Contributions to structural mechanics and durability in structural engineering

by Gideon PAG van Zijl

Dissertation presented for the Degree of Doctor of Engineering in the Faculty of Engineering, at Stellenbosch University

Supervisor: Professor WP Boshoff

December 2016

Declaration

By submitting this dissertation electronically, I declare that the entirety of the work contained therein is my own, original work, that I am the sole author thereof (unless to the extent explicitly otherwise stated), and that I have not previously in its entirety or in part submitted it for obtaining any qualification.

Signature:

Date: December 2016

Abstract

Contributions to structural engineering have been made since 2001 from the basis of the Department of Civil Engineering of Stellenbosch University (SU). The inauguration of the Centre for Development of Sustained Infrastructure (CDSI) in 2002 has been instrumental in defining, directing and scoping the research and development in the categories *Advanced cement-based construction materials*, *Crack formation and durability towards durability design*, *Renovation and retrofitting towards extended life span* and *Sustainable energy harvesting structures*. The contributions are structured along these categories as chapters of this dissertation.

Early career background in structural Engineering at the Institute for Structural Engineering (1987-1989) and Bureau for Mechanical Engineering (1989-1992) and higher education in computational and structural mechanics (PhD 1995-1999, Research Fellow 1999-2001, TU Delft), shaped the research interests in these fields. Continued affiliation with TU Delft (30%) and SU (70%) in the years 2001-2009 provided access to collegial expertise in related fields of experimental research, materials engineering, risk and reliability, and structural design at these institutions and beyond. In this way, national and international collaboration complemented structural and computational mechanics in well-rounded research programs in the mentioned categories. Clearly, the contributions are the result of collaboration in which the author to various degrees led, participated in and supervised research and development. Highlights of the contributions in the four categories are described at a relatively high level towards conveying the contributions in the national and international context. To a degree selective reporting is done, and the reader directed to detailed elaborations in roughly 200 dissertations, theses and technical papers supervised or co-supervised, authored and co-authored.

Approach by the infrastructure pre-fabrication industry in South Africa towards development of accelerated and new product lines led to the development of advanced cement-based construction materials (ACM) with local ingredients, and appropriate adaption of the materials to industrial fabrication process of high-pressure extrusion. What started as fibre inclusion towards reduced traditional steel reinforcement in concrete pipes, led to development, characterisation, manufacturing and constitutive modelling of steel fibre concrete and strain-hardening cement-based composites (SHCC). Roles of international leadership in co-chairing and chairing RILEM technical committees followed, as well as co-editing of books on the state-of-the-art of Durability of SHCC and a Framework of durability design with SHCC respectively. Particular contributions of significant potential towards the ability to design for durable, sustainable infrastructure, were made in chloride-induced corrosion and alkali silica reaction. In both cases crack formation and durability, i.e. structural durability in service conditions are the points of departure in order to assess actual structural performance in presence of such deteriorating processes.

The work in ACM was extended to ultra-high strength concrete, and recently to lightweight aerated concrete (LWAC) and lightweight foam concrete (LWFC). The thermal, acoustic and potential mechanical advantages of LWAC and LWFC are subjects of a current significant research effort in the CDSI towards developing these lightweight materials for structural application in residential infrastructure. Constitutive models developed for traditional construction materials, as well as several of the ACM, enabled the iterative computational-experimental development and validation of retrofitting strategies for both unreinforced load-bearing masonry and reinforced concrete structures for new functionality or extended structural life span. Finally, a role of leadership and collaboration was fulfilled in research of the solar chimney power plant concept with national and international partners, bringing the concept for harvesting of sustainable energy to a pre-feasibility level.

The contributions have laid the link between construction material properties, structural behaviour and durability. Through the fundamental experimental research, structural mechanics and computational mechanics,

it has been made possible to utilise the advanced properties of ACM to advance structural performance and durability. Human capital well-versed in the fundamental principles of this multi-level structural engineering approach has been developed in the process of research supervision by the author.

Opsomming

Bydraes tot struktuuringenieurswese is gemaak sedert 2001 met die Department van Siviele Ingenieurswese van Universiteit Stellenbosch (US) as basis. Die stigting van die Sentrum vir Ontwikkeling van Volhoubare Infrastruktuur (CDSI) in 2002 was instrumenteel in die bepaling, afbakening en stuur van navorsing en ontwikkeling in die kategorië *Gevorderde sementbasis konstruksiemateriale, Kraakvorming en duursaamheid met die oog op duursaamheidsontwerp, Renovering and versterking tot verlengde lewenspan* en *Strukture vir ontginning van volhoubare energie*. Die bydraes word gestruktureer aan die hand van hierdie kategorië as hoofstukke van hierdie proefskrif.

Vroë-loopbaan ervaring in struktuuringenieurswese by die Instituut vir Struktuuringenieurswese (1987-1989) en die Bureau vir Meganiese Ingenieurswese (1989-1992), en hoër opleiding in berekenings- en struktuurmeganika (PhD 1995-1999, Navorsingsgenoot 1999-2001, TU Delft), het die navorsingsbelang in hierdie velde gevorm. Voortgesette affiliasie met TU Delft (30%) en US (70%) in die jare 2001-2009 het toegang verleen tot kollegiale kundigheid in verwante velde in eksperimentele navorsing, materiaalingenieurswese, risiko en betroubaarheid, en struktuurontwerp by hierdie instansies en andere. Op hierdie manier het nasionale en internasionale samewerking struktuur- en berekeningsmeganika gekomplementeer in afgeronde navorsingsprogramme in die vermelde kategorië. Die bydraes is duidelik die gevolg van samewerking, waarin die outeur navorsing en ontwikkeling tot verskillende mate gelei het, aan deelgeneem het, en studieleiding verskaf het. Hoogtepunte van die bydraes in die vier kategorië word beskryf op ‘n relatief hoë vlak, met die doel om die bydraes in die nasionale en internasionale konteks te plaas. Die beskrywings is tot ‘n mate selektief, en die leser word verwys na gedetaileerde beskrywings in rofweg 200 proefskrifte, tesisse en tegniese artikels wat deur die outeur begelei, mede-begelei, of geskryf is as hoof- of mede-outeur.

Toenadering deur die infrastruktuur voorafvervaardigingsindustrie in Suid-Afrika ter versnelde en nuwe produksielyne het gelei tot die ontwikkeling van gevorderde sement-basis konstruksiemateriale (ACM) met plaaslike ingrediente, en geskikte aanpassing van die materiale om met ‘n industriële vervaardigingsproses van ekstrusie onder hoë druk vervaardig te kan word. Wat begin het as insluiting van vesels om tradisionele staalbewapening in betonpype te verminder of te vervang, het gelei tot die ontwikkeling, karakterisering, vervaardiging en konstitutive modellering van staalvesel beton en vervormingsverhardende sementbasis saamgestelde materiale (SHCC). Dit is gevolg deur internasionale leierskap as mede-voorsitter en voorsitter van RILEM tegniese komitees, en mede-redakteurskap van boeke oor die huidige stand van Duursaamheid van SHCC en ‘n Raamwerk vir Duursaamheidsontwerp met SHCC onderskeidelik. Spesifieke bydraes van potensieel noemenswaardige belang is gelewer tot die vermoë om duursame, volhoubare infrastruktuur te ontwerp, met spesifieke verwysing na chloriede geïnduseerde korrosie en alkali silika reaksie. In beide gevalle is kraakvorming en duursaamheid, dit wil sê strukturele duursaamheid onder dienstoestande, die vertrekpunt om ware strukturele gedrag in die teenwoordigheid van hierdie degradasieprosesse te assesseer.

Die werk in ACM is uitgebrei tot ultra-hoë sterkte beton, en onlangs ook tot liggewig belugte beton (LWAC) en liggewig skuimbeton (LWFC). Die termiese, akoestiese en potensiele meganiese voordele van LWAC en LWFC is die onderwerp van ‘n huidige intense navorsingsprogram in die CDSI ter ontwikkeling van hierdie liggewig materiale tot strukturele toepassing in residensiële infrastruktuur. Konstitutiewe modelle wat ontwikkel is vir tradisionele konstruksiemateriale, sowel as verskeie van die ACM, het die iteratiewe numeriese-eksperimentele ontwikkeling en validasie van versterkingstrategië moontlik gemaak, vir beide ongewapende lasdraende messelwerk en gewapende betonstrukture vir nuwe funksionaliteit of verlengde lewenspan. Laastens, is ‘n rol van leierskap en samewerking vervul in navorsing oor die sontoring kragsentrale konsep,

saam met nasionale en internasionale vennote, wat hierdie konsep vir ontginning van volhoubare energie gebring het tot die vlak kort voor lewensvatbaarheid.

Die bydraes vorm ‘n skakel tussen konstruksiemateriaal eienskappe, struktuurgedrag en duursaamheid. Deur die fundamentele eksperimentele navorsing, struktuurmeganika en berekeningsmeganika, is dit moontlik gemaak om die gevorderde eienskappe van ACM te benut om struktuurgedrag en -duursaamheid te bevorder. Hoogsopgeleide menslike kapitaal, goed vertroud met die fundamentele beginsels van hierdie multi-vlak ingenieursbenadering is ontwikkel in die proses van navorsingsbegeleiding deur die outeur.

Acknowledgements

The contributions in this dissertation are the result of laboratory and numerical experiments, modelling and the development of innovative and practical solutions by research students who have worked with me over the past decades. They are too many to name here. In acknowledgement of their respective contributions, Appendix A lists all students whom I have supervised or co-supervised. In most instances, the papers cited in this dissertation bear your names as co-authors, testimony to your invaluable contributions. I am indebted to you all for your enthusiasm, hard work, and friendship.

In reflection on my career, the mentorship by Professor Johan Retief since my return from The Netherlands is a beacon. As colleague over the past 25 years, I attribute my early South African research network and the conceptualisation of the CDSI to him.

Professor Billy Boshoff embodies many firsts in my career, as first Master's student at Stellenbosch University, PhD, Post Doc, and ex-student to become Professor. I acknowledge your tireless striving for excellence. Thank you for supervising this dissertation, with the perspective of having traversed most of this road with me since 2001.

I acknowledge the laboratory staff of the Structural Division of Stellenbosch University, for their diligence, at times tolerance with an impatient professor, and their pride in the achievements of the research students whom they assisted.

The staff of the Department of Civil Engineering has been a warm, collegial and excellent unit in challenging times when our very existence was in doubt, and in times of collective achievement. My association with you over the past decade is the finest period of my career.

My family has offered me firm personal support and inspiration throughout my career. Making the yearly commute to Delft over the first decade of this century, and making it fun, is evidence of your commitment. Allowing and accepting my long hours as HOD is evidence of your sacrifice to my calling.

Contents

List of Abbreviations

AAC	Autoclaved aerated concrete
AAR	Alkali aggregate reaction
ACM	Advanced cement-based materials
AE	Acoustic emission
ASR	Alkali silica reaction
BE	Beam-end
CAC	Calcium aluminate cement
CDSI	Centre for development of sustainable infrastructure
CFRP	Carbon fibre reinforced polymers
CoV	Coefficient of variation
CT	Computer tomography
CWV	Crack width value
CWV_{WP}	Crack width value for water permeability
DIC	Digital image correlation
DTU	Dresden University of Technology, Germany
ECC	Engineered cementitious composites
FE	Finite element
FEA	Finite element analysis
FRC	Fibre reinforced concrete
GGCS	Ground granulated corex slagment
HPFRCC	High-performance fibre reinforced cement-based composites
IPI	Ingress potential index
IPI_{WP}	Ingress potential index for water permeation
IPI_{Cl}	ıngress potential index for chloride diffusion
ISE	Institute of structural engineering, Stellenbosch
LEC	Levelised electricity cost (investment, operations and maintenance cost per kWh of electricity produced over the project lifetime)
LVDT	Linear variable differential transducer
LWAC	Lightweight aerated concrete
LWFC	Lightweight foamed concrete
MOR	Modulus of rupture
MTM	Materials testing machine
NDT	Non-destructive test
NWC	Normal weight concrete
PO	Pull-out bond
PP	Polypropylene
PVA	Polyvinyl-alcohol
RAC	Recycled aggregate concrete, i.e. concrete containing RCA
RCA	Recycled concrete aggregate
R&D	Research and development
R_e	Reynold's number

RILEM	*Reunion Internationale des Laboratoires et Experts des Materiaux, Systemes de Construction et Ouvrages* International Union of Laboratories and Experts in Construction Materials, Systems, and Structures
RIM	Radical innovation methodology
SCCN	Solar chimney competency network
SEM	Scanning electron microscopy
SFRC	Steel fibre reinforced concrete
SHCC	Strain-hardening cement-based composites
SCPP	Solar chimney power plant
SP	Superplasticiser
SU	Stellenbosch University, South Africa
TUD	Delft University of Technology, The Netherlands
TUE	Eindhoven University of Technology, The Netherlands
UHPC	Ultra-high performance concrete
VMA	Viscosity modifying agent
XRF	X-ray florescence
Y10, Y12, Y20	10 mm, 12 mm and 20 mm diameter respectively, high tensile strength reinforcing steel bar

Chapter 1 Introduction

Research results over an academic career spanning more than two decades are collected under appropriate themes, highlighting the contributions to the structural and civil engineering sciences. Founded by a structural engineering education and early career, the research activities span the development of advanced construction materials and constitutive modelling, computational and structural mechanics, to crack formation and durability. Premature infrastructural deterioration internationally gives context to these contributions to infrastructure sustainability and life span extension, and motivates the international collaborations. This contextualisation of the collection of the candidate's works is presented as basis for evaluation and awarding the DEng degree by Stellenbosch University.

1.1 Sustainability in structural engineering

The fundamental role of infrastructure in driving economies, as enabler in all economy sectors, is undisputable. Structural Engineering contributes through the development of appropriate construction materials, design to resist environmental and process actions with acceptable level of reliability, functionality for its intended use, and overall cost efficiency in all phases over the full life cycle. Ecological perspective has received justified attention, obligating Structural engineers to constrain solutions to structural integrity with energy efficiency and minimised or zero harmful emissions embodied in construction materials and construction technologies, during the operation of infrastructure, and re-use or demolition at the end of its life span.

However, the cost to maintain and repair reinforced concrete (R/C) structures has grown to a significant portion of total construction expenditure world-wide, up to 50% in many industrial countries. Whilst typical design life for infrastructure is 50 years, or in cases 100 years, the average intervention-free service life of German infrastructure is reported to be 18.5 years (Wittmann and Van Zijl 2006). This does not compare well with Roman bridges, which had service lives of 2000 years, e.g. a Roman bridge in Augusta Treverorum, Trier. This has led to significant research and development efforts internationally towards developing advanced construction materials to resist aggressive environmental exposure that causes premature deterioration, and excessive cost of the repair intervention and that caused by the partial or full functional loss of the particular economic infrastructure for the duration of repair (Lepech 2011).

Contributions to structural sustainability described in this dissertation relate to advanced construction materials with potential for reduced volume of construction and associated reduced ecological impact. Construction materials with particular durability potential are developed, and their actual durability performance characterised to ensure appropriate use in structural systems and environmental exposure for low-intervention, durable structures. In addition to advanced materials and structural systems for new structures, the significant portfolio of existing, affected infrastructure requires suitable intervention strategies to reach or extend its service life, guided by the same principles of energy efficiency, ecology and economy. Also in cases where new insight has developed in environmental action, including natural or industry-induced seismicity, intervention strategies are required to efficiently address inappropriately high levels of risk, with least impact to the industry or society. This has led to the development of a range of advanced construction materials, constitutive laws to capture their mechanical behaviour with sufficient accuracy, and structural systems to exploit their superior characteristics.

1.2 Contributions to structural mechanics and durability

Six forming years in structural and computational analyses for civil engineering, manufacturing, mining and chemical processing industries in the late 1980's, led to an academic career in structural engineering commencing in 1992 at Stellenbosch University. In 1995 the author joined Delft University of Technology (TUD) as researcher, and completed a PhD on *Computational modelling of masonry creep and shrinkage* (Van Zijl 2000) in the groups for structural mechanics and computational mechanics. This introduced a major theme of contributions in structural, load bearing masonry. Constitutive models for masonry for both discrete (meso-scale, including embedded interface representation of joints) as well as continuum (macro) modelling, developed first by a preceding PhD candidate in the group (Lourenço 1996), were extended for time and rate dependence, and improved in aspects of mechanical simulation by Van Zijl (2000). These augmented models were implemented in commercial finite element software DIANA as first models dedicated to structural masonry. Bulk creep and cracking rate-dependence were developed by the author, and the latter was demonstrated to regularise continuum representation of localisation (cracking) in masonry and concrete. These masonry models are still included in the FE package DIANA, and used widely internationally. In continued improvement of the models, a dilatancy formulation was included, avoiding significant potential overestimation of shearing resistance in compressive-shear conditions dominating in seismic and wind action. The publication of this contribution is well-cited in ISI listed journals. The models were used by the author's research students at Stellenbosch University to predict damage to historical masonry buildings along the North-South Metro line in Amsterdam by tunnelling-induced subsidence expected and observed. This was done in collaboration with the Structural Mechanics group at TUD in the period 2002-2004.

Required retrofitting of residential buildings erected in South Africa before 1989, when the requirement for structural resistance to seismic action was standardised, motivated the development of strain-hardening cement-based composites (SHCC) directly after the author's return to Stellenbosch University in 2001. While the initial concept was fathered by VC Li and his co-workers (eg. Li 1993), significant contributions from the author's research group included the first creep tests on these advanced construction materials. What is more, the group (Boshoff et al. 2009a,b) discovered and presented the dominating mechanism of SHCC tensile creep under sustained load as being time-dependent fibre pull-out from the matrix. While SHCC was demonstrated to retain fine crack widths under quasi-static tensile and flexural load up to extreme levels of deformation, crack widening and eventual creep fracture occur under sustained load once cracks have formed. This phenomenon has to be carefully considered in structural design.

SHCC bond to concrete and masonry substrates is another contribution of significance. A bond interface constitutive model incorporating a strain-softening Coulomb-friction limit state, capped with a softening tensile cut-off and a strain-hardening-softening compressive cap, was characterised by the author's student (Van Zijl and Stander 2009). These results were extensively modelled in a recent PhD study at TUD (Luković 2016). This work is included as a book chapter on the state-of-the-art of durability design with SHCC (Van Zijl and Slowik 2016). In addition to the interface constitutive model, a constitutive model for SHCC based in multi-surface plasticity, including strain-hardening-softening in both tensile and compressive regimes was developed by the author (Van Zijl 2009), and is one of three models currently available for this class of materials. The first was developed in a PhD study (Boshoff 2007) supervised by the candidate and based in computational damage. The model by Van Zijl (2009) incorporates creep and rate-dependence, and was used by Van Zijl and Stander (2009) to simulate physical experiments. Overlays to load bearing masonry are currently being developed, including a spraying (shotcrete) application, to enhance seismic resistance of historical or other structures vulnerable to seismic damage (Van Zijl and De Beer 2016). Other advanced cement-based construction materials with

retrofitting potential (self-compacting steel fibre reinforced concrete; ultra-high performance concrete) have been developed by the author's group.

Deteriorating infrastructure nationally and internationally inspired investigation of structural durability, i.e. resistance to deterioration processes under operational conditions. The fine, controlled cracks in SHCC were thought to restrict ingress of deleterious materials, and thereby prevent or limit deterioration. The author's student (Paul 2015, Paul and Van Zijl 2014, Paul et al. 2016) was the *first* to determine chloride profiles for cracked reinforced SHCC (R/SHCC). Paul and Van Zijl (2016) were the *first* to investigate and present evidence of the influence of crack spacing on corrosion rate in R/SHCC, as opposed to the widely believed dominant influence of crack width on corrosion rate. Next to corrosion in coastal regions, alkali silica reaction has been studied by the author's group. ASR has affected several structures world-wide, of which the most well-known cases in South Africa are the destroyed concrete pavement of the National Road (N2) in the Western Cape, and deterioration of the concrete sleepers of the Sishen-Saldanha iron ore railway line. ASR remains a major source of deterioration in South Africa, affecting for instance the Danie Craven Stadium in Stellenbosch, the Kleinplaas Dam in Stellenbosch and the Good Hope Centre in Cape Town designed by Nervi in the late 1970's. Results of physical experiments and modelling of the combined mechanical cracking and ASR (Alaud and Van Zijl 2015, 2016) are novel.

Infrastructural sustainability is not the sole responsibility of Structural Engineers, but a multi-disciplinary challenge. A collaborative research program was performed with colleagues in Mechanical Engineering towards developing aspects of the Solar Chimney Power Plant for solar energy harvesting. Main contributions stemming from this work are the three PhD graduates Van Dyk (2008) on the tower structure, Fluri (2007) on optimal turbine layout and Pretorius (2007) on the performance and control of the SCPP, supervised by the author, Professors Theo von Backström and Detlev Kröger respectively. The extended collaboration with international colleagues Professors Reinhard Harte (Wuppertal, Germany), Wilfried Krätzig, Hans-Jürgen Niemann and Rüdiger Höffer (Bochum, Germany), brought the SCPP concept to the verge of implementation, with ongoing international attempts at raising capital to erect a full-scale plant. Important contributions from this Solar Chimney Competence Network (SCCN) are the well-cited collaborative papers on the "State and recent advances in research and design of Solar Chimney Power Plant Technology" (Von Backström et al. 2008) and a detailed cost model developed by the research team for large scale SCCPs, including the cost of the tower, collector and the power conversion units (Fluri et al. 2009). Contributions by the author's team to sustainable energy harvesting structures extended to the design of tall wind turbine support structures for South Africa (Way and Van Zijl 2015, Van Zyl and Van Zijl 2015), to inform the local structural engineering community on appropriate design strategies, and relative cost of locally designed and constructed alternative construction materials for large towers.

1.3 The Platform

The contributions documented here are to be seen against the background of collaborative research with various colleagues nationally and internationally and, importantly, senior research students who performed the bulk of physical experimental, numerical and analytical research under the author's supervision or co-supervision. The research has been performed under the auspices of the Centre for Development of Sustainable Infrastructure (CDSI) inaugurated by the author in 2002, in the Institute of Structural Engineering (ISE) at Stellenbosch University. The vision of sustainable infrastructure towards supporting the South African economic development has focussed the research efforts in relevant themes, and encouraged industry support and participation.

The collaborations with various colleagues at Stellenbosch University and across the world are evident from the lists of co-authors in the cited references at the end of each chapter of this dissertation. An attempt has been made to distinguish the author's contributions in the relevant descriptions, but clearly the contributions would not have been possible without the collaborative efforts, facility sharing and expertise of the many co-authors. Their contributions are acknowledged.

Appendix A lists the graduated and current PhD and Master's students who are credited with the research described in this dissertation, and whose contributions are described to varying levels of detail in the chapters of this dissertation. They are listed chronologically since the author's return to the Department of Civil Engineering of Stellenbosch University in 2001. Whilst the 31 Master's Theses have brought valuable research insights and results, it is natural that more fundamental and extensive contributions have been presented by Doctoral candidates. Their achievements justify a brief summary here, also in chronological sequence:

- Dr. ir. Ad T. Vermeltfoort, Associate Professor at Eindhoven University of Technology, The Netherlands, performed physical experiments on masonry specimens in the Pieter van Musschenbroek Laboratory of TUE, culminating in his PhD dissertation *Brick-mortar interaction in masonry under compression (2005, co-supervised by the author).* His work, and that of Dr.ir. Rob van der Pluijm in the same Laboratory was heavily relied on in the author's PhD and subsequent research towards development of constitutive models for masonry.
- Professor Billy (W.P.) Boshoff, through his PhD dissertation entitled *Time-dependent behaviour of Engineered Cementitious Composites (ECC)* (March 2007), and Post-doctoral research (2007) has pioneered the strain-hardening cement-based composite research at Stellenbosch University under the author's supervision. He received the Reitz Medal for best postgraduate student in Civil Engineering at Stellenbosch University in 2007. After his appointment as Lecturer in 2008, he has traversed the academic ranks to full professor at Stellenbosch University in minimum time, and was awarded the Upcoming Researcher of 2015 by the Engineering Faculty at SU.
- Dr Cobus van Dyk, Associate at UWP Consulting in East London, South Africa, performed one of three themes of the Solar Chimney Power Plant collaborative research project, culminating in his PhD dissertation *A methodology for radical innovation – illustrated by application to a radical civil engineering structure* (December 2008). He received the Reitz Medal for best postgraduate student in Civil Engineering at Stellenbosch University in 2008. Dr van Dyk was elected as South African Institute of Civil Engineers (SAICE) Young Engineer of 2014.
- Adjunct Professor Peter W. Day, under academic mentorship and supervision of Professor Johan Retief, and co-supervision by the author, was awarded the Senior Doctorate (DEng) for his dissertation *A contribution to the advancement of Geotechnical Engineering in South Africa* (March 2013). As a leading Geotechnical Engineer in South Africa and internationally, he co-supervises the author's research students in soil-structural interaction of wind turbine structures in South Africa. Amongst various awards, he has been SAICE Engineer of 2014.
- Dr Jin Zang was the first to develop ultra-high strength concrete without heat curing in the Materials Laboratory of Stellenbosch University, leading to his PhD dissertation *Developing non-heat treated UHPC in South Africa* (March 2015).
- Emeritus-Professor Johan Verster Retief, the author's colleague and mentor over the past decades, co-supervised Mrs Susan Engelbrecht and Dr Cobus van Dyk in structural reliability, and was main supervisor of Prof Peter Day's DEng. Amongst his many achievements, Prof Retief received the Jennings Award in 2014. The author was honoured to supervise Professor Retief for his DEng dissertation *Contributions to the implementation of the principles of reliability to the standardized basis of structural design* (December 2015), with Dr Celeste Viljoen as co-supervisor.

- Dr Suvash Chandra Paul, Research Fellow at Nanyang Technological University (NTU) in Singapore, performed ground-breaking experimental research on chloride ingress and steel bar corrosion in SHCC. His dissertation *The role of cracks and chlorides in corrosion of reinforced strain-hardening cement-based composites (R/SHCC)* (December 2015) was awarded the Reitz medal for best PhD work in the Department of Civil Engineering, Stellenbosch University. In 2013, during his PhD research, Dr Paul won two best paper awards at international conferences.
- Mr Salhin Alaud's PhD dissertation entitled *Durability of concrete under combined action - mechanical load and alkali silica reaction (ASR)* (2016) is in process of assessment. As an experienced lecturer from the Department of Civil Engineering, Al-Mergib University, Libya he has undertaken PhD studies at Stellenbosch University on full-time basis. He has designed and overseen the manufacturing of accelerated ASR testing equipment in the Structures and Concrete Materials laboratories of Stellenbosch University.
- Mr Stephan Zeranka, full-time Laboratory Manager of the Structures and Concrete Materials Laboratories of the Department of Civil Engineering at Stellenbosch University. In his PhD dissertation entitled *Design-oriented shear constitutive model for steel fibre-reinforced concrete (SFRC)* currently being written with envisaged graduation March 2017, he developed design principles for self-compacting steel fibre-reinforced concrete (SFRC). He subsequently performed multi-scale physical experiments and modelling of shear resistance of SFRC with and without steel bar reinforcement. This included single fibre pull-out tests, as well as novel Iosipescu-type single fibre pure shear tests and as control, single fibre push-through tests. On the macro-scale, results of Iosipescu shear tests of pre-cracked SFRC specimens serve as verification of a semi analytical modelling and simplified shear analysis of SFRC, based on single fibre pull-out and dowel effect results.
- Mrs Susan A. Engelbrecht has performed PhD research on part-time basis, with dissertation entitled *Flexural design guidelines for strain–hardening fibre reinforced cement-based composites.* Insight in the flexural behaviour of, and a design strategy for steel bar reinforced SHCC beams have been presented, and the manuscript is in process of assessment for graduation in December 2016.
- Mr Peter B.K. Mbewe, Lecturer at the Polytechnic Malawi, received his MScEng entitled *Development of analytical flexural models for steel fibre reinforced concrete beams with and without steel bars* in December 2011 (Cum Laude), and his current PhD entitled *Structural system performance evaluation towards sustainable housing* is key to the CDSI's contribution to sustainable housing in South Africa. His novel non-linear structural analysis strategy is elaborated in this DEng dissertation.
- Mr Tata (A.S.) van Rooyen, Lecturer in Structural Engineering at Stellenbosch University, initiated the CDSI research activities in lightweight aerated concrete and lightweight foam concrete, starting with his MScEng (March 2013) and continued in his PhD dissertation *Mechanics and durability of surface treated foamed concrete*. He has supervised several BEng final year projects and MEng[Research] theses on the topic.
- Mr Mohamad Pourbehi continues the work started by Salhin Alaud on ASR. He is responsible for the development of a computational strategy and implementation in a finite element setting in his dissertation entitled *Computational modelling of ASR*. He is supervised by Dr JAvB Strasheim, and co-supervised by the author.

1.4 Layout

The dissertation devotes a chapter to each of four main themes, as follows:

- Chapter 2 Advanced cement-based construction materials. Highlights of strain-hardening cement-based composites (SHCC) and industrial manufacturing processes developed by the CDSI are described.

Development of ultra-high strength concrete (UHPC), steel fibre-reinforced concrete (SFR) and light-weight aerated (LWAC) and lightweight foam concrete (LWFC) by the CDSI is also described.

- Chapter 3 Crack formation and durability, towards durability design. Contributions to simulating, understanding and characterising deterioration processes of chloride-induced corrosion of steel in SHCC, as well as ASR in reinforced concrete are elaborated in this chapter. A common theme is the combined action of mechanically induced cracks and these deterioration processes of corrosion and ASR.
- Chapter 4 Renovation and retrofitting towards extended structural life span. This chapter is devoted to bonded overlays of Carbon Fibre Reinforced Polymer (CFRP) on masonry and concrete substrates, as well as SHCC bonded overlays on masonry and concrete substrates. The use of appropriate constitutive models developed by the author for these construction and retrofitting materials is presented. Adaption of the SHCC mix for a suitable sprayed application is also described, along with validating experimental results on increased resistance of retrofitted structural elements.
- Chapter 5 Sustainable energy harvesting structures. The collaborative, multi-disciplinary research on aspects of the Solar Chimney Power Plant is described, and an overview of the current status is given. An overview of contributions towards the design of Wind turbine support structures appropriate for South Africa is also given.

The dissertation is concluded with Chapter 6, where the main contributions are summarised, followed by the list of students supervised in Appendix A.

References

Alaud SM and Van Zijl GPAG 2014. Role of mechanical load and Alkali Silica Reaction in concrete, International Congress on Durability of Concrete ICDC, 4-6 December 2014, New Delhi, India.

Alaud SM and Van Zijl GPAG 2016. Role of pre-crack formation and Alkali Silica Reaction in concrete. 15th International Conference on Alkali Aggregate Reaction (15th ICAAR), 3-7 July 2016, Sao Paulo, Brazil.

Boshoff, WP 2007. Time-Dependant Behaviour of Engineered Cement-Based Composites. PhD dissertation, Stellenbosch University, South Africa.

Boshoff WP, Mechtcherine V and Van Zijl GPAG 2009a. Characterising the time-dependent behaviour on the single fibre level of SHCC: Part 1: Mechanism of fibre pull-out creep, *Cement and Concrete Research*, 39 (2009) 779-786.

Boshoff WP, Mechtcherine V and Van Zijl GPAG 2009b. Characterising the time-dependent behaviour on the single fibre level of SHCC: Part 2: Rate effects in fibre pull-out tests, *Cement and Concrete Research*, 39 (2009) 787-797.

Fluri TP 2008. Turbine layout for and optimization of solar chimney power conversion units. PhD dissertation, Stellenbosch University, South Africa.

Fluri TP, Pretorius JP, Van Dyk C, Von Backström TW, Kröger DG, Van Zijl GPAG 2009. Cost Analysis of Solar Chimney Power Plants, Solar Energy 83(2) 246–256.

Lepech MD 2011. Durability, economical, ecological and social aspects (life-cycle considerations). Chapter 8 in Durability of Strain-Hardening Fibre-Reinforced Cement-Based Composites (Van Zijl GPAG, Wittmann FH, eds.), State-of-the-art report, Rilem TC 208 HFC, SC 2, Springer Publishers, ISBN-13: 978-94-007-0337-7.

Li VC 1993. From Micromechanics to Structural Engineering – the Design of Cementitious Composites for Civil Engineering Applications, JSCE J. Struc. Mechanics and Earthquake Engineering, 10 (2) 37-48.

Lourenço PB 1996. Computational strategies for masonry structures. PhD dissertation, Delft University of Technology, The Netherlands.

Luković, M 2016. Influence of interface and strain-hardening cementitious composite (SHCC) properties on the performance of concrete repairs, PhD dissertation, Delft University of Technology, The Netherlands.

Paul SC 2015. The role of cracks and chlorides in corrosion of R/SHCC. PhD dissertation, Stellenbosch University, South Africa.

Paul SC, Van Zijl GPAG 2014. Crack formation and chloride induced corrosion in reinforced strain-hardening cement-based composite (R/SHCC), Journal of Advanced Concrete Technology 12 (Sept 2014) 340-351.

Paul SC, Van Zijl GPAG 2016. Chloride-induced corrosion modelling of cracked reinforced SHCC. Archives of Civil and Mechanical Engineering (ACME) 16: 734-742, DOI 10.1016/j.acme.2016.04.016.

Paul SC, Van Zijl GPAG, Babafemi J, Ming Jen TAN 2016. Chloride ingress in cracked and uncracked specimens made from strain-hardening cement-based composite (SHCC). Construction and Building Materials 114, 232-240.

Pretorius JP 2007. Optimization and control of a large-scale solar chimney power plant. PhD dissertation, Stellenbosch University, South Africa.

Van Dyk C 2008. A methodology for radical innovation – illustrated by application to a radical civil engineering structures. PhD dissertation, Stellenbosch University, South Africa.

Van Zijl GPAG 2000. Computational modelling of masonry creep and shrinkage. PhD dissertation, Delft University of Technology, The Netherlands.

Van Zijl GPAG 2009. Computational modelling of SHCC – an anisotropic constitutive model incorporating creep and rate dependence. ISE report 2009-020, Stellenbosch University, South Africa.

Van Zijl GPAG, De Beer L 2016. An SHCC overlay retrofitting strategy for unreinforced load-bearing masonry, Proceedings of 9th International Conference on Fracture Mechanics of Concrete and Concrete Structures - FRAMCOS-9, V. Saouma, J Bolander, E Landis (Eds), 29 May-2 June 2016, Berkeley, USA.

Van Zijl GPAG, Slowik V (eds.) 2016. A framework for durability design with strain-hardening fibre-reinforced cement-based composites (SHCC), State-of-the-art report, Rilem TC 240-FDS, Springer Publishers.

Van Zijl GPAG, Stander H 2009. SHCC repair overlays for RC: Interfacial bond characterization and modeling, CDROM Proc. International Conference on Concrete Repair, Rehabilitation and Retrofitting (ICCRRR 2008), University of Cape Town, South Africa, pp. 995-1003.

Van Zyl WS, Van Zijl GPAG 2015. Dynamic behaviour of normally reinforced concrete wind turbine support structures. J SAICE 54(4) 35-44.

Von Backström ThW, Harte R, Höffer R, Krätzig WB, Kröger DG, Niemann H-J, Van Zijl GPAG 2008. State and Recent Advances in Research and Design of Solar Chimney Power Plant Technology, VGB PowerTech Journal, July-edition 2008.

Way A, Van Zijl GPAG 2015. Material cost comparison between steel, concrete and hybrid wind turbine support structures in South Africa. J SAICE 54(4) 45-54.

Wittmann FH, Van Zijl GPAG 2006. Task Group B – Durability of SHCC Conclusions. In: Proceedings Rilem International Workshop on High Performance Fiber Reinforced Cement-Based Composites (HPFRCC) in Structural Applications, May 22-27, Honolulu, Hawaii, pp. 109 – 114.

Chapter 2 Advanced cement-based construction materials

2.1 Introduction

Over millennia, materials from various sources have been used in construction of infrastructure, ranging from natural stone, wood, clay and even ice, to man-made composites like fired clay bricks and blocks, concrete, metals and plastics. In societies across the world, preferences in construction materials appear to have developed, fuelled by aesthetic appeal, tradition, availability of ingredient materials and greater versatility of some materials over others. Concrete is used in most structures world-wide for its mouldability into required form, availability of ingredient materials, relative low sensitivity to material and production process variabilities, and durability. Recently, remarkable improvements have been made in the ability to design cement-based materials to specific performance criteria, including self-compaction or self-levelling, ductility and inherent crack control. These developments enable significant advances in structural performance over the design life span, which must be borne in mind when considering the material cost. The Centre for Development of Sustainable Infrastructure (CDSI), has played a significant role in developing advanced cement-based construction materials (ACM), as elaborated in this chapter.

Strain-hardening cement-based composites (SHCC) have been developed, characterised, modelled and applied in large scale experimental studies by the CDSI during the past one and a half decade. Developed initially by the group in Michigan under leadership of Victor Li in the 1990s under the acronym ECC (engineered cementitious composites) (Li 1993, 1998, Li et al. 2001), international research activity was stimulated by the work of a RILEM Technical Committee 208-HFC, chaired by professor Li in the period 2005 to 2009. The three subcommittees *SC1: Mechanical characterisation and testing*, *SC2: Durability* and *SC3: Structural design and performance* produced three state-of-the-art reports (Fischer 2011, Van Zijl and Wittmann 2011, Rokugo and Kanda 2013). The work on durability of SHCC of SC2 was continued by RILEM TC 240-FDS in the period 2010 to 2016, chaired by the author (Van Zijl and Slowik 2016). The energy dissipating mechanism of multiple cracking under general loading actions has led to the structural application of SHCC in buildings and highway bridges in earthquake prone regions (eg. Rokugo and Kanda 2013, Van Zijl and Slowik 2016), and the proposal of a retrofitting strategy by bonded SHCC overlay on unreinforced load bearing masonry structures in seismic regions (see Chapter 4). The inherent crack-control has the potential of structural durability, as elaborated in Chapter 3, where for instance significantly reduced corrosion rates observed in steel reinforced SHCC is elaborated.

An interesting study on acoustic emission (AE) monitoring of SHCC during tensile and flexural tests was performed by the author's PhD-student Suvash Paul while on a study visit to BAM in Berlin, Germany. The tensile and flexural specimens were instrumented with AE sensors, and clear distinction could be made between frequencies above 120 kHz associated with fibre pull-out or rupture and below 90 kHz associated with matrix cracking. The latter was confirmed by AE monitoring of mortar tensile test specimens of the same base mix, but without the PVA fibres (Paul et al. 2015). This first approach and publication of AE monitoring of SHCC holds significant potential not only in laboratory experiments, but as non-destructive test (NDT) method in practice.

Ultra high-performance concrete (UHPC) has been developed by the CDSI with local ingredients except the high-strength short straight steel fibres imported from Belgium (Zang 2015, Zang and Van Zijl 2015). Structural applications of UHPC are increasing, in elegant pedestrian bridges (eg. Perry and Seibert 2008), slender highway bridge girders (Graybeal 2006) and highly durable bridge deck repairs by bonded overlay to the existing concrete bridge deck as substrates (eg. Brühwiler and Denarié 2006). Volume reduction of structural elements holds potential for cost savings on structural level in carefully considered and designed structural systems. Steel fibre reinforced concrete (SFRC) has found application in performance-based designed applications, for instance in tunnel lining structures, slabs on grade, and suspended slabs. Lack of standardisation has influenced application of SFRC, but recent inclusion of design guidelines in the Model Code (MC2010) has potentially paved the way for the introduction of this ACM into the next generation Eurocode standards. Despite having been subject of significant research efforts over the past five decades, understanding of micro-mechanisms of fibre pull-out and dowel effect in resisting general stress fields in SFRC is limited. Self-compacting SFRC (SC-SFRC) has been developed by the CDSI, and a multi-level characterisation and modelling approach followed (Zeranka and Van Zijl 2015) for the envisaged development of systematic and reliable structural shear design guidelines for SFRC. A model for flexural design with SFRC and steel reinforced SFRC (R/SFRC) has recently been developed (Van Zijl and Mbewe 2013).

The development of lightweight foamed concrete (LWFC) started already in 1920 for applications such as thermal and acoustic insulation, soil stabilisation, lightweight backfill. Recently, significant improvement in compressive strength has been achieved, leading to research efforts towards structural application of LWFC and steel reinforced LWFC (R/LWFC). A research team of the CDSI has studied lightweight aerated concrete (LWAC) and LWFC since 2011 as a candidate construction material for residential infrastructure in South Africa, to exploit its light weight in seismic regions of South Africa, and simultaneously benefitting from its potential for thermal insulation and an acoustic barrier.

While existing and emerging contributions to several ACMs have been described above, the contributions with regard to SHCC and LWFC are selected for further elaboration in the following sections.

2.2 Strain-hardening cement-based composites (SHCC)

The energy dissipative and crack control characteristics of SHCC motivated local development of various classes of this material by the author's research team at Stellenbosch University. These characteristics hold potential for structural durability (Chapter 3) and application in seismic resistant infrastructure, for instance for retrofitting (see Section 4.3). SHCC was developed by the CDSI with local ingredient materials, except polyvinyl alcohol (PVA) fibres imported from Kuraray, Japan. Boshoff (2007) was the first to successfully manufacture highly ductile SHCC at Stellenbosch University, supported by research MScEng students (Gao Song and Van Zijl 2004, De Koker and Van Zijl 2004, Stander and Van Zijl 2006).

2.2.1 Mechanical response of SHCC

Typical tensile stress-strain responses of SHCCs developed at Stellenbosch University are shown in Figures 2.1 and 2.2, in comparison with a high strength HPFRCC. The SHCC mixes are given in Table 2.1, comprising of imported polyvinyl-alcohol (PVA) fibres, fine local silica sand, local CEM I 42.5 cement, South African fly-ash and ground granulated corex slagment (GGCS) from Saldanha in the Western Cape of South Africa, as well as chemical additives for appropriate rheology. The role of aggregate particle size and amount was reported by

Van Zijl (2005a), with a coarse sand version of SHCC developed by Paul and Van Zijl (2013). High-volume fly-ash and GGCS inclusion was reported by Van Zijl (2005b).

The strain-hardening response is associated with multiple crack formation, as shown in Figures 2.1 and 2.2. Typically, the cracks remain fine, in the range 40-100 μm for a significant range in tensile strain. This can be seen in the crack width distribution representation of Figure 2.3a, which was first proposed by the author and incorporated in the proposed test method for SHCC (Van Zijl et al. 2016) together with digital image correlation (DIC) from high resolution photos for contactless crack width measurement (Figure 2.3a). From this figure, an important observation is that although the average crack width remains in a tight range, a wider crack is present already at strain levels significantly below the ultimate strain. This is shown more clearly in Figure 2.3b, where the average crack width remains below 60 μm for tensile strain up to 3%, but the maximum crack width continuously increases with increased strain. The presence of these wider cracks was identified as a potential concern for durability by TC 208-HFC SC2. Durability is treated in Chapter 3.

Table 2.1: Typical SHCC mix proportions (normalised by cement mass, except fibres by volume fraction)

Ingredient	[1]SHCC1	[2]SHCC2
Cement (CEM I 42.5)	1	1
Fly Ash	1.2	0.6
Ground granular Corex slag (GGCS)	-	0.6
Water	0.7	1.0
Sand (φ_s< 0.21 mm)	1	1
Fibre: PVA RECS15:		
L_f = 12 mm, d_f = 0.04 mm	V_f = 2.0%	V_f = 2.5%

[1]Adendorff et al. (2009), [2]Gao Song and Van Zijl (2004)

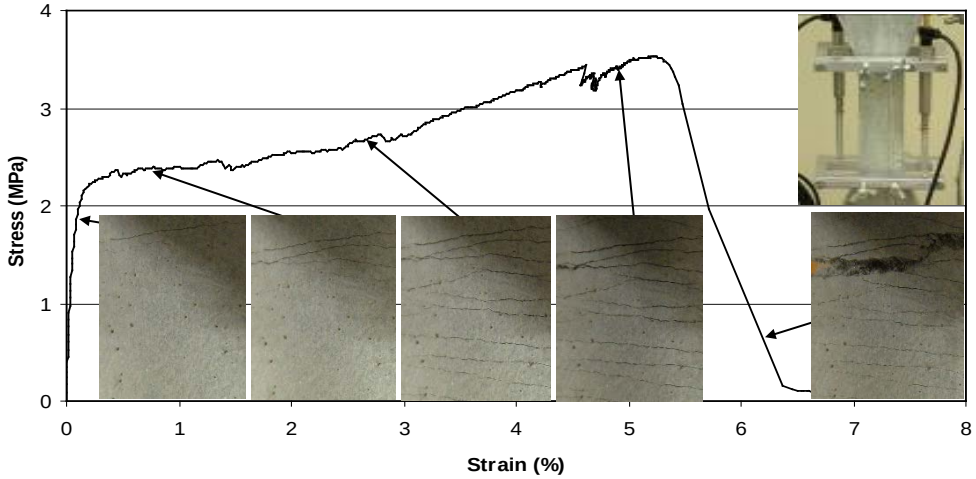

Figure 2.1: Multiple crack formation in SHCC under uniaxial tensile test

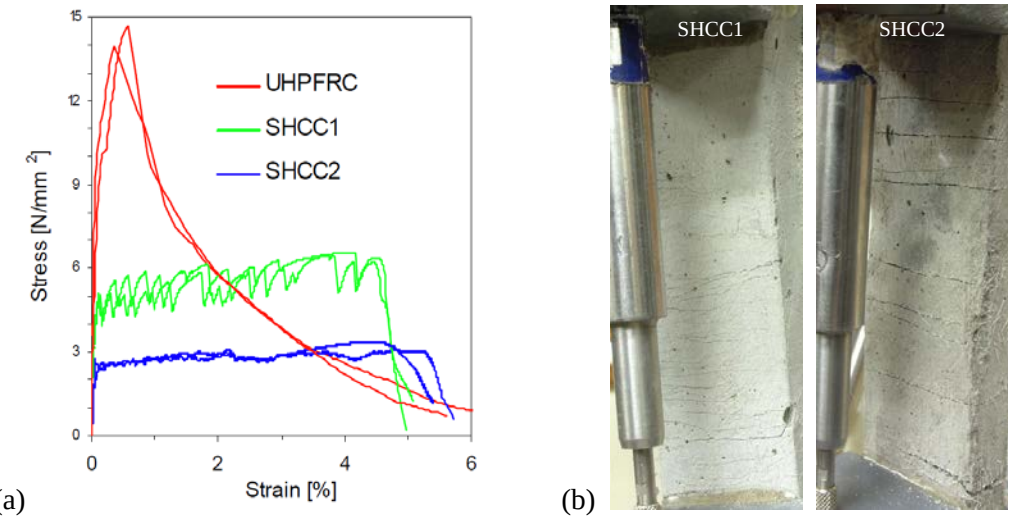

(a) (b)

Figure 2.2: (a) Typical tensile responses of classes of SHCC compared to UHPFRC and (b) the crack patterns.

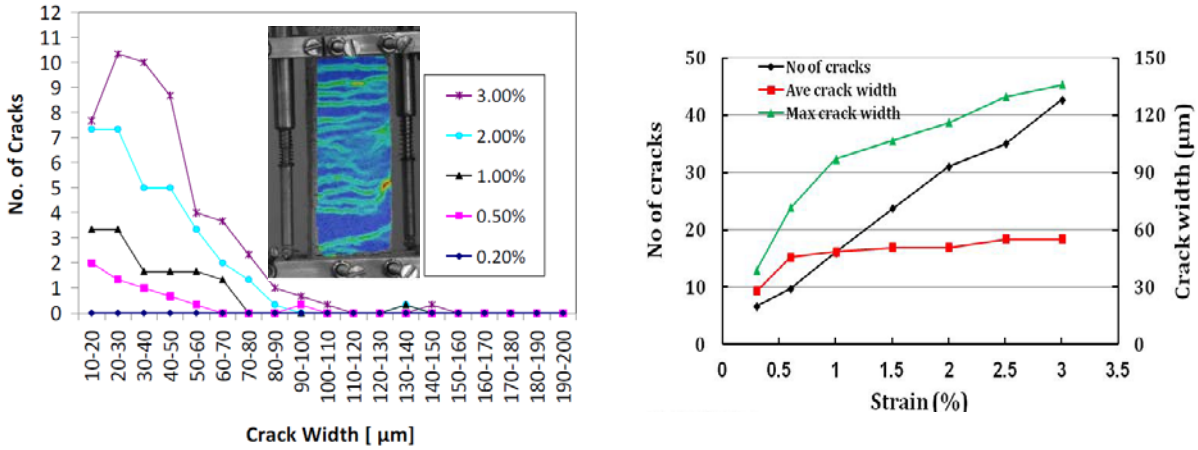

(a) (b)

Figure 2.3: (a) Crack width distribution in a particular SHCC at various average tensile strain levels (Adendorff *et al*. 2010). (b) Average and maximum crack width, as well as number of cracks developing with tensile strain in SHCC (Paul and Van Zijl 2013).

The multiple cracking and crack width control was shown to be retained in cyclic tensile testing (Adendorff et al. 2009, Van Zijl et al. 2016), in flexure (Van Zijl 2009b) and shear (Van Zijl and Shang 2007). An Iosipescu-shear test was designed for SHCC to study, as shown in Figure 2.4a. The notched shear specimen size is 320x140 mm and 20 mm thick. For detailed dimensions of the notches, the reader is referred to Van Zijl and Shang (2007). They were specially designed, supported by finite element analysis to optimise uniformity of the shear stress distribution in the notched central section, and to ensure that the maximum principal stress occurs in that section to enforce shear dominant failure. Diagonal deformation was recorded in the notched area throughout the tests by an linear variable differential transducer (LVDT) mounted at 45 degrees over a 25 mm gauge length as shown in Figure 2.4a. The average shear stress in the central pure shear cross-section is shown in Figure 2.4b as function of the diagonal strain, i.e. the deformation along the 45^{o} angle divided by the 25 mm original gauge length.

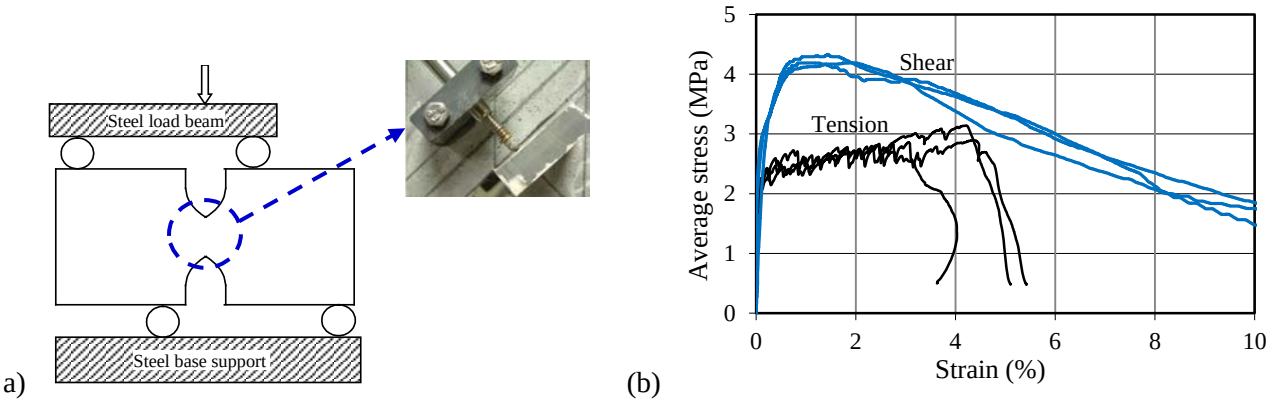

a) (b)

Figure 2.4: (a) Ioscipesco-type shear test setup for SHCC and (b) a comparison of the average shear stress versus diagonal strain with uniaxial tensile stress-strain (Van Zijl and Shang 2007).

Also shown in Figure 2.4b are the tensile stress-strain responses of dumbbell specimens of the same batch of SHCC, in order to show that the shear strength is significantly higher than the ultimate tensile strength. The mechanism of shear strengthening is illustrated in Figure 2.5. In the ascending linear-elastic stress-strain branch, equal diagonal tension (σ_1) and compression (σ_2) exists in the central section in pure shear. This holds until the first diagonal crack arises. Beyond the first cracking shear force, the tensile resistance can be maintained or gradually increased due to the strain-hardening characteristic of SHCC. In compression, a significant capacity remains. This means that the situation illustrated in Figure 2.5b can arise. A compressive stress σ'_2 which is increasingly higher than the principal tensile stress σ_1 acts in each material point, albeit in a rotated principal stress orientation (θ'). The orientation angle can be derived from the Mohr circle shown in Figure 2.5c. Multiple fine cracks aligned at an angle of roughly 60° with the horizontal were indeed found in the SHCC Iosipescu specimens – Figure 2.5d. In Section 4.3, the multiple shear cracking is shown to be beneficial in a retrofitting strategy of SHCC bonded overlays on masonry shear walls.

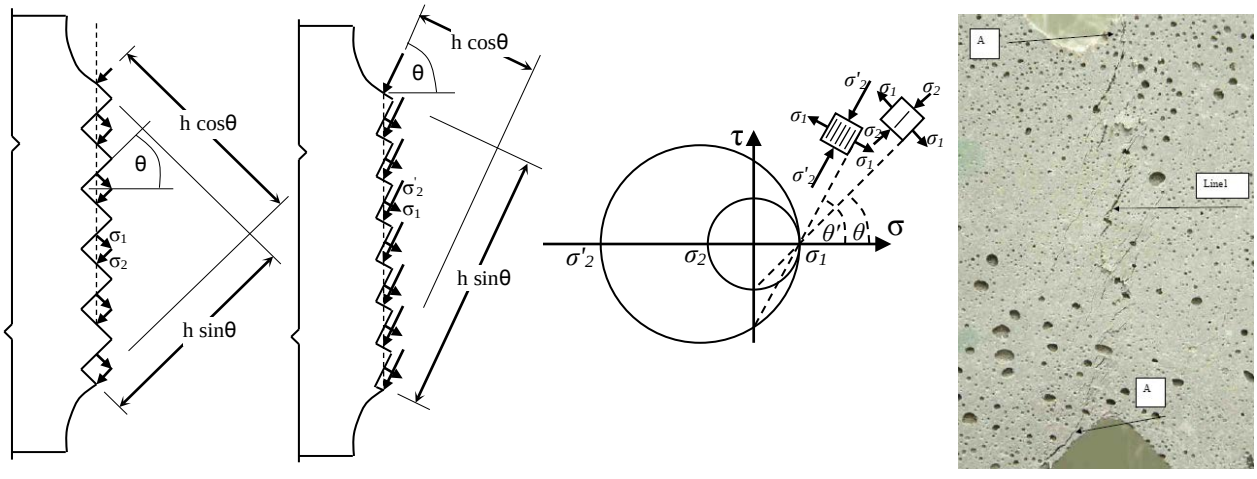

(a) (b) (c) (d)

Figure 2.5: (a) Diagonal tension-compression in the elastic shearing regime until first crack, (b) subsequent principal stress rotation beyond first cracking, (c) Mohr-Coulomb circles for these stress states demonstrating increased shear resistance and (d) verification of aligned multiple shear cracks (Van Zijl and Shang 2007).

2.2.2 Fabrication processes of SHCC

In addition to standard casting of SHCC mixes into steel, perspex or wooden moulds, extrusion and spraying applications have been developed. Whereas highly flowable mixes are preferred for good fibre dispersion in cast manufacturing (Paul and Van Zijl 2013), a zero-slump, dough-like consistency was successfully used by Visser and Van Zijl (2007) to extrude SHCC that retained its shape satisfactorily. For spraying application, the SHCC must be pumped from the position of mixing to the nozzle, which is typically a distance of 10 m or more. In the nozzle a high-pressure air jet accelerates the fresh material towards the substrate. For successful spraying, the fresh SHCC should adhere to the substrate or previously sprayed layers, and not run off. Figure 2.6 shows photos of suitably flowable and dough-like consistencies for casting and extrusion. In Figure 2.6c, too high run-off of freshly sprayed SHCC is shown.

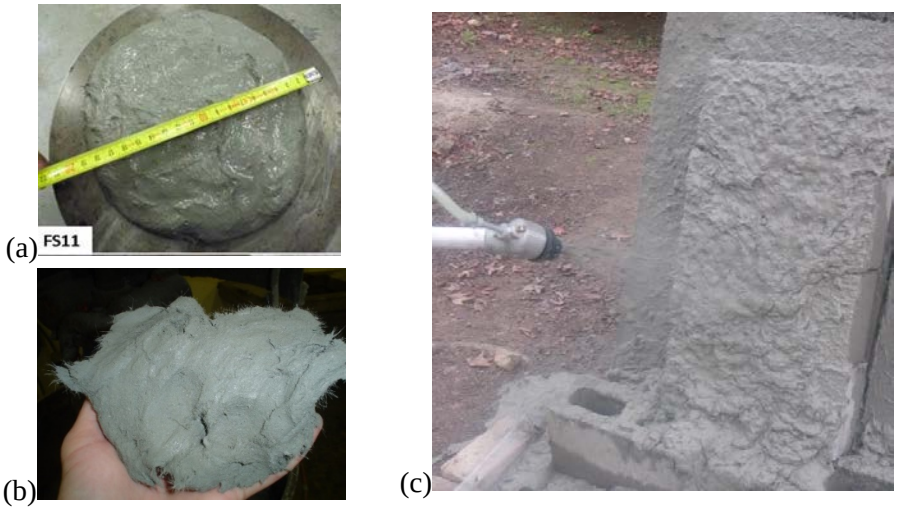

Figure 2.6: Fresh consistency, showing (a) preferred flowable, self-levelling SHCC for cast applications, (b) zero-slump, dough-like SHCC for extrusion and (c) excessive run-off for too flowable and non-adhesive SHCC for spraying application.

Mix adjustments for extrusion may be restricted to adjusted superplasticiser (SP) and viscosity modifying agent (VMA) content, but careful aggregate grading may be required to prevent segregation in the high-pressure extrusion process, where pressures of 3 to 4 MPa may build-up (Visser and Van Zijl 2007). Modification of the binder composition was made by De Beer and Van Zijl (2016), by inclusion of a small percentage (3-5%) of locally available calcium aluminate cement (CAC). The mix adjustments and manufacturing processes were shown to retain strain-hardening behaviour of the respective cast, extruded and sprayed elements by manufacturing and testing dumbbell specimens in uniaxial tension. Dumbbell specimens were carefully cut from extruded plates, while specimens for testing sprayed SHCC were prepared by direct spraying into dumbbell moulds. Both extruded and sprayed specimens showed reduced ductility of about 1.5% to 2% ultimate strain, compared with about 3% of cast specimens. Figure 2.7 shows the reduced ductility of extruded specimens compared with that of cast specimens. The reduced ductility in the range 1.5% to 2% is nevertheless considered to be sufficient for many applications (Van Zijl et al. 2016).

A different outcome was achieved in terms of tensile strength, with a 30% decreased tensile strength found for sprayed SHCC specimens compared with cast specimens with the same base mix. In contrast, extruded specimens showed significantly higher tensile strengths (Figure 2.7). While further optimisation of the sprayed

SHCC mixes and process may be required, the higher strength of extruded specimens was investigated and reported by Visser and Van Zijl (2007) to be due to entrained air forced from the SHCC in the high-pressure extrusion, and fibre alignment dominantly in the direction of in the extrusion action. As an indication of the reduced entrained air, the E-modulus of the extruded specimens was determined on cylindrical specimens cored from extruded beams, as well as from the tensile test results. The average E-modulus of extruded specimens was found to be more than double that of cast specimens, as can be seen from the summarised results in Tables 2.2 and 2.3.

Table 2.2: E-moduli of SHCC specimens tested in uniaxial tension on dumbbell specimens (Visser 2007)

Specimen [#]	Cast specimens Cast [GPa]	Extruded specimens	
		Cut from plate [GPa]	Cut from beam [GPa]
1	9.53	24.20	23.10
2	9.71	24.37	24.95
3	9.94	24.63	25.62
4	10.02	26.37	25.94
5	10.32	26.86	25.97
6	11.39		
7	12.08		
Average	10.43	25.59	25.12
StdDev	0.95	1.23	1.20
CoV	9.09%	4.88%	4.77%

Table 2.3: Compressive E-moduli of 50 mm diameter and 100 mm long cylindrical specimens prepared by casting and cut from extruded beams (Visser 2007)

Specimen [#]	Cast specimens [GPa]	Extruded specimens [GPa]
1	9.24	20.71
2	9.55	21.32
3	10.71	22.47
4	10.84	22.59
5	11.84	23.82
Average	10.44	22.18
StdDev	1.05	1.21
CoV	10.08%	5.45%

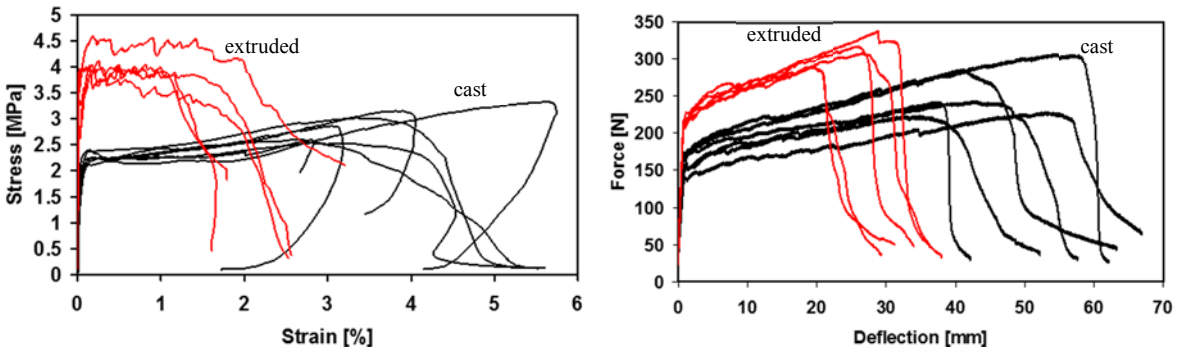

Figure 2.7: Tensile stress-strain and flexural responses of extruded and cast SHCC specimens (Visser and Van Zijl (2007)

Considering the SHCC volume fraction comprised by aggregate (V_a) and paste (V_p) with respective elastic moduli E_a and E_p, the elastic modulus of the matrix (E_m) can be expressed as (Hashin 1962):

$$E_m = \frac{(1+V_a)E_a + V_p E_p}{V_p E_a + (1+V_a)E_p} E_p \tag{2.1}$$

An alternative formulation is based on a representative matrix volume with a central concentration of solid aggregate surrounded by hardened cement paste (Helmuth and Turk 1966):

$$\frac{1}{E_m} = \frac{\left(1-\sqrt{V_a}\right)}{E_p} + \frac{\sqrt{V_a}}{E_a\sqrt{V_a} + E_p\left(1-\sqrt{V_a}\right)} \tag{2.2}$$

Neither Equation (2.1) nor (2.2) account for the air entrainment, but a well-known cubic relation between porosity (ρ) and E-modulus of cement paste is expressed as follows:

$$E_p = E_p^*(1-p)^3 \tag{2.3}$$

where E_p^* is the paste modulus for zero porosity (p=0). Equation (2.3) expresses the significant role of entrained air, and was shown by Visser and Van Zijl (2007) to account for the significant difference in E-moduli of extruded and cast SHCC specimens.

In a step towards production of one-way spanning structural elements, steel bar reinforced SHCC (R/SHCC) beams were extruded by Visser. Figure 2.8 shows the provision for two steel bars to be inserted into the extruder chamber. During extrusion, the extrudate drew the bars into the SHCC by friction. In Figure 2.9, flexural test results of extruded SHCC and R/SHCC are compared, also showing the flexural crack pattern typically found for SHCC beams. In comparison, a shear-dominant failure mode is seen in the figure for R/SHCC, which indicates sufficient bond of the steel reinforcing bars and their contribution to flexural resistance. Thereby, the shear becomes the weaker mode of failure, marked clearly by diagonal shear cracks.

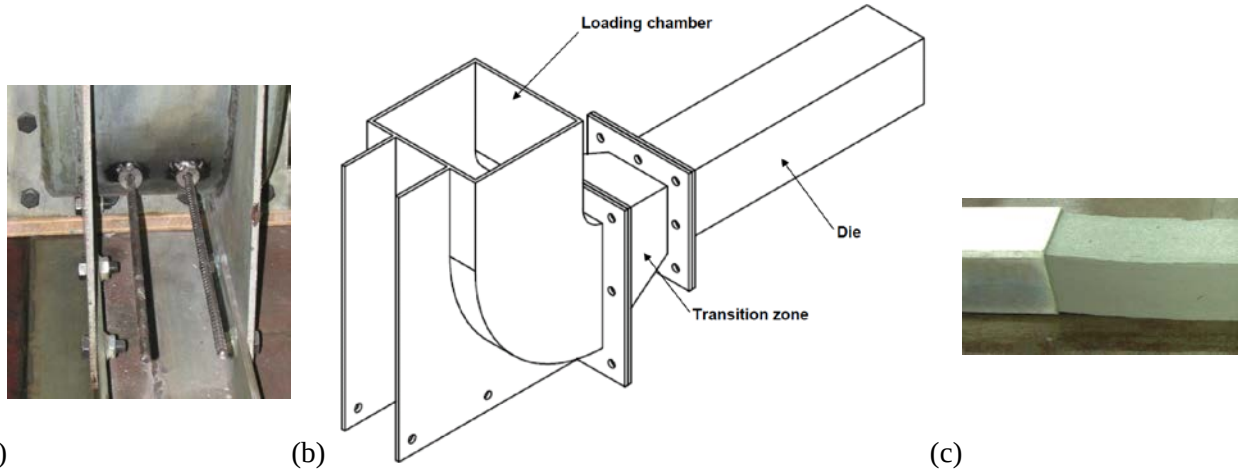

(a) (b) (c)

Figure 2.8: (a) Provision for steel bars to be placed in the back of (b) the piston extrusion chamber, where it is drawn into (c) the extrudate (Visser and Van Zijl 2007).

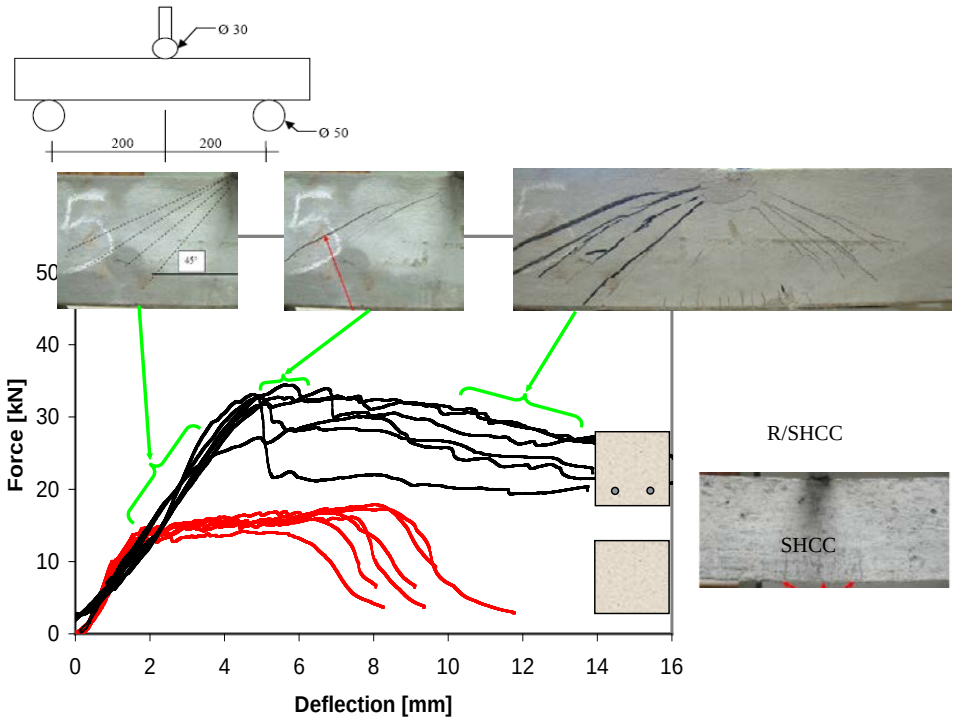

Figure 2.9: Load-deflection responses of extruded SHCC and R/SHCC beams of dimension 100x100 mm cross-section, 500 mm long and tested with a 400 mm span in three point bending. 2Y8 bars were used as reinforcement, with a 20 mm cover (Visser 2007).

2.2.3 SHCC creep and rate dependence

An important contribution by the CDSI research to understanding of SHCC long term behaviour, lies in characterisation of its response under sustained load, as well as under various loading rates.

2.2.3.1 Loading rate dependence of SHCC

The earliest contributions (Boshoff and Van Zijl 2005, 2007) reported rate-dependence of SHCC with regard to first cracking, ultimate resistance, ultimate strain and deflection in uniaxial tension as well as flexure over four orders of quasi-static loading rate – Figure 2.10. Relatively small loss of ultimate strain with increased loading rate was found, compared with Yang and Li (2006), as observed by Van Zijl (2010b) – see Figure 2.11. To investigate the reason for these differences, single fibre pull-out tests were performed. See Figure 2.11 for typical single fibre pull-out rate dependence as performed by Boshoff et al. (2009b). Significantly increased resistance is apparent at higher pull-out rates ($\dot{\delta}$), leading to dominant fibre breakage at high rates indicated by the vertical drop in pull-out force P after peak resistance. The rate-dependent single fibre response suggests that rate-increased macroscopic resistance should occur, and with increasing brittleness. Nevertheless, the fibre rupture in the tests performed by Boshoff et al. (2009b) occurred at significantly higher pull-out displacement as seen in Figure 2.12. It is postulated that different matrix-fibre interfacial conditions cause fibre rupture at lower pull-out displacements, leading to embrittlement of such composites at higher tensile loading rates.

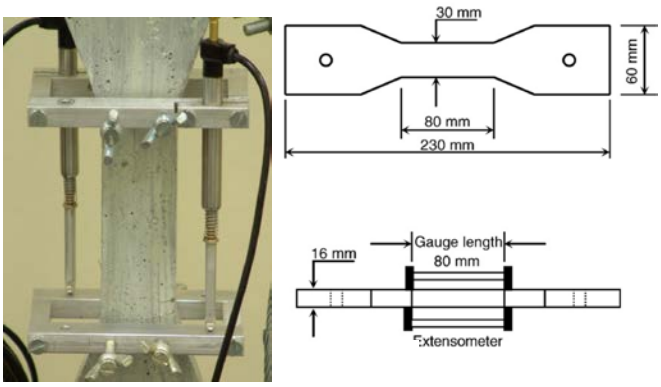

(a) Tension: test specimen and setup

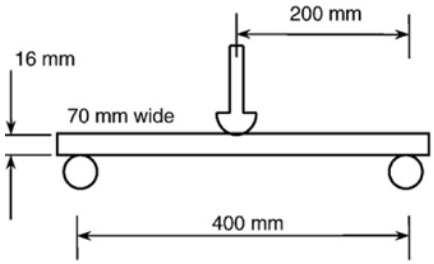

(e) Flexure: test specimen and setup

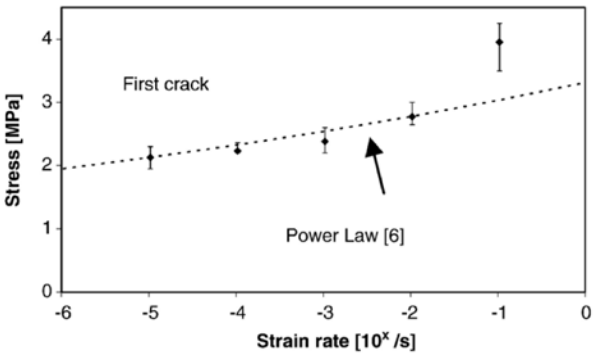

(b) Tension: first cracking stress

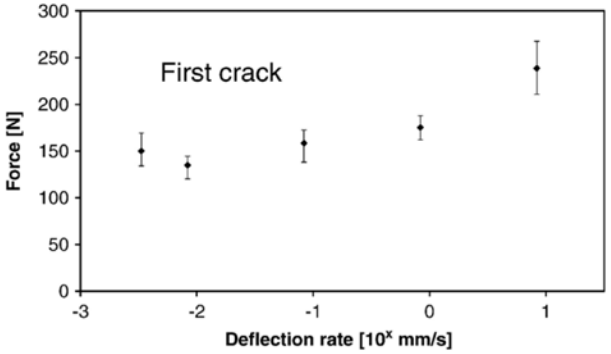

(f) Flexure: first cracking force

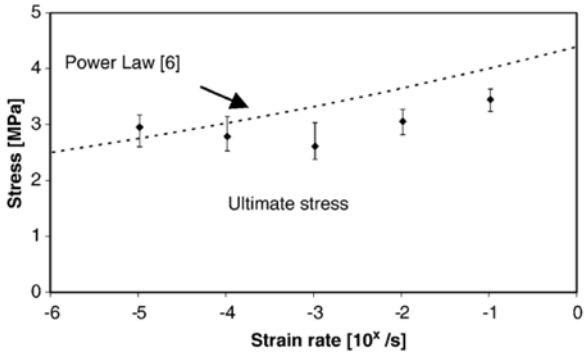

(c) Tension: ultimate stress

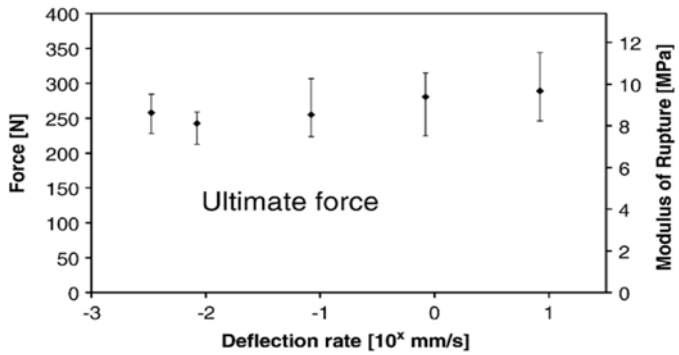

(g) Flexure: ultimate force and MOR

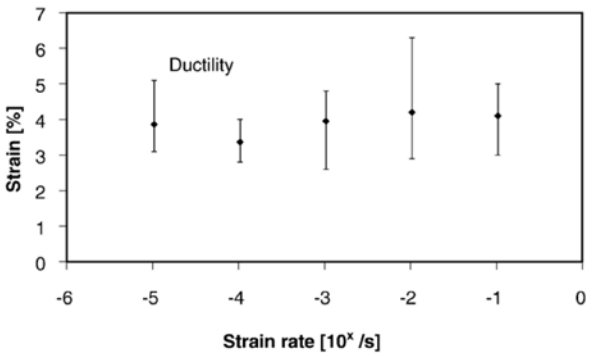

(d) Tension: ultimate strain

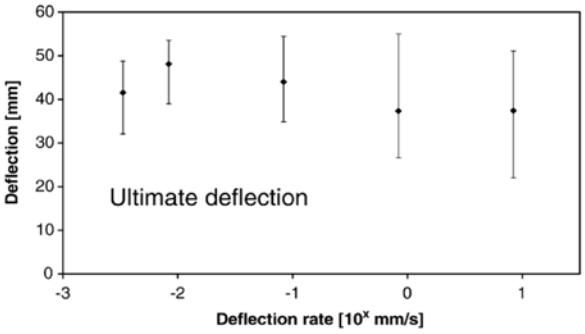

(h) Flexure: Ultimate deflection

Figure 2.10: SHCC rate-dependence in uniaxial tension (left) and flexure (right) (Boshoff and Van Zijl (2007).

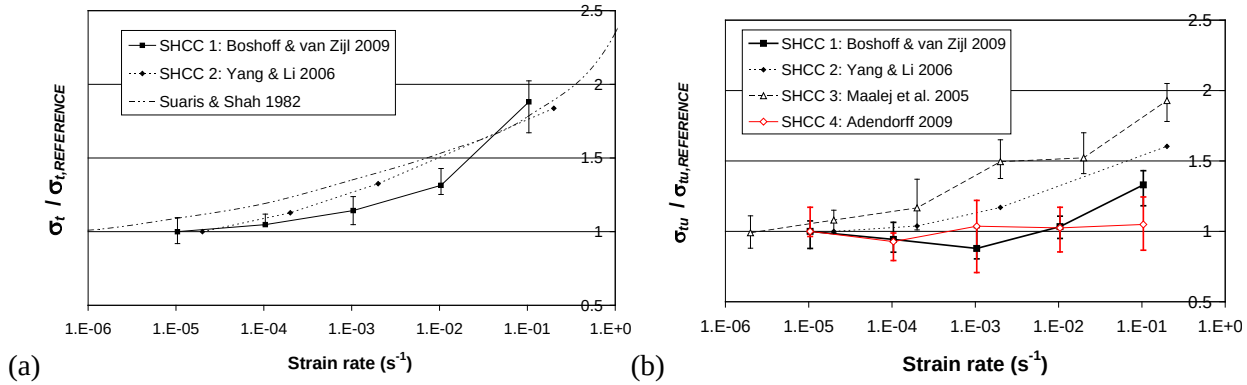

Figure 2.11: (a) First cracking and (b) ultimate tensile strength (Van Zijl 2010b).

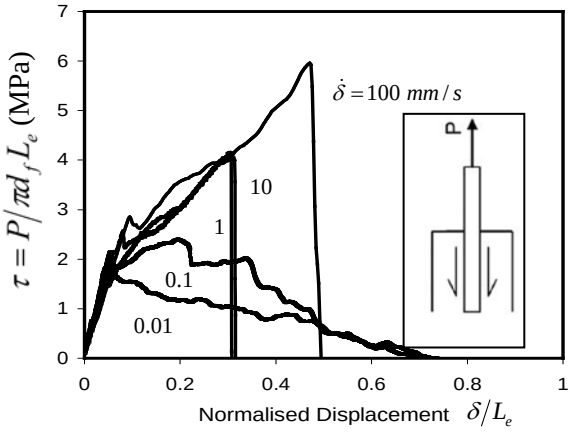

Figure 2.12: Rate-dependent single fibre pull-out responses (Boshoff et al. 2009b), showing typical responses as analysed by Van Zijl (2010b).

2.2.3.2 SHCC tensile creep response

The results of SHCC creep under sustained tensile load reported by Boshoff and Van Zijl (2009a) are summarised in Figure 2.13. SHCC dumbbell specimens were pre-cracked by tensile loading to 1% strain, unloading and subsequent reloading to the required sustained stress level, as shown in Figure 2.13a. The resulting creep stress-strain responses indicated with symbols in Figure 2.13b show the phenomena of creep limit and creep fracture, first to be reported by the author's research group for SHCC. For cracked specimens loaded to sustained stress levels below 70% of the average ultimate strength, strains recorded over the time span of one year remained relatively low, and appeared to approach the so-called creep limit. For 70 % and 80% sustained tensile stress levels, significant tensile strain ensued over the corresponding period. While none of the specimens finally fractured completely, those loaded to 80% are expected to have fractured within a finite period of time, should the test have been continued. To understand and characterise fibre pull-out time dependence, sustained load single fibre pull-out tests were conducted and reported by Boshoff et al. (2009a). In these tests, a tensile load that causes an average shear stress of 1.2 MPa in the embedded fibre-matrix interface, was sustained on each fibre. All fibres eventually completely pull-out of the matrix under this sustained load. Fibres that were fully de-bonded by prior tensile loading, after which the sustained bond stress was applied and maintained, pulled out in just under 20 hours on average, while fully bonded fibres remained in-tact for about three times this duration, pulling out after about 60 hours on average. This confirmed fibre-matrix interfacial bond-slip is an important mechanism of tensile creep in cracked SHCC. An important time-dependent effect is widening of cracks in SHCC under sustained tensile load, as observed by Boshoff et al. (2009a).

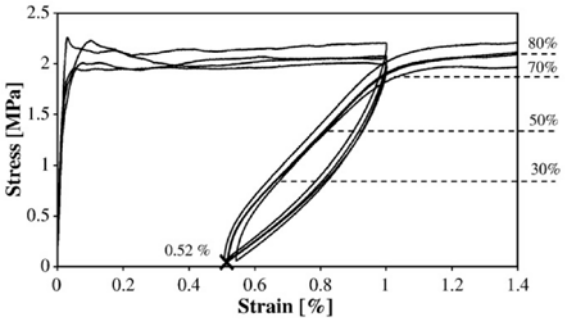

(a)

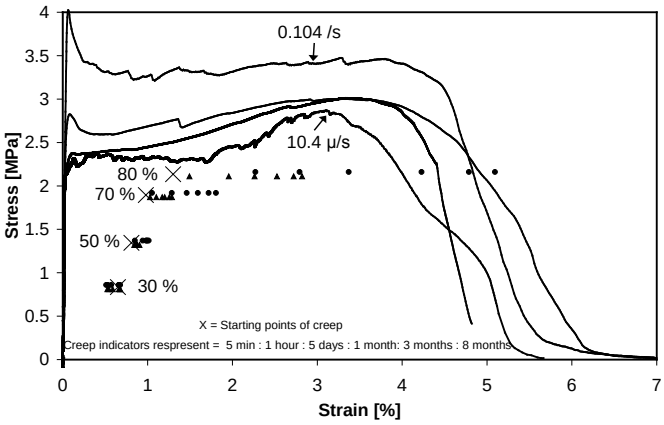

(b)

(c)

Figure 2.13: (a) Pre-cracking and subsequent (b) sustained tensile load testing in (c) specially designed and manufactured creep frames at RH 65±5%, T 23±2 ^{o}C (Boshoff and Van Zijl 2009a).

2.2.4 Constitutive model for SHCC

Design models are required for sound design and structural application of SHCC as construction material. Such models do not yet exist and the pool of experimental data is relatively limited, certainly in comparison with traditional construction materials like RC and structural steel. Computational models, verified and validated against physical experiments, may contribute significantly towards understanding and derivation of design guidelines, within the limits of applicability of the models and reasonable extrapolation to other boundary value problems by analysts with expertise in computational and structural mechanics. Hereby, the computational model may assist in deriving rational design guidelines.

A macroscopic constitutive model for SHCC was developed, implemented, verified and validated by Van Zijl (2009). The computational model captures main mechanisms of behaviour with reasonable accuracy, despite considering a homogeneous continuum of the actual heterogeneous composite and discontinuous physical crack formation. The model is based in computational plasticity, and uses a multi-surface plasticity limit function shown by the solid lines in Figure 2.14. It comprises a maximum principal stress criterion (Rankine-type) in tension, and an algebraic minimum principal stress criterion in compression. Once the respective limit function is activated, strain-hardening and subsequent softening ensues in tension, as well as in compression. Figure 2.15 illustrates the linear strain-hardening and subsequent exponential softening. Provision is made for different values for first cracking stress (f_{ty}), ultimate tensile stress (f_{tuy}), strain at ultimate stress (κ_{tuy}), and fracture energy (G_{ty}) in the *y*-direction, than those for the *x*-direction (f_{tx}, f_{tux}, κ_{tux} G_{tx}). This is to account for anisotropy. For instance, in extruded products, dominant fibre orientation in the extrusion direction has been shown to cause

flexural strength in the extrusion direction of roughly 2.5 times that in the orthogonal direction (Visser and Van Zijl 2007; see Section 2.2.2). The same is valid for compression.

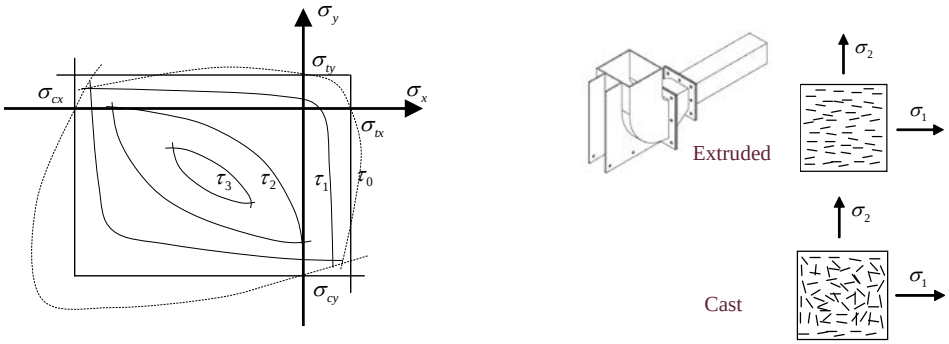

Figure 2.14: Multi-surface limit function for biaxial behaviour of SHCC.

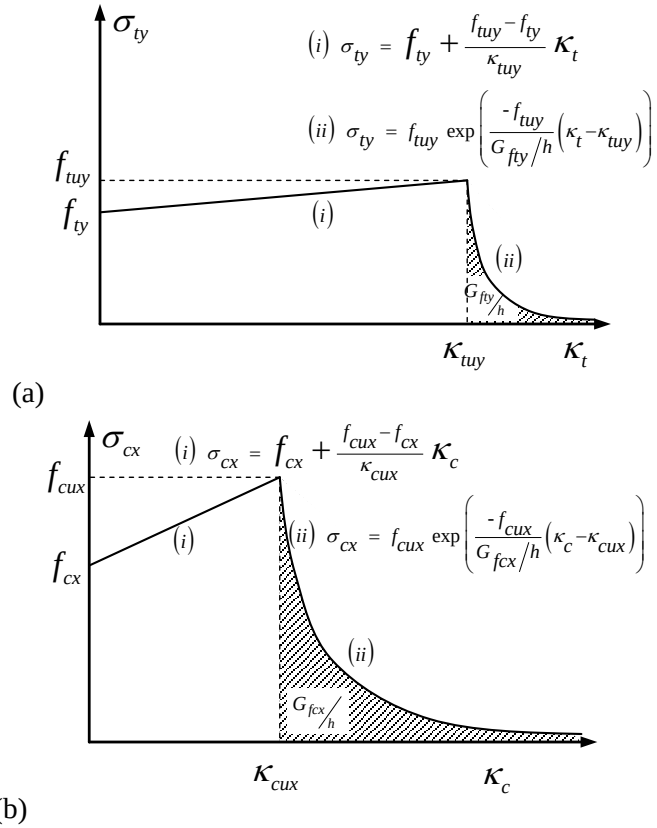

Figure 2.15: Inelastic linear hardening, followed by exponential softening in (a) tension and (b) compression (Van Zijl 2009c). Note that the parameters for tension in the y-direction are shown, and those for the x-direction in compression.

Note that a plane stress state is considered and shown in Figure 2.14 in terms of the two orthogonal normal stresses and a single shear plane. This is appropriate for the thin-walled SHCC specimens. Note further that the dashed lines in Figure 2.14 illustrate biaxial strengthening through confinement, of which evidence was reported by Molapo (2010) and Swanepoel (2011) who performed physical biaxial tests – see Figure 2.16. The Rankine-

type limit functions are considered to be conservative. The use of linear hardening and exponential softening also for compression is for simplicity, but improved resemblance with the measured compressive responses can easily be obtained by defining alternative hardening-softening curves, for instance parabolic hardening and exponential softening.

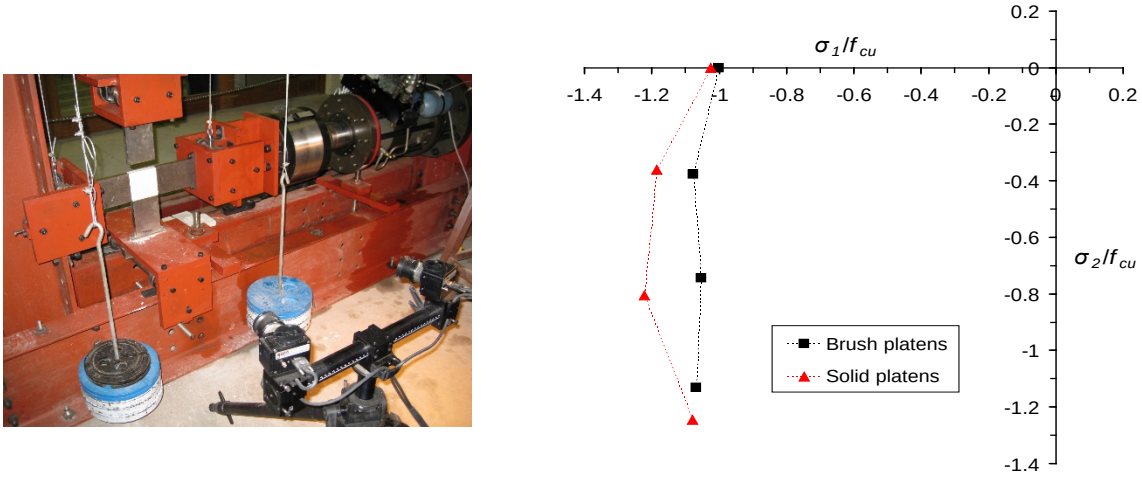

Figure 2.16: Biaxial test results by Molapo (2010) and Swanepoel (2011) for cast SHCC.

In the plane stress setting with stress and strain vectors

$$\boldsymbol{\sigma}^T = \lfloor \sigma_x \ \sigma_y \ \tau \rfloor, \ \boldsymbol{\varepsilon}^T = \lfloor \varepsilon_x \ \varepsilon_y \ \gamma \rfloor \tag{2.4}$$

the constitutive law can be expressed as follows

$$\dot{\boldsymbol{\sigma}} = \boldsymbol{D}^{ve}\dot{\boldsymbol{\varepsilon}}^{ve} + \boldsymbol{\Sigma} = \boldsymbol{D}^{ve}\left(\dot{\boldsymbol{\varepsilon}} - \dot{\boldsymbol{\varepsilon}}^{p} - \dot{\boldsymbol{\varepsilon}}^{0}\right) + \boldsymbol{\Sigma} \tag{2.5}$$

where $\boldsymbol{D}^{ve}$ is an equivalent time-dependent stiffness modulus, $\dot{\boldsymbol{\varepsilon}}^{ve}$, $\dot{\boldsymbol{\varepsilon}}^{p}$ and $\dot{\boldsymbol{\varepsilon}}^{0}$ are the visco-elastic, plastic and initial strain vector respectively and $\boldsymbol{\Sigma}$ is a viscous stress vector accounting for the history. Full detail of the computational treatment is given by Van Zijl *et al.* (2001). There, it is shown that the visco-elastic stiffness is computed from the spring stiffnesses (E_i) and dashpot viscosities (η_i) of the elements in the Maxwell chain shown in Figure 2.17. The stress history term accumulates the stresses in each chain element at the end of the previous time step. Linear time integration is used to integrate Equation (2.5). To incorporate the various sources of time dependence, the limit functions and their evolutions according to the hardening-softening shown in Figure 2.15 are enhanced by consideration of bulk visco-elasticity through the Maxwell-chain, as well as cracking viscosity (η_{cr}), as schematised in Figure 2.17. Note that the latter is activated only in tension.

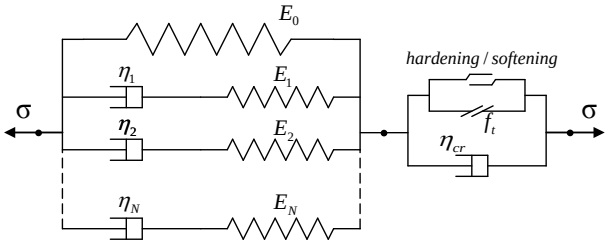

Figure 2.17: Schematic representation of the constitutive model.

The limit stresses are treated in multi-surface plasticity fashion, whereby the plastic strain increment is expressed as follows:

$$\Delta\boldsymbol{\varepsilon}^p = \Delta\lambda \frac{\partial f}{\partial \boldsymbol{\sigma}} \tag{2.6}$$

with λ the amount of plastic flow/crack strain and f the flow function. For tension, the anisotropic Rankine yield (limit) function is chosen, represented by the solid line in Figure 2.14, which is a maximum principal stress failure criterion, formulated as

$$f_t = \frac{(\sigma_x - \sigma_{tx}) + (\sigma_y - \sigma_{ty})}{2} + \sqrt{\left(\frac{(\sigma_x - \sigma_{tx}) + (\sigma_y - \sigma_{ty})}{2}\right)^2 + \alpha_t \tau^2} \tag{2.7}$$

The current admissible stresses in the material *x*, *y* directions are denoted by σ_{tx} and σ_{ty} respectively. Simple expressions for the tensile resistance are given in Figure 2.15. As stated in the previous section, separate expressions are used in the orthogonal directions, with separate sets of model parameters. The hardening-softening is governed by equivalent tensile strain κ_t, with an appropriate measure for SHCC considered to be the maximum principal plastic strain given by

$$\dot{\kappa}_t = \dot{\varepsilon}_1^p = \frac{\dot{\varepsilon}_x^p + \dot{\varepsilon}_y^p}{2} + \sqrt{\left(\frac{\dot{\varepsilon}_x^p - \dot{\varepsilon}_y^p}{2}\right)^2 + \left(\frac{\dot{\gamma}}{2}\right)^2} \tag{2.8}$$

The strain increment can be shown to be directly related to the plastic flow increment $\Delta\kappa_t = \Delta\lambda_t$. The parameter α_t controls the shear contribution to tensile failure. In compression, the limit function is

$$f_c = -\frac{(\sigma_x - \sigma_{cx}) + (\sigma_y - \sigma_{cy})}{2} + \sqrt{\left(\frac{(\sigma_x - \sigma_{cx}) + (\sigma_y - \sigma_{cy})}{2}\right)^2 + \alpha_c \tau^2} \tag{2.9}$$

and the equivalent compressive strain is

$$\dot{\kappa}_c = -\dot{\varepsilon}_2^p = -\frac{\dot{\varepsilon}_x^p + \dot{\varepsilon}_y^p}{2} + \sqrt{\left(\frac{\dot{\varepsilon}_x^p - \dot{\varepsilon}_y^p}{2}\right)^2 + \left(\frac{\dot{\gamma}}{2}\right)^2} \tag{2.10}$$

As for tension, it can be shown that $\Delta\kappa_c = \Delta\lambda_c$. The intersection between the two limit surfaces is treated in a consistent way, as proposed by Koiter (1953)

$$\Delta\boldsymbol{\varepsilon}^p = \Delta\lambda_t \frac{\partial f_t}{\partial \boldsymbol{\sigma}} + \Delta\lambda_c \frac{\partial f_c}{\partial \boldsymbol{\sigma}} \tag{2.11}$$

In tension, a cracking rate-dependence is introduced following Wu & Bažant (1993) and Van Zijl *et al.* (2001) as follows:

$$\Delta w = \Delta w_r \sinh\left[\frac{\sigma - \sigma_t(w)}{c_1\left[\sigma_t(w) + c_2 f_t\right]}\right] \tag{2.12}$$

where $\dot{w}_r$ is a constant, reference crack opening rate. The crack width w, which is assumed to be spread uniformly across the fracture process zone of width l_b, can be related to the equivalent strain as follows:

$$\kappa_t = w/l_b \tag{2.13}$$

With Equations (2.12, 2.13) the tensile strength equations (Figure 2.15) can be rewritten as

$$\sigma_{ti} = \left(f_{ti} + \frac{f_{tui} - f_{ti}}{\kappa_{tui}}\kappa_t\right)\left[1 + c_1 \sinh^{-1}\left(\frac{\dot{\kappa}_t}{\dot{\kappa}_r}\right)\right] + c_1 c_2 f_{tui} \sinh^{-1}\left(\frac{\dot{\kappa}_t}{\dot{\kappa}_r}\right) \qquad \forall \kappa_t \le \kappa_{tui} \tag{2.14}$$

$$\sigma_{ti} = f_{tui} \exp\left(\frac{-f_{tui}}{G_{fti}/l_b}(\kappa_t - \kappa_{tui})\right)\left[1 + c_1 \sinh^{-1}\left(\frac{\dot{\kappa}_t}{\dot{\kappa}_r}\right)\right] + c_1 c_2 f_{tui} \sinh^{-1}\left(\frac{\dot{\kappa}_t}{\dot{\kappa}_r}\right) \qquad \forall \kappa_t > \kappa_{tui} \tag{2.15}$$

where the index i refers to the material axes x or y. The coefficient c_2 is a small offset value to prevent singularity of Equation (2.12). The reference strain rate $\dot{\kappa}_r$ is directly related to $\dot{w}_r$ cf. Equation (2.13). It should be a sufficiently low cracking rate at which the cracking strengths are rate-independent. In the current model, the rate terms represent all physical processes causing rate dependence, here both cracking viscosity and fibre pull-out rate-dependence. The constitutive model was implemented as a user material in DIANA (2008).

The model has been shown to be able to accurately simulate experimental tests of SHCC, both quasi-static and in terms of rate and time dependence (Van Zijl 2009c). As an example, the flexural tests of SHCC and R/SHCC beams of Section 2.2.2, and shown in Figure 2.9, were analysed based on the tensile responses of the dumbbell specimens tested by Visser and Van Zijl (2007). Full characterisation of the model parameters is elaborated in Van Zijl (2009c), and a summary given in Table 2.4. The computed responses are shown in Figure 2.18.

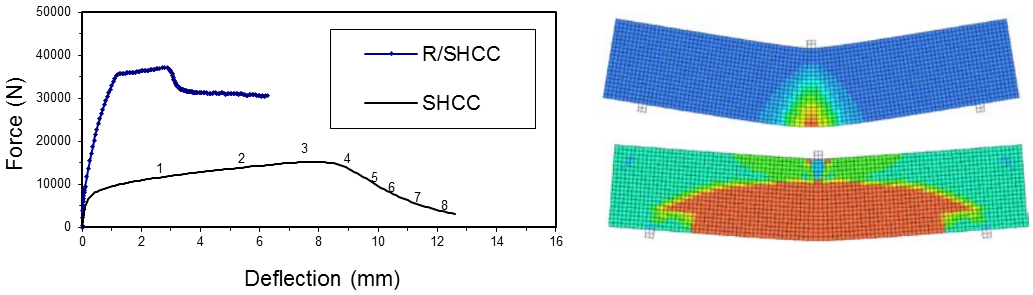

Figure 2.18: Simulation of the SHCC and R/SHCC beams of Visser and Van Zijl (2007), showing the FE meshes and inelastic strain contours at ultimate flexural resistance.

Table 2.4. Model parameters for R/SHCC beams by Visser (2007).

Tension		Compression	
$f_{tx} = f_{ty}$ (MPa)	1.8	$f_{cx} = f_{cy}$ (MPa)	20
$f_{tux} = f_{tuy}$ (MPa)	2.0	$f_{cux} = f_{cuy}$ (MPa)	30
$\kappa_{tux} = \kappa_{tuy}$ (-)	0.04	$\kappa_{cux} = \kappa_{cuy}$ (-)	0.02
$g_{ftux} = g_{ftuy}$ (N/mm^2)	0.01	$g_{ftux} = g_{ftuy}$ (N/mm^2)	5
Creep			
E_0 (MPa)	360	v	0.3
E_1 (MPa)	3380	$\zeta_1 = \eta_1/E_1$ (s)	10^0
E_2 (MPa)	3380	$\zeta_2 = \eta_2/E_2$ (s)	10^1
E_3 (MPa)	3380	$\zeta_3 = \eta_3/E_3$ (s)	10^2
E_4 (MPa)	375	$\zeta_4 = \eta_4/E_4$ (s)	10^3
E_5 (MPa)	375	$\zeta_5 = \eta_5/E_5$ (s)	10^4
E_6 (MPa)	375	$\zeta_6 = \eta_6/E_6$ (s)	10^5
E_7 (MPa)	375	$\zeta_7 = \eta_7/E_7$ (s)	10^6
Rate:			
m_x (N.s.mm^{-2})	1200	m_y (N.s.mm^{-2})	1200
Steel: Elastic-perfect plastic			
E (GPa)	200	*Yield stress* (MPa)	450
v	0.3	*Steel area* (mm^2)	101

In Van Zijl (2009a, 2009c) the model is shown to capture the phenomena of creep fracture and creep limit, and to simulate the quasi-static Iosipescu shear tests of Section 2.2.1 (Figure 2.4b) with reasonable accuracy.

2.3 Lightweight foamed concrete

The self-weight of concrete may dominate the loads to be resisted in infrastructure. Reduction in weight holds significant benefits in high-rise buildings, and in seismic regions. Over the past century, lightweight concrete has been developed typically by replacement of standard coarse aggregate with lightweight aggregate, entrainment of air, or foam bubbles. Lightweight aggregate concrete is well researched and standardised (SANS10100, BS EN 1992-1-1:2004) for structural use. LWAC and LWFC have received considerable attention, but have not been included in design standards for structural use. The concept of foam concrete has been developed already in the early 20th century, and it has been used successfully as fire protection, acoustic barriers, thermal insulation and void filling material. A comprehensive review of LWFC is given by Ramamurthy et al. (2009). Autoclaved aerated concrete (AAC), a type of LWAC manufactured under high, controlled temperature and pressure to reduce shrinkage and improve strength, was developed in the 1920s. However, only relatively recently research programs have been launched to investigate the structural use of non-heat treated LWFC (Jones and McCarthy 2005) and LWAC (van Rooyen et al. 2013). In particular, it has been reported that high volume fly-ash inclusion is beneficial in significantly increasing compressive strength of LWFC at higher age (1 year) compared with mixes without fly ash (Kearsley and Wainwright 2002).

A team of CDSI researchers under supervision of the author is studying LWFC as a potential construction material for medium-rise residential buildings in seismic regions of South Africa. Successes to date include the ability to design LWFC mixes to acceptably accurate densities in the range 1200-1600 kg/m^3 with compressive strengths in the range suitable for structural application for densities 1400 kg/m^3 and above, with attention for mechanical properties, durability and assessment strategies.

2.3.1 Mechanical properties of LWFC

Table 2.5 summarises the mechanical properties of LWFC developed by de Villiers et al. (2016a), also showing properties for a typical class of normal weight concrete (NWC). For 1400 and 1600 kg/m^3, average cube compressive strengths of 19 MPa and 32 MPa were obtained, with coefficients of variation (CoV) of 0.053 and 0.105 respectively, which are in the range for structural application. However, the E-modulus (E_c) and fracture energy (G_f) are disproportionately low, as illustrated graphically in Figure 2.19. For details of the carefully designed and executed wedge-splitting tests for fracture energy, as well as pull-out (PO) and beam-end (BE) bond tests of reinforcing bars embedded in LWFC (R/LWFC), the reader is referred to de Villiers (2015) and de Villiers et al. (2016). Currently, inclusion of low quantities of polymeric fibres in LWFC is studied by the research team, due to its reported improvement in strength and stiffness (Jones and McCarthy 2005). It is postulated to significantly increase the fracture energy, whereby the bond strength in R/LWFC is believed to be increased as well.

Table 2.5: LWFC mix compositions, also showing a typical NWC (de Villiers et al. 2016a).

Target casting density [kg/m^3]	12F	14F	16F	NWC
	1200	1400	1600	2366
CEM I-52.5	447.2	526.7	606.2	336.2
Fly-ash, Class S	447.2	526.7	606.2	0
Coarse aggregate	0	0	0	1000
Sand	0	0	0	835
Water	277.3	326.6	375.9	195
Foam [Litre]	377.0	266.3	155.5	0
f_{cu} [MPa] (cube)	10.41 (0.057)	19.1 (0.053)	32.26 (0.105)	38.66 (0.038)
E_c [GPa]	6.46 (0.030)	8.75 (0.001)	12.15 (0.022)	31.48 (0.114)
f_t [MPa]	1.31 (0.061)	2.14 (0.062)	3.63 (0.092)	4.15 (0.017)
G_f [N/m]	4.67	5.72	7.32	123.55
l_c [mm]	15.42	11.06	6.75	938

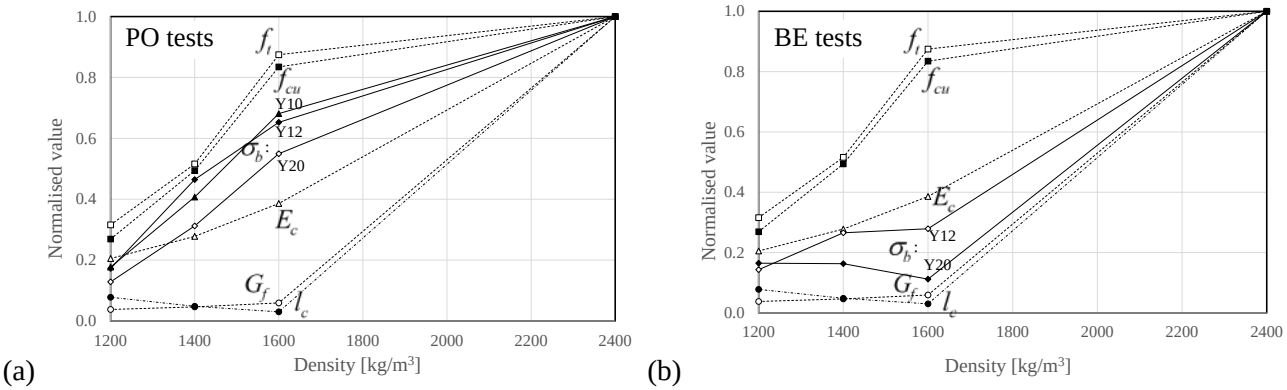

(a) (b)

Figure 2.19: Normalised mechanical properties and bond stress obtained from (a) PO and (b) BE tests.

2.3.2 Durability properties of LWFC

Studies on carbonation and carbonation-induced corrosion of steel in R/LWFC, as well as chloride-induced corrosion in R/LWFC have just been started by research students in the CDSI. The influence of coatings, pore blockers and pore lining to reduce permeability of LWFC to deleterious substances is studied, as means of preventing or slowing down ingress of deleterious gases and fluids into LWFC. An appropriate level of durability has to be ensured for the structural use of R/LWFC for sustainable housing.

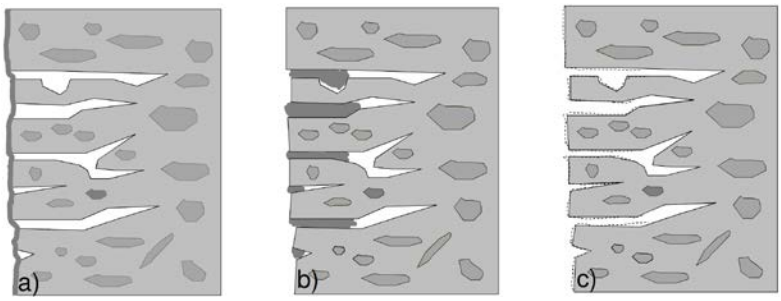

Figure 2.20: Categories of surface treatment agents; (a) coatings, (b) pore blockers and (c) pore liners (Medeiros and Helene 2009).

2.3.3 Towards assessment of R/LWFC structural systems

Unreinforced load bearing masonry (ULM) and masonry infilled reinforced concrete (RC) framed structures are favoured construction materials and systems in low to medium-rise buildings for housing. In the Western Cape of South Africa, several two to four storey ULM buildings have been built for housing. As elaborated in Section 4.3, regions of the Western Cape are prone to low-moderate earthquakes, as it lies on the Milnerton fault. A retrofitting strategy is proposed for ULM buildings in the region. However, LWFC is studied by the CDSI as a low mass alternative construction material for new medium-rise housing in the region. In this regard, assessment tools are developed for objective comparison of building systems for housing by PhD-student Peter Mbewe under supervision of the author. Structural assessment of wall systems has been the starting point, and a truss analogy combined with a novel nonlinear solution method has been developed (Mbewe and Van Zijl 2016a,b), using reduced stiffness upon exceeding linear elasticity in the truss members. The load-deformational response of the truss shown in Figure 2.21a is shown in Figure 2.21b. Two cases were studied, one for elastic-perfect plastic elements, and the second for strain-hardening elements. The computed results are shown to be accurate compared with detailed nonlinear finite element analysis results of the truss. This reduced stiffness solution method is subsequently used to analyse a masonry infilled RC frame shown in Figure 2.22. Well-known diagonal strut approaches are followed for in-plane stiffness of the wall panel to characterise the truss member properties, while the RC frame is simplified by static condensation to a truss with two diagonals – see Figure 2.21a, b. Hardening and/or softening material behaviour of the truss elements can be considered in the simple solution method. For elaboration of the mathematical framework and solution algorithm the reader is referred to Mbewe and Van Zijl (2016b).

The push-over response of wall systems is intended for assessment of the resistance of existing housing structures, for instance to evaluate seismic resistance and retrofitting strategies as described in Section 4.3. Characterisation studies of R/LWFC wall systems are envisaged, to assist in evaluation of various structural systems and construction materials for new housing construction. The next step is the analysis of an ULM shear wall, a retrofitted ULM shear wall (Section 4.3) and an R/LWFC shear wall. The purpose is to compare the

shear resistances of these walls for typical thickness and nominal reinforcement, and secondly to determine the required thickness and reinforcement of a LWFC shear wall to give equivalent resistance to that of a retrofitted ULM wall. Thermal, acoustic and durability assessment functionalities will also be included in future work in the CDSI.

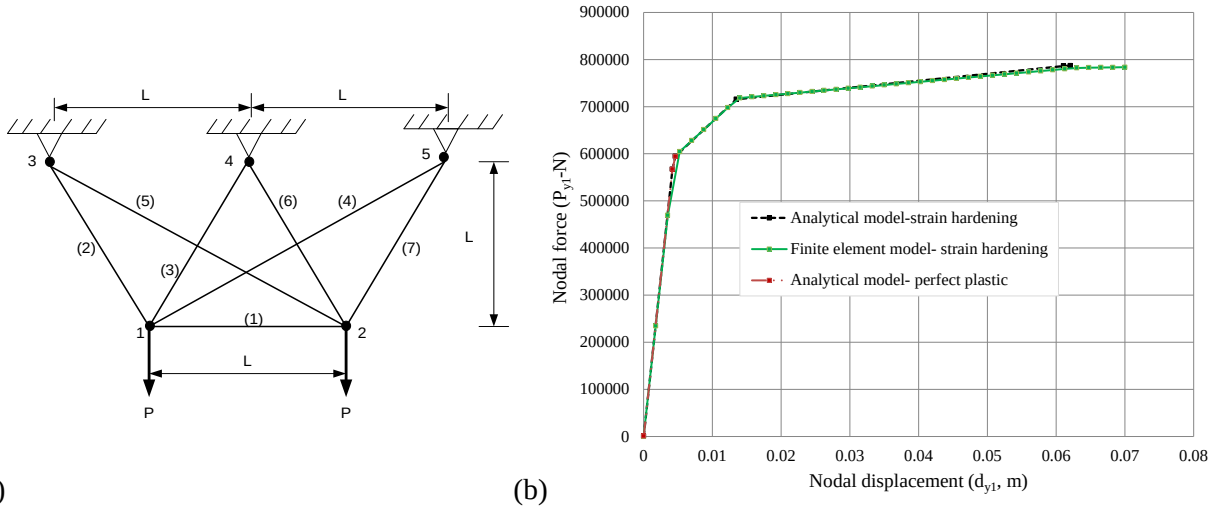

(a) (b)

Figure 2.21: (a) Truss example with elastic-perfect plastic elements, and hardening elements, solved (b) by detailed finite element analysis and with the proposed reduced member stiffness strategy (Mbewe and Van Zijl 2016a).

2.4 Concluding remarks

Through the development of advanced cement-based materials described in this chapter, the endeavour was to contribute to the level of insight, characterisation, constitutive modelling and structural modelling capacity nationally and internationally. Particular leading contributions by the author's group were made in experimental investigation of tensile creep of pre-cracked and uncracked SHCC, and on the single fibre level. The phenomena of tensile creep limit and tensile creep fracture, as well as the time-dependent widening of existing cracks ánd formation of new cracks under sustained load were demonstrated and brought to the attention of the international research community. This led to more laboratories investigating these phenomena. A new shear test method was developed for SHCC and the fundamental mechanism of high shear resistance in SHCC explained. This was presented in a keynote lecture at the International Conference Advances in Cement and Concrete X in Davos, July 2006, and was selected for publication in a leading journal (Van Zijl 2007). Another leading contribution was the extrusion of steel reinforced SHCC beams (Visser and Van Zijl 2007), in addition to pipes and plate elements. This expertise on extrusion and spraying of SHCC (see Section 4.3) was instrumental in the author's invitation as visiting Professor to Nanyang Technological University (NTU) Centre for 3D Printing, and the group for Building and Construction of the School of Mechanical and Aerospace Engineering in April 2016.

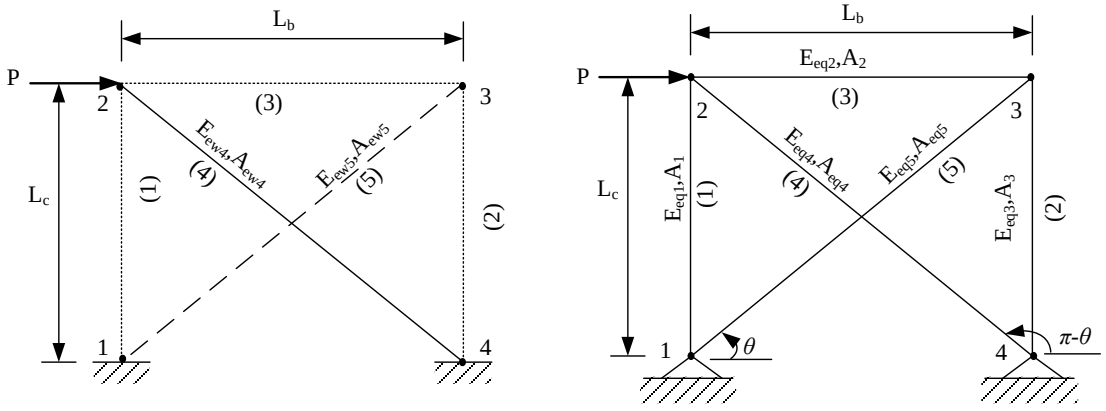

(a) Equivalent diagonal strut for infill wall (active strut shown with continuous lines)

(b) Overall equivalent truss system for RC infilled frame

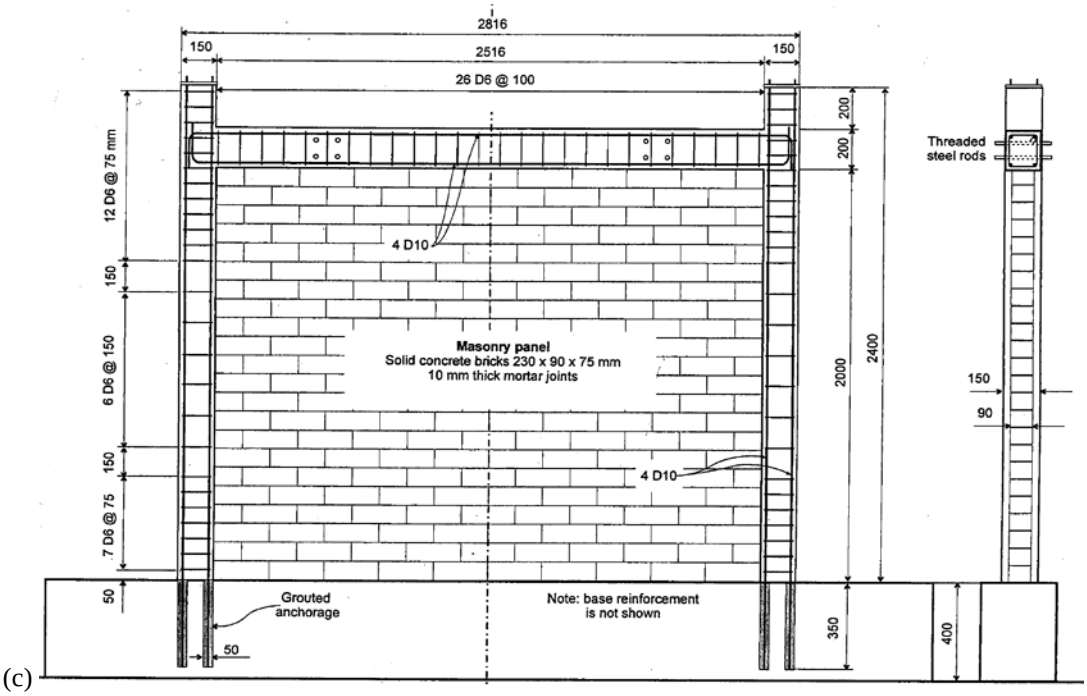

(c)

Figure 2.22: (a) Truss model with diagonal strut and (b) inclusion of the RC frame to represent (c) the infilled masonry RC frame tested by (Crisafulli 1997).

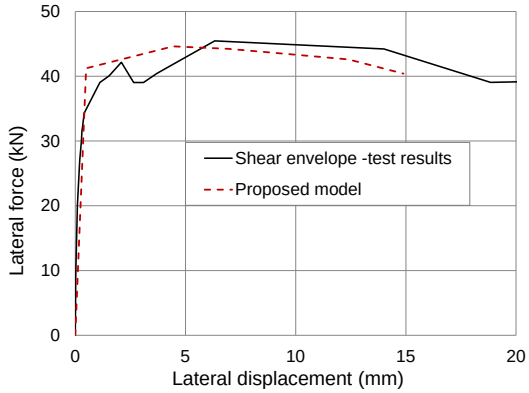

Figure 2.23: Push-over load-deformation response of the masonry infilled RC frame of Figure 2.22 by Crisafully 1997) compared to the response computed with the equivalent truss analogy and reduced truss member stiffness strategy (Mbewe and Van Zijl 2016b).

The research activities in SHCC led to appointment of the author as co-chair of the subcommittee 2: Durability of RILEM Technical Committee 208-HFC for the period 2005-2009, and co-editorship of this TC subcommittee's state-of-the-art report published as a book (Van Zijl and Wittman 2011). At the end of life of TC 208-HFC, the author was requested to chair a new TC 240-FDS to define a Framework for Durability design with SHCC. This relates to durability, described in Chapter 3, but also entailed comparative mechanical testing in five participating laboratories in order to derive a set of guidelines for a suitable tensile test method and procedure for SHCC, as well as accurate measurement of the fine, multiple cracks by digital image correlation (DIC) and appropriate reporting of crack width distributions. The resulting paper (Van Zijl et al. 2016) was selected as one of the ten outstanding papers in 2015 by the Materials and Structures Board of Editors. The author is also a co-founder and Vice-President of the International Association for Strain-Hardening Cement Composites (SHCC). The fourth conference in the SHCC series will be held in Dresden in September 2017, following on SHCC3-2014 in Dordrecht, SHCC2-2011 in Rio de Janeiro, with the roots of this series in the International Conference on Advanced Cement-based Materials (ACM-2009) hosted in Stellenbosch by the author, and the International Conference on High Performance Fibre-Reinforced Cementitious Composites held in Hawaii in 2005.

Keynote lectures on ACM were also presented in Kaiserslautern, Germany at the Symposium *Strain-hardening concrete with short fibers*, in October 2005 (Van Zijl 2005b), at the International Concrete Conference and Exhibition held in Sun City, South Africa in February 2008, and the National Symposium on *Concrete for a Sustainable Environment* held in August 2010 in Johannesburg, South Africa.

References

Adendorff CJ, Boshoff WP, Van Zijl GPAG 2010. Crack characterisation in SHCC: towards durability assessment, Advances in cement-based materials: Proceedings International Conference on Advanced Concrete Materials, 17-19 November 2009, Stellenbosch, South Africa, pp. 215-221.

Boshoff W 2007. Time-Dependant Behaviour of Engineered Cement-Based Composites. PhD dissertation, Stellenbosch University, South Africa.

Boshoff WP, Mechtcherine V and Van Zijl GPAG 2009. Characterising the time-dependent behaviour on the single fibre level of SHCC: Part 1: Mechanism of fibre pull-out creep, Cement and Concrete Research, 39 (2009) 779-786.

Boshoff WP, Mechtcherine V and Van Zijl GPAG 2009. Characterising the time-dependent behaviour on the single fibre level of SHCC: Part 2: Rate effects in fibre pull-out tests, Cement and Concrete Research, 39 (2009) 787-797.

Boshoff WP, Van Zijl GPAG 2006. Creep and creep fracture of engineered cement-based composites, Int. J. Restoration of Buildings and Monuments, 12(2), pp. 133-142

Boshoff WP, Van Zijl, GPAG 2007a. A computational model for strain-hardening fibre-reinforced cement-based composites. J SAICE, 49(2) 24-31.

Boshoff WP, Van Zijl GPAG 2007b. Time-dependent response of ECC: Characterisation of creep and rate dependence. Cement and Concrete Research, 37 725-734.

British Standard BS EN 1052-3: 2002. Method of test for masonry- Part 3 Determination of initial shear strength. BSI British standards.

Boshoff WP and Van Zijl GPAG 2004. Computational and experimental modelling of creep behaviour of Engineered Cement-based Composites. Proceedings SEMC 2004, Cape Town, South Africa, 1061-1066.

Boshoff WP and Van Zijl GPAG 2004. Numerical modelling of ECC. Proceedings 5th Fracture Mechanics of Concrete and Concrete Structures (FRAMCOS-V), (eds VC Li et al.), Vail, USA, 1037-1043.

Brühwiler E, Denarié E 2006. Rehabilitation of concrete structures using Ultra-High Performance Fibre Reinforced Concrete, In: Proceedings of the 2nd International Symposium on Ultra High Performance Concrete, March 05 - 07, 2008, Kassel, Germany.

De Koker D and Van Zijl GPAG 2004. Extrusion of engineered cement-based composite material. Proceedings 6th Rilem Symposium on Fibre reinforced Concrete (FRC), Varenna, Italy, 1301-1310.

De Koker D, Van Zijl GPAG and Mostert D 2004. Manufactoring processes for engineered cement-based composite material. CDROM Proceedings SEMC 2004, Cape Town, South Africa, 1055-1060.

De Villiers JP 2015. Bond behaviour of deformed steel reinforcement in lightweight foamed concrete, MEng-thesis, Stellenbosch University.

De Villiers JP, Van Zijl GPAG, van Rooyen AS 2016a. Fracture of light weight foamed concrete in evaluation of bond behaviour of steel reinforcement in LWFC. In Proceedings of FRAMCOS-9, 29 May-1 June 2016, Berkeley, USA, DOI 10.21012/FC9.289

De Villiers JP, Van Zijl GPAG, van Rooyen AS 2016b. Bond of steel reinforcement in lightweight foamed concrete (LWFC). Journal of the FIB, Structural Concrete, in print.

DIANA v. 9.3, 2008. DIANA User's Manual, TNO DIANA BV, Delft, The Netherlands.

Fischer G (ed.) 2011. Mechanical characterization and testing of strain-hardening fiber-reinforced cement-based composites (SHCC), State-of-the-art report, Subcommittee 1 of RILEM TC 208-HFC, RILEM.

Gao Song and Van Zijl GPAG 2004. Tailoring ECC for commercial application. Proceedings 6th Rilem Symposium on Fibre reinforced Concrete (FRC), Varenna, Italy, 1391-1400.

Graybeal BA 2006. Material Property Characterisation of Ultra-High Performance Concrete. Publication No. FHWA-HRT-06-103, US Department of Transportation, Federal Highway Administration, Research, Development and Technology, McLean, USA.

Habel K, Viviani M, Denarié E, Brühwiler E 2006. Development of the Mechanical Properties of an Ultra-High Performance Fiber Reinforced Concrete (UHPFRC). Cement and Concrete Research, 36(7).

Hashin Z 1962. The elastic moduli of heterogeneous materials, J Appl. Mech. 29 143-150.

Helmuth RA, Turk DM 1966. Symposium on Structure of Portland Cement Paste, Special Report 90, National Academy of Sciences, Washington (1966).

Jones MR, McCarthy A 2005. Preliminary views on the potential of foamed concrete as a structural material, Magazine for Concrete Research, 57(1), 21-31.

Kearsley EP, Wainwright PJ 2002. Ash content for optimum strength of foamed concrete. Cement and Concrete Research, 32 241–6.

Kearsley EP, Mostert HF 2005. Designing mix composition of foamed concrete with high fly ash contents. Proceedings of the International Conference on the Use of Foamed Concrete in Construction, R. H. Dhir, M. D. Newlands, and A. McCarthy, eds., Thomas Telford, London, 29-36

Koiter WT 1953. Stress-strain relations, uniqueness and variational theorems for elastic-plastic materials with singular yield surface, Q. Appl. Math. 11(3) 350-354.

Li VC 1993. From Micromechanics to Structural Engineering – the Design of Cementitious Composites for Civil Engineering Applications, JSCE J. Struc. Mechanics and Earthquake Engineering, 10 (2) 37-48.

Li VC 1998. Engineered cementitious composite (ECC)-tailored composites through micromechanical modelling, in Fiber Reinforced Concrete: Present and the Future (eds. N. Banthia, A. Bentur, A. and A. Mufti), Canadian Society for Civil Engineering, Montreal, pp. 64-97.

Li VC, Wang S, Wu C 2001. Tensile strain-hardening behavior of PVA-ECC, ACI Materials Journal, 98 (6) 483–492.

Li VC, Mishra DK, Naaman AE, Wigh JK, LaFave JM, Wu HC, Inada Y 1994. On the shear behavior of engineered cementitious composites, J. Advanced Cement Based Materials 1(3) 142-149.

Lopez AL, Serna P, Camacho E, Coll H, Navarro-Gregori J 2014. First Ultra-High-Performance Fibre-Reinforced Conrete Footbridge in Spain: Design and Construction. Structural Engineering International, 101-104.

Lourenço PB, Rots JG, Blaauwendraad J (1998). Continuum model for masonry: parameter estimation and validation. J. ASCE J. Struct. Eng., June, 642-652.

Maalej M, Quek ST, Zhang J 2005. Behavior of hybrid fiber engineered cementitious composites subjected to dynamic tensile loading and projectile impact. ASCE J Mater Civil Eng 17(2):143–152

Madeiros MHF, Helene P 2009. Surface treatment of reinforced concrete in marine environment: Influence on chloride diffusion coefficient and capillary water absorption. Construction and Building Materials 23, 1476-1484.

MC2010 2010. The Model Code, fib CEB-FIP, Walraven (fib convenor Special Activity Group 5).

Mbewe PBK and Van Zijl GPAG 2016a. Towards development of a non-linear structural analysis analytical model for evaluation of structures. FIB Symposium, November 2016, Cape Town.

Mbewe PBK, Van Zijl GPAG 2016b. A simplified non-linear structural analysis of RC infilled frames subjected to seismic loading. Submitted to ASCE J Structural Engineering

Molapo KT 2010. The behaviour of strain-hardening cement composites under biaxial compression, MScEng-thesis, Stellenbosch University, South Africa.

Paul SC, Pirskawetz S, Van Zijl GPAG, Schmidt W 2015. Acoustic Emission in Determining the Crack Propagation in Strain-hardening Cement-Based Composites (SHCC). Cement and Concrete Research 69, 19-24.

Paul SC, Van Zijl GPAG 2013. Mechanically induced cracking behaviour in fine and coarse sand strain-hardening cement based composites (SHCC) at different load levels. Journal of Advanced Concrete Technology, 11 (Nov 2013) 301-311.

Perry VH, Seibert PJ 2009. The use of UHPFRC (DuctalR) for bridges in North America: the technology, applications and challenges facing commercialization. 2nd International Symposium on Ultra High Performance Concrete, 2008, pp. 815–822.

Ramamurthy K, Kunhanandan Nambiar EK, Indu Siva Ranjani G 2009. A classification of studies on properties of foam concrete, Cement & Concrete Composites 31 (2009) 388–396.

RILEM Recommendation AAC13.1, Determination of the specific fracture energy and strain softening of AAC, RILEM Technical Recommendations for the testing and use of construction materials, E & FN Spon, 1994, pp. 156–158.

Rokugo K, Kanda T (eds.) 2013. Structural design and performance, State-of-the-art report, Subcommittee 2 of RILEM TC 208-HFC, SPRINGER.

SANS 10249. 2012. Masonry walling. Pretoria: SABS Standards Division, South Africa.

SANS 10160-4. 2011. Basis of structural design and actions for buildings and industrial structures. Part 4: Seismic actions and general requirements for buildings. Pretoria: SABS Standards Division, South Africa.

Shang QJ 2006. Shear behaviour of engineered cement-based composites, Thesis, Stellenbosch University, South Africa.

Slowik V, Luković M, Wagner C, Van Zijl GPAG 2016. Behaviour of bonded SHCC overlay systems, Chapter 8 of A framework for durability design with strain-hardening fibre-reinforced cement-based composites (eds. GPAG Van Zijl, V Slowik), State-of–the-art-report of RILEM Technical Committee 240-FDS, SPRINGER.

Stander H 2007. Experimental and computational characterisation of SHCC-Concrete interfacial bond. MScEng-thesis, Stellenbosch University, South Africa.

Swanepoel W 2011. The behaviour of fibre reinforced concrete (SHCC) under biaxial compression and tension, MScEng-thesis, Stellenbosch University, South Africa.

Van der Pluijm R 1992. Deformation controlled shear tests on masonry. Rep. BI-92-104, TNO Building and Construction, Delft, The Netherlands (in Dutch).

Van der Pluijm R 1998. Overview of deformation controlled combined tensile and shear tests. Rep. TUE/CCO/98.20, Eindhoven Univ. of Technology, Eindhoven, The Netherlands.

Van Zijl GPAG 2000. Computational modelling of masonry creep and shrinkage. PhD dissertation, Delft Univ. of Techn., The Netherlands.

Van Zijl GPAG 2004a. Modeling Masonry Shear-Compression: Role of Dilatancy Highlighted. Journal of Engineering Mechanics 130(11): 1289-1296.

Van Zijl GPAG 2004b. Masonry shear response characterization. Masonry International, Journal of the British Masonry Society, 17(1), 26-32.

Van Zijl GPAG 2005a. The role of aggregate in high performance fibre reinforced cement-based composites. Concrete / Beton, Nr 110, September 2005, 7-13.

Van Zijl GPAG 2005b. Optimisation of the composition and fabrication methods, applications for precast concrete members, Invited lecture in Hochductile Betone mit Kurzfaserbewehrung – Entwicklung, Prüfung, Anwendung (ed. V. Mechtcherine), pp. 37-54.

Van Zijl GPAG 2006. ECC shear behaviour characterization, Advances in Cement and Concrete: Sustainability, July 2-7 2006, Davos, Switzerland, pp. 66-71.

Van Zijl GPAG 2007. Improved mechanical performance: Shear behaviour of strain-hardening cement-based composites (SHCC). Cement and concrete reseach 37:1241-1247.

Van Zijl GPAG 2009a. Constitutive model for fibre-reinforced strain-hardening cement composites (SHCC), Concrete / Beton, Journal of the Concrete Society of Southern Africa, November, 124: 8-15.

Van Zijl GPAG 2009b. Durability of strain-hardening cement composites (SHCC) - an overview, CDROM Proceedings International Conference on Concrete Repair, Rehabilitation and Retrofitting (ICCRRR 2008), University of Cape Town, South Africa, pp. 199-205.

Van Zijl GPAG 2009c. Computational modelling of SHCC – an anisotropic constitutive model incorporating creep and rate dependence. ISE report 2009-020, Stellenbosch University, South Africa.

Van Zijl GPAG 2010a. Computational modeling of strain-hardening cement composites (SHCC), International Conference on Advanced Concrete Materials, 17-19 November 2009, Stellenbosch, South Africa, pp. 263-270

Van Zijl GPAG 2010b. Modelling the rate effects in cracking and fracture of strain-hardening cement-based composites (SHCC), Fracture and Damage of Advanced Fibre-reinforced Cement-based Materials, Symposium organized with 18th European Conference on Fracture, 30 Aug – 3 Sept 2010, Dresden, Germany, pp. 185-193.

Van Zijl GPAG, De Beer L 2016a. An SHCC overlay retrofitting strategy for unreinforced load-bearing masonry, Proceedings of 9th International Conference on Fracture Mechanics of Concrete and Concrete Structures - FRAMCOS-9, V. Saouma, J Bolander, E Landis (Eds), 29 May-2 June 2016, Berkeley, USA.

Van Zijl GPAG, De Beer L 2016b. Retrofitting unreinforced load-bearing masonry with a sprayed SHCC overlay, Proceedings of FIB 2016 Symposium, 21-23 November 2016, Cape Town, South Africa.

Van Zijl GPAG, De Borst R, Rots JG 2001a. The role of crack rate dependence in the long-term behaviour of cementitious materials. Int. J. Solids and Structures, 38(30-31), 5063-5079.

Van Zijl GPAG, De Borst R, Rots JG 2001b. A numerical model for the time-dependent cracking of cementitious materials. Int. J. Numerical Methods in Engineering, 52(7), 637-654. DOI: 10.1002/nme.211

Van Zijl GPAG, De Vries PA 2005. Masonry wall crack control with CFRP. ASCE Journal of Composites for Construction, 9(1), 84-89.

Van Zijl GPAG, De Vries PA, Vermeltfoort AT 2004. Masonry wall damage by restraint to shrinkage. ASCE Journal of Structural Engineering. 130(7), 1075-1086.

Van Zijl GPAG and Mbewe PBK 2013. Flexural modeling of steel fibre -reinforced concrete beams with and without steel bars. Engineering Structures 53 (2013) 52–62.

Van Zijl GPAG, De Borst R and Rots JG, 2001. A numerical model for the time-dependent cracking of cementitious materials. Int. J. Numerical Methods in Engineering 52(7) 637-654.

Van Zijl GPAG, Rots JG, Vermeltfoort AT 2001. Modelling of shear-compression in Masonry. CDROM-Proc. 9th Canadian Masonry Symposium, PH Bischoff, JL Dawe AB, Schriver and AJ Valsangkar, eds., Fredericton, Canada.

Van Zijl GPAG and Stander H 2006. The effect of admixtures on the fresh and consolidated behaviour of ECC. Proceedings Advanced Cement-Based Materials, June 2005, Denmark University of Technology, Denmark, BYG-DTU 2005: 89-102

Van Zijl GPAG, Slowik V (eds.) 2016. A framework for durability design with strain-hardening fibre-reinforced cement-based composites (SHCC), State-of-the-art report, Rilem TC 240-FDS, Springer Publishers.

Van Zijl GPAG, Stander H 2009. SHCC repair overlays for RC: Interfacial bond characterization and modeling, CDROM Proc. International Conference on Concrete Repair, Rehabilitation and Retrofitting (ICCRRR 2008), University of Cape Town, South Africa, pp. 995-1003.

Van Zijl GPAG, Wittmann FH (eds.) 2011. Durability of strain-hardening fibre-reinforced cement-based composites (SHCC), State-of-the-art report, Rilem TC 208-HFC, SC 2, Springer Publishers, ISBN-13: 978-94-007-0337-7.

Van Zijl GPAG, Wittmann FH, Toledo Filho RD, Slowik V, Mihashi H 2016. Comparative testing of crack formation in strain-hardening cement-based composites (SHCC). Materials and Structures, 49(4) 1175-1189.

Vermeltfoort AT, Raijmakers TMJ, Janssen HJM 1993. Shear tests on masonry walls.

Visser G 2009. FRP external reinforcement of bridges in SA, MEng-thesis, Stellenbosch University, South Africa.

Visser CR 2007. Mechanical and structural characterization of extrusion moulded SHCC, MScEng-thesis, Stellenbosch University, South Africa.

Visser CR and Van Zijl GPAG 2007. Mechanical characteristics of extruded SHCC. Proc. International RILEM CONFERENCE on High performance fibre reinforced cement composites, 10-13 July 2007, Mainz, Germany, pp. 165-173.

Wille K, Parra-Montesinos GJ 2012. Effect of Beam Size, Casting Method, and Support Conditions on Flexural Behavior of Ultra-High-Performance Fiber-Reinforced Concrete. ACI Materials Journal 109(3).

Wille K, Parra-Montesinos GJ 2012. Ultra-High Performance Concrete with Compressive Strength Exceeding 150 MPa (22 ksi): A Simpler Way, ACI Materials Journal 108(1) 46-54.

Wu ZS, Bazant ZP 1993. Finite element modelling of rate eDect in concrete fracture with inRuence of creep. In: Creep and Shrinkage of Concrete BaKzant ZP, Carol I (eds), E&FN Spon, London, 427–432.

Yang E, Li VC 2006. Rate dependence in engineered cementitious composites, RILEM PRO49, 8pp

Zang Jin 2015. Developing non-heat treated UHPC in South Africa. PhD dissertation, Stellenbosch University, South Africa.

Zang Jin, Van Zijl GPAG 2015. Developing non-heat treated ultra-high performance concrete with local materials. J. Concrete society of Southern Africa, Concrete / Beton, 142 (September 2015) 12-23.

Zeranka S, Van Zijl GPAG 2013. Characterising the shear behaviour of steel fibre reinforced concrete, SEMC, September 2013, Cape Town

Zeranka S, Van Zijl GPAG 2015. Multi-scale characterisation of the shear-dominant fracture in a steel fibre-reinforced cement-based composite. In: Proceedings of 5th International Conference on Construction Materials (ConMat'15), Whistler, BC, Canada, August 19-21, 2015

Chapter 3 Crack formation and durability, towards durability design

3.1 Introduction

Maintenance cost of reinforced concrete (R/C) structures has been growing steadily and has become a significant portion of total construction industry expenditure world-wide. According to ASCE reports (2005, 2013) annual direct cost of maintenance of bridges in the US exceeded $ 8 billion in the USA in 2005, and this amount grew to $ 12.7 billion in 2013, while it is estimated that $ 20.3 billion should in fact be spent annually. In 2005, US drivers paid more than $ 54 billion per annum in addition for vehicle repair and operating cost, and the amount increased to $ 67 billion in 2013. Forty percent of the German infrastructure needs repair measures. There, the average intervention-free service life is reported to be 18.5 years, which does not compare well with Roman bridges, which had service lives of 2000 years, e.g. a Roman bridge in Augusta Treverorum, Trier. It is acknowledged that cost restrictions most likely did not apply to Roman construction. Roughly fifty percent of the total expenditure for construction is needed for maintenance and repair in many industrial countries (Wittmann and Van Zijl 2006).

This motivates care when developing new construction materials, such as HPFRCC, UHPC and SHCC. Construction materials for infrastructure should be inherently durable, and contribute to more durable structures. In this regard SHCC in particular presents a strong potential, by the nature of strain-hardening, which is physically controlled micro-crack formation. This potential durability of SHCC was studied by RILEM TC 208-HFC subcommittee 2 with Professor Folker Wittmann as chairman and the author as co-chairman, and a state-of-the art report written (Van Zijl and Wittmann 2011) and summarized by Van Zijl et al. (2012). Collaborative testing by participating laboratories in this TC led to recommendations for tensile testing of SHCC for durability (Van Zijl et al. 2016). One of the main findings of this TC was that significant amounts of water or other deleterious substances may be absorbed by dry, or non-saturated SHCC containing multiple fine cracks. Capillary absorption of water (Zhang et al. 2010) and chloride (Wittmann et al. 2011) has since been reported, showing that water is absorbed deep into the fine cracks within minutes of exposure. Nevertheless, chloride-induced experiments by Miyazato and Hiraishi (2005, 2013) indicated low corrosion rates in cracked R/SHCC subjected to absorption of chloride aqueous solution. This motivated a research program in chloride-induced corrosion of cracked and uncracked R/SHCC by the author, studying non-destructive testing of corrosion potential and rates, the influence of crack spacing and steel cover depth, as well as the level of deformation on corrosion of steel reinforcing bars in R/SHCC. The most important results thus far are summarised in this chapter, but can be found in various recent publications (Paul and Van Zijl 2013a, 2014, 2016, Paul et al. 2016).

Most of these results on corrosion in R/SHCC have been included in the state-of-the-art report of RILEM TC 240-FDS (Van Zijl and Slowik 2016), as are first attempts to relate the recently proposed crack ingress potential index (IPI) for water permeation (IPI_{WP}) and for chloride diffusion (IPI_{Cl}) (Boshoff et al. 2015), as well as the crack width value (CWV) for water permeability (CWV_{WP}) (Wagner and Slowik 2011, Wagner 2016) to actual observed ingress, as well as actual corrosion damage in cracked R/SHCC (Van Zijl and Paul 2016).

Several structures in South Africa, but also world-wide, are affected by alkali silica reaction (ASR), including the Danie Craven Stadium in Stellenbosch, the Kleinplaas dam wall in Jonkershoek, Stellenbosch and the Good Hope Centre in Cape Town. To assist condition assessment and intervention planning, a research program was

started in 2012. PhD-student Salhin Alaud developed accelerated ASR test equipment in the laboratories under supervision of the author. A particular focus is combined action of mechanical cracks, and continued ASR reaction in unreinforced concrete, as well as in steel bar RC elements. The results indicate that cracks induced by tensile mechanical action reduce in width as the ASR reaction continues, with the cracked region acting as region of reduced restraint in concrete or RC (Alaud and Van Zijl 2014, 2016a,b).

Durability investigation of other construction materials has also been performed under supervision of the author within the CDSI, or is currently in progress, for instance for R/LWFC as briefly described in Section 2.3.2. In preparation for a drive towards recycling of demolished concrete also in South Africa, mechanical and durability properties of concrete including various percentages of recycled concrete aggregate (RCA) were studied and reported by Paul and Van Zijl (2013b,c), but is not further elaborated in this dissertation. In the following sections the contributions to durability studies on SHCC and ASR are described in more detail, with the emphasis on durability in the cracked state.

3.2 Crack formation and durability of SHCC

The contributions towards developing, mechanical characterisation and modelling of SHCC in Section 2.2 have been made in parallel with durability studies. Seismic activity in the Western Cape of South Africa justifies consideration of the appropriate use of SHCC or R/SHCC as construction material for its energy dissipating multiple crack characteristic, whether in new structures or in retrofitting strategies described in Sections 4.3 and 4.4. On the other hand, corrosion of steel reinforcement in RC in coastal regions in South Africa and elsewhere demands careful durability design of such structures. This applies also to regions in the world where de-icing practise leads to significant and premature deterioration of RC infrastructure. Two main contributions from the author's research group are time-dependent crack widening and corrosion of steel in R/SHCC.

3.2.1 SHCC crack width time dependence

Various studies on crack width were performed in the author's research group, making use of three-dimensional digital image correlation (DIC) (Van Zijl et al. 2016), for instance producing the crack width histogram in Figure 2.3a. The crack widths are typically determined from snapshots at particular strain levels, with the aim of deriving durability design indices (Boshoff et al. 2015, Wagner and Slowik 2011). However, in cases of high sustained load, creep deformation may include the development of more cracks, or alternatively widening of existing cracks, or a combination of these two phenomena. Boshoff and Van Zijl (2009) reported crack width development in time under sustained uniaxial tensile load. A typical PVA-SHCC mix similar to SHCC1 in Table 2.1 was used. In an attempt to isolate cracks, notches were cut in specimens with geometry and setup shown in Figure 3.1. The specimens were carefully loaded to about 60% of the average ultimate stress, which was determined in monotonic tensile tests on 5 notched specimens. Due to slight differences in load (with two specimens hanging in series as shown in Figure 3.1d) and notch geometry, the sustained stresses on the 6 creep specimens are given in Figure 3.2.

High resolution (8 MP) photos were taken at regular intervals with a camera connected to a Leica microscope. From these photos optical measurement of the crack widths along the central line (Figure 3.1c) was performed. Figure 3.3 summarises the number of cracks and the central crack width development in time under the sustained load. It is clear that more cracks initiate under the sustained load (Figure 3.3a). Also, crack widening occurs under the sustained load in time, at first gradually, but at a higher rate at later stages approaching creep fracture along the central wide crack in the notch.

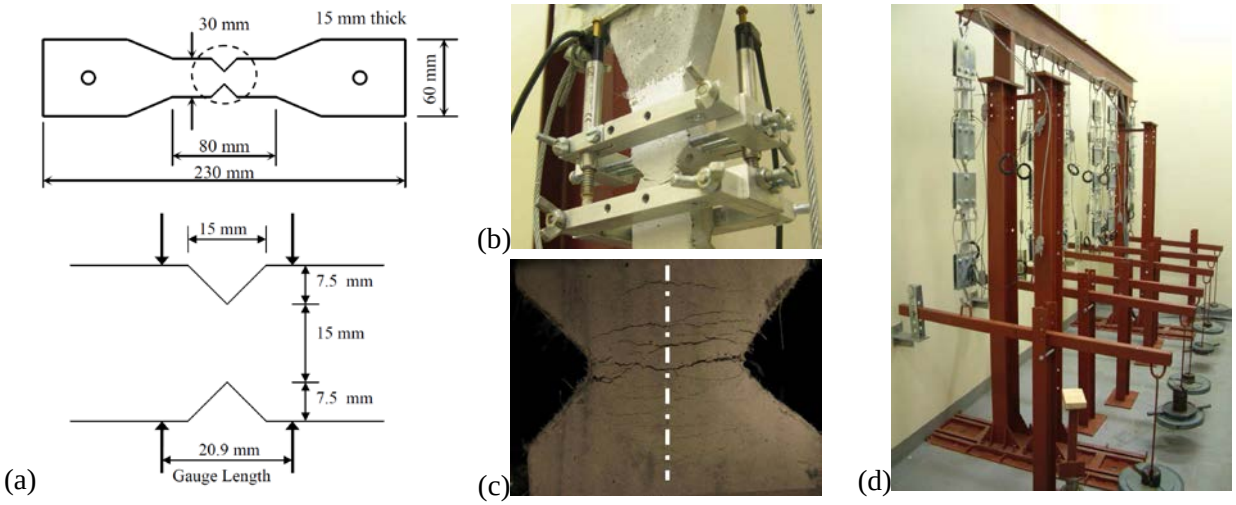

Figure 3.1: Dumbbell (a) specimen and notch geometry, (b) deformation measurement, (c) central line along which the number of cracks and crack width were determined, and (d) the test frames (Boshoff et al. 2009).

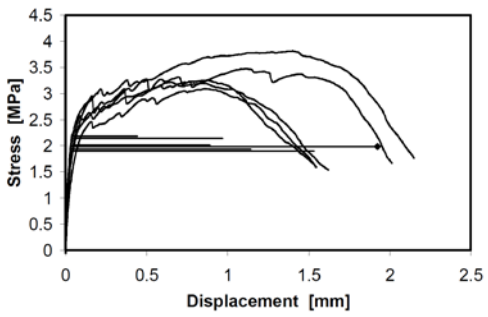

Specimen number	Sustained tensile stress (MPa)
1	2.01
2	1.94
3	2.14
4	1.90
5	2.18
6	1.99

Figure 3.2: Tensile creep and monotonic stress-displacement responses (left), and the sustained tensile stress level (right) (Boshoff et al. 2009).

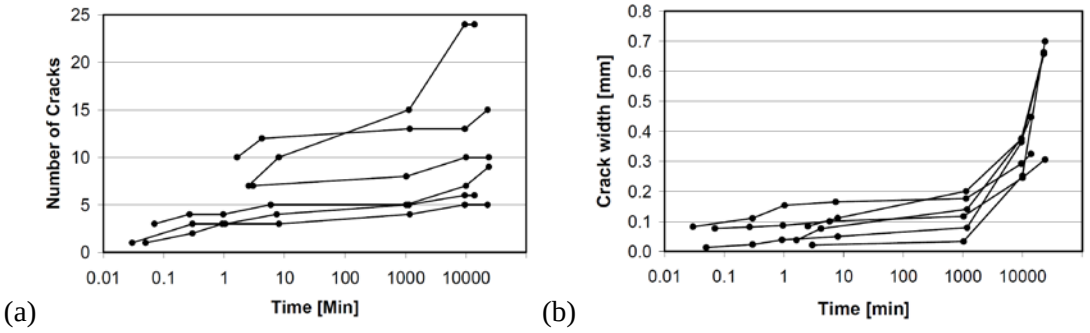

Figure 3.3: (a) Number of cracks and (b) crack width development with time under sustained tensile load.

The crack widening is visualised in Figure 3.4, where also unnotched dumbbell specimens of Boshoff (2007) are shown (Figure 3.4 right). Unfortunately, Boshoff (2007) did not measure and report the crack width development in time. It is emphasised that the observations are for the extreme case of sustained high tensile load. Also, under these circumstances it appears that the dominant initial mechanism of creep deformation is the initiation of more cracks, while the widths of existing cracks are controlled. However, as creep fracture is

approached, the number of cracks and crack width both increase rapidly. For such exceptional conditions of sustained high loading, the time-dependent change in crack pattern in terms of the number of cracks and crack width must be considered by the designer. This may influence structural safety, as creep fracture may be approached or activated. Even in absence of structural stability, increased ingress of deleterious substances into wider and more cracks may change the structure's durability performance, leading to faster deterioration.

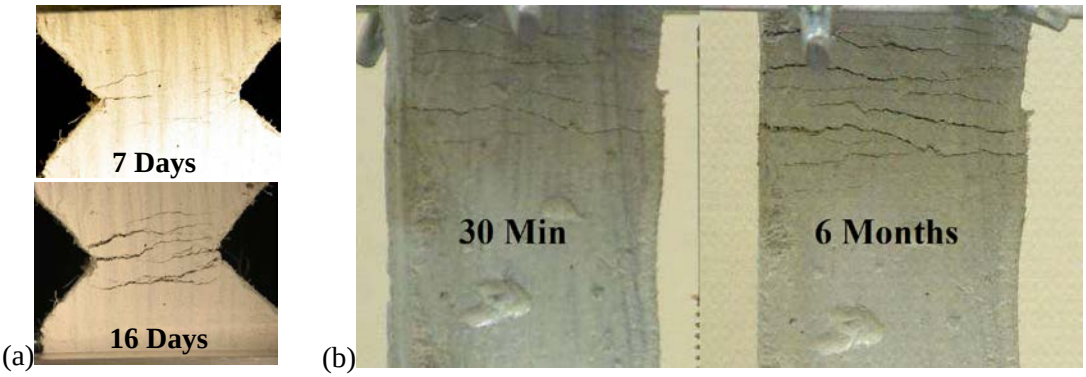

(a) (b)

Figure 3.4: Time-dependent crack widening observed by (a) Boshoff et al. (2009) and (b) Boshoff (2007).

3.2.2 Chloride-induced corrosion in R/SHCC

While reduced water permeability and chloride diffusivity of cracked SHCC was reported by various authors (eg. Lepech and Li 2005, Sahmaran et al. 2007) for saturated SHCC, evidence of quick ingress of water and chlorides into SHCC has been reported. The cracks act as pathways for the quick access, followed by gradual diffusion into the adjacent matrix between cracks (Zhang et al. 2010, Paul et al. 2016). This leads to the presence of significant amounts of chloride at the level of steel bar reinforcement in cracked R/SHCC, which, together with oxygen and water are the required ingredients for corrosion of the steel bars. However, low corrosion rates are reported in cracked R/SHCC under such circumstances (Miyazato and Hiraishi 2005, 2013). In the next sections, the author and PhD student Suvash Chandra Paul's investigation into crack patterns, chloride ingress and corrosion in R/SHCC to study this anomaly, is described.

3.2.2.1 Cracking of R/SHCC

Deterioration by chloride-induced corrosion is considered to be directly linked to cracking. The inherent crack control of SHCC in tension, flexure and shear has been described in Section 2.2. In Figure 3.5, crack spacing development with tensile strain in uniaxial tensile testing of dumbbell specimens is shown, as reported by Paul and Van Zijl (2013a) for SHCC of similar type as SHCC1 in Table 2.1, but with one set of specimens containing the typical fine sand used in SHCC, and also another set containing coarser sand. See Figure 3.5a for the sand gradings. The coarse sand was tested to investigate possible cost reduction of SHCC, to avoid expensive and time consuming preparation of fine graded sands from natural sands or by crushing of rock. In Figure 3.5b it is clear that, for these SHCCs, crack saturation was approached at about 2.5% tensile strain. A reduced tensile ultimate strain was found for the coarse sand version, but considered still to be practical in many applications of this advanced material.

The same SHCC mixes were used to prepare beam specimens of 100 mm square cross-sections and 500 mm long for three-point bending tests with span length of 400 mm. The beam specimens were reinforced by one

central, or two Y10 steel bars, as illustrated in Figure 3.6, and subjected to flexure up to a deflection of 3.5 mm to achieve saturated flexural cracking.

In Figure 3.7 the average crack spacing in the R/SHCC specimens is shown. For fine sand, the crack spacing appears to be influenced by cover depth, with an apparent threshold cover of roughly 25 mm, beyond which the crack spacing is not influenced by cover depth. For coarse sand, the crack spacing is insensitive to cover depth. An explanation may be found in RC and R/SHCC tensile tests results of Fischer and Li (2002), shown in Figure 3.8. It appears that the steel bar ribs influence crack spacing adjacent to the bar, by stress concentrations in the concrete at the ribs. Thus, a crack runs towards the surface from the position of each rib. Further away from the bar, more cracks form in between, reducing the crack spacing from that of the rib spacing. With too small cover depth, the stress concentrations dominate, and cracks do not form in between, causing a larger average crack spacing. It is postulated that the fine crack spacing may reduce corrosion rate, by the relatively small cathode to anode size ratio in the electrochemical corrosion process. Paul and Van Zijl (2016) reported crack spacing, average width and maximum in another set of R/SHCC beams, summarised in Figure 3.9.

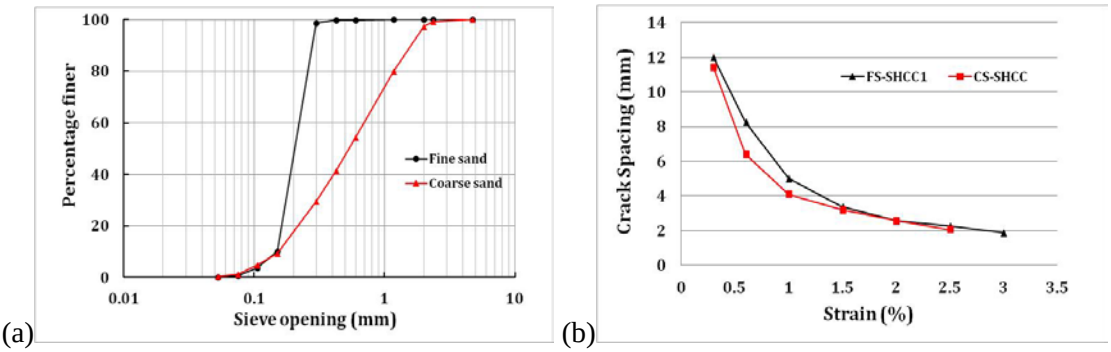

(a) (b)

Figure 3.5: (a) Sand grading for fine and coarse sand, used in SHCC specimens to prepare dumbbell specimens. (b) Average crack spacing development with tensile strain (Paul and Van Zijl 2013a).

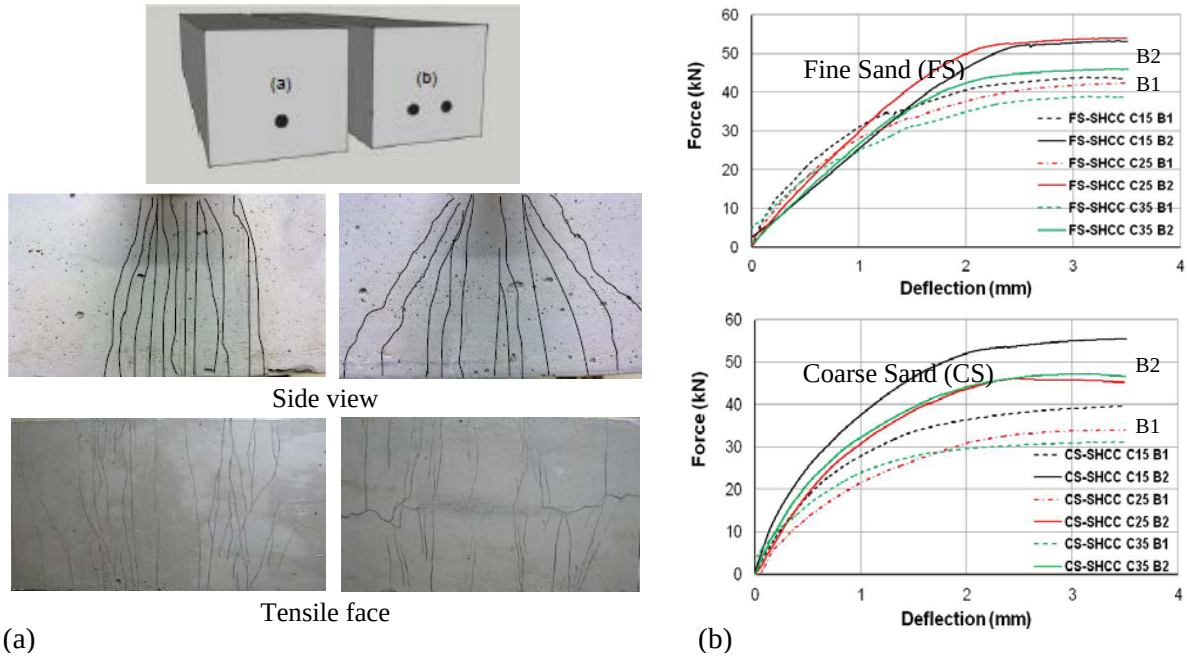

(a) (b)

Figure 3.6: (a) Typical crack patterns over the central 200 mm in a SHCC beam reinforced by (a) a single steel bar (B1) and (b) two steel bars (B2). (b) Load-deflection responses of fine and coarse sand R/SHCC beams.

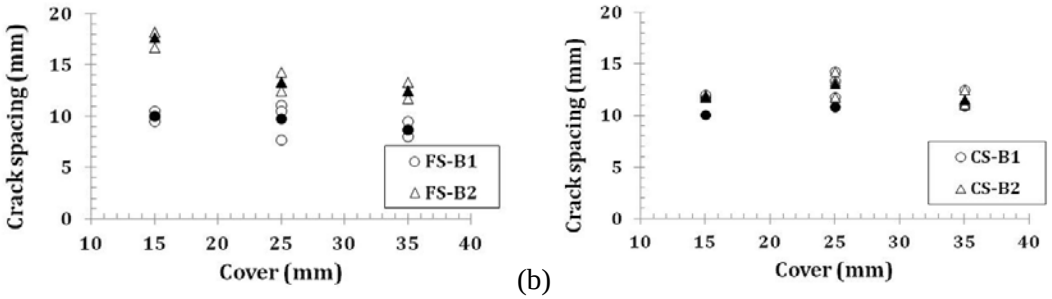

Figure 3.7: Crack spacing as function of cover depth in R/SHCC specimens containing (a) fine sand and (b) coarse sand. The average spacing is shown by infilled symbols (Paul and Van Zijl 2013a).

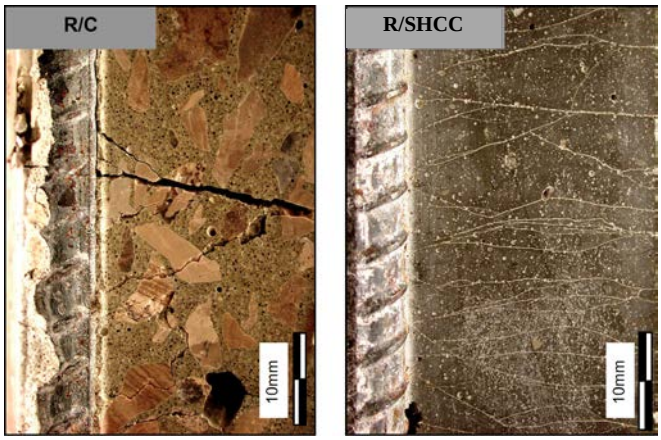

Figure 3.8: Cracking in RC and R/SHCC in uniaxial tension (adapted from Fischer and Li 2002).

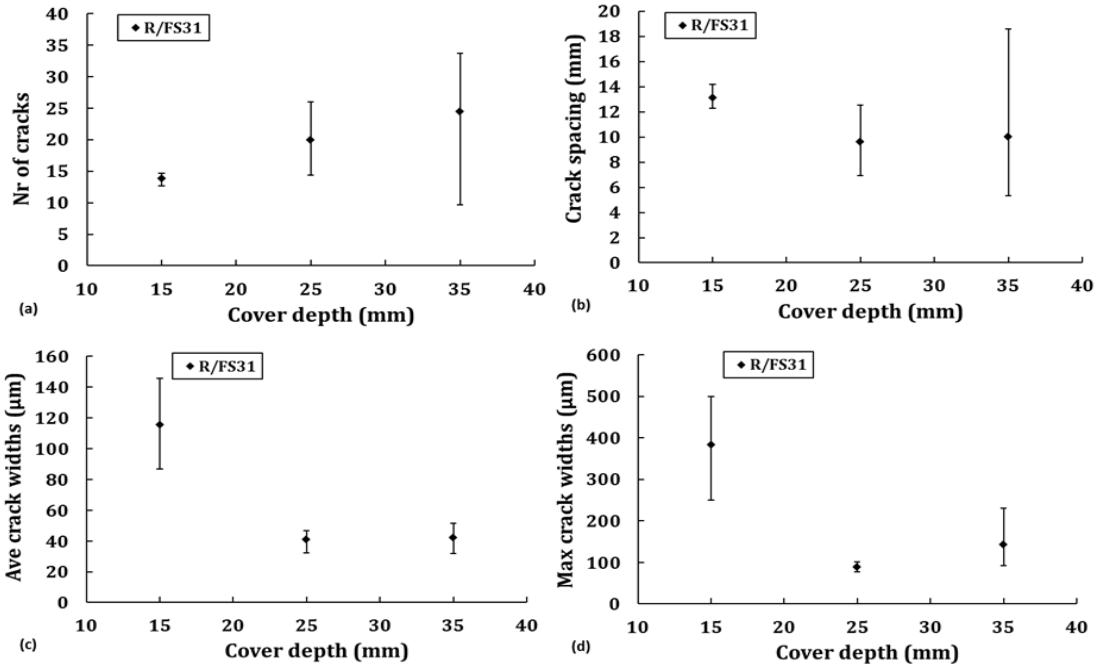

Figure 3.9: (a) Number of cracks, (b) average crack spacing, (c) average crack width and (d) maximum crack width in R/SHCC specimens in three-point bending (Paul and Van Zijl 2016).

3.2.2.2 Chloride into cracked SHCC and R/SHCC

Fast ingress of chloride into unreinforced SHCC beams that were pre-cracked by three-point bending, is visualised by silver nitrate discolouring seen in Figure 3.10 (Paul and Van Zijl 2016). The pre-cracked SHCC beams were exposed to ponding of sodium chloride (NaCl) aqueous solution on the top, cracked face of the beams for durations of one hour, one day and seven days respectively. Already after one hour of ponding, chloride is seen to have reached deep into the cracks. After one day, the affected area is clearly larger, with chloride also penetrating from the crack faces into the uncracked matrix. This phenomenon is continued, and after seven days the matrix between cracks has nearly been filled with chloride in places. In Figure 3.10b, chloride profiles are shown. Full details of drilling into cracked regions of the SHCC specimens to successive depth intervals of 3 mm to produce the chloride profiles with 3 mm depth intervals, are given in Paul (2015).

Also described in detail are the X-ray florescence (XRF) tests for chloride content of the powder collected by drilling, and comparisons with total chloride content determined by chemical titration for acid soluble chloride according to RILEM TC 178-TMC (2002a), as well as free chloride content by determining water-soluble chloride content according to RILEM TC 178-TMC (2002b) (Paul 2015, Paul et al. 2016). In Figure 3.11a chloride profiles determined in a cracked reinforced beam by the XRF method are shown together with the profiles determined by chemical titration for total and free chloride content. From the figure it is clear that significant chloride binding occurs, given the difference between total and free chloride. Note that all chloride profiles are expressed as percentage of binder mass.

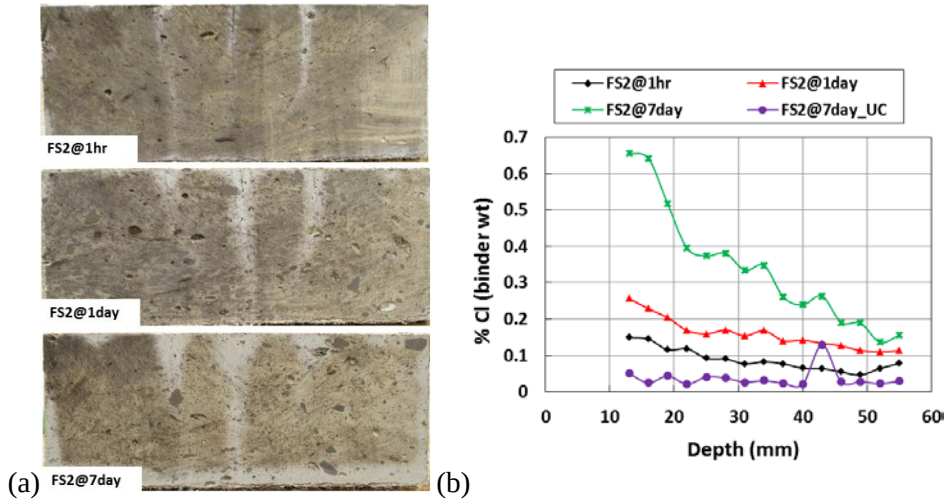

Figure 3.10: (a) Chloride penetration depth in cracked SHCC visualised by silver nitrate solution application after various durations (1 hour, 1 day, 7 days) of ponding with aqueous solution. (b) Total chloride content profiles determined by XRF in unreinforced, cracked SHCC specimens after different exposure periods.

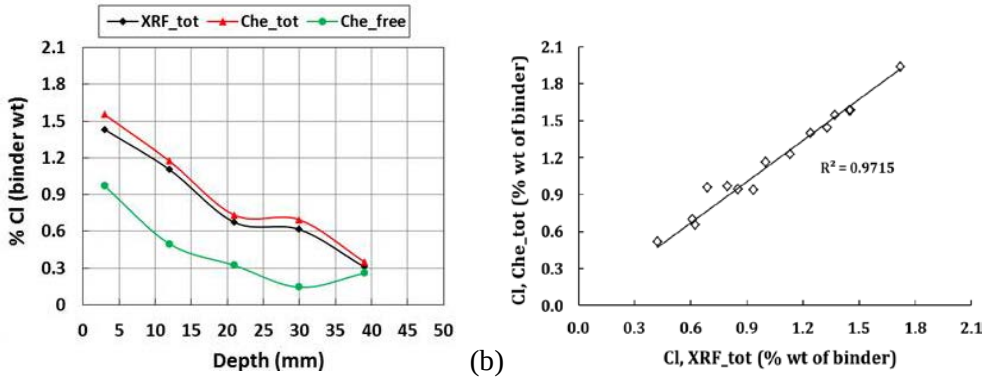

(a) (b)

Figure 3.11: (a) Chloride profiles determined by XRF and chemical titration for total and free chloride content in a cracked R/Mortar specimen with cover depth 25 mm after 29 weeks of cyclic ponding and drying. (b) Relationship between total chloride content obtained from chemical testing and from XRF testing and in a number of cracked R/SHCC specimens (Paul et al. 2016).

Chloride profiling was also performed for cracked R/SHCC subjected to cyclic ponding and drying with chloride aqueous solution, in order to correlate them with corrosion in the embedded steel bars. Figure 3.12 summarises the beam geometry, and the setup in steel frames to maintain a pre-determined level of deflection. This was done to cause a saturated crack pattern and subsequently keep the cracks open in the loaded state. Note that two levels of deflection were enforced, namely 5 mm in one set of specimens and 7 mm in another set, as described in detail by Paul (2015). These deflections are more than what is expected for operational conditions for R/SHCC, to investigate chloride ingress and corrosion in a worse-case scenario. The crack patterns for these R/SHCC specimens are shown in Figure 3.9 for a central deflection of 5 mm. The chloride profiles determined by XRF, and considered to represent total chloride content based on the good correlation shown in Figure 3.11b, are shown in Figure 3.13.

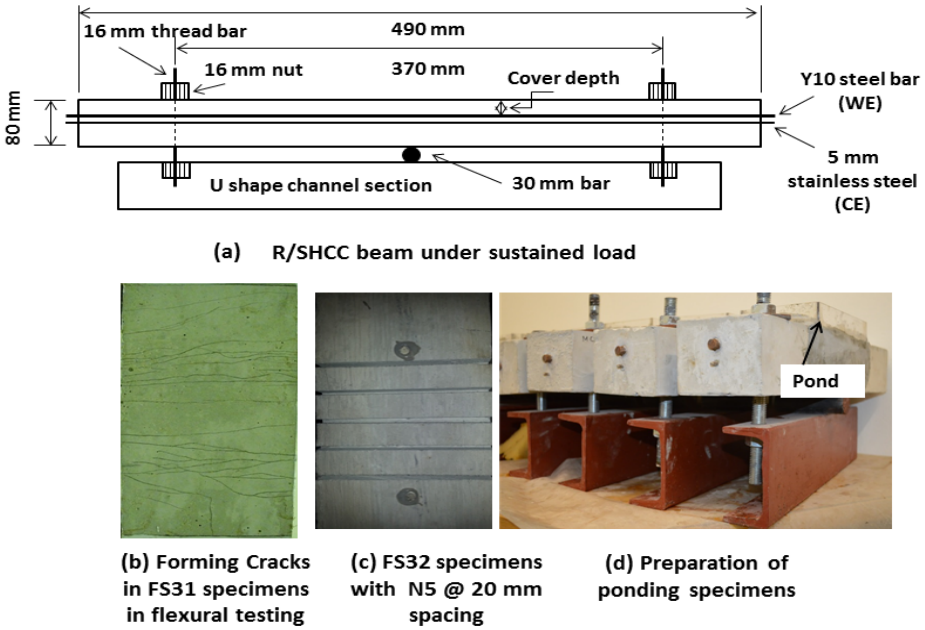

Figure 3.12: (a) R/SHCC specimen geometry and setup in steel frames, (b) crack pattern on the upper, tensile face, (b) notches for pre-set crack spacing of 20 mm on the upper, tensile face and (d), R/SHCC beams subjected to ponding on the upper, tensile faces (Paul and Van Zijl 2016).

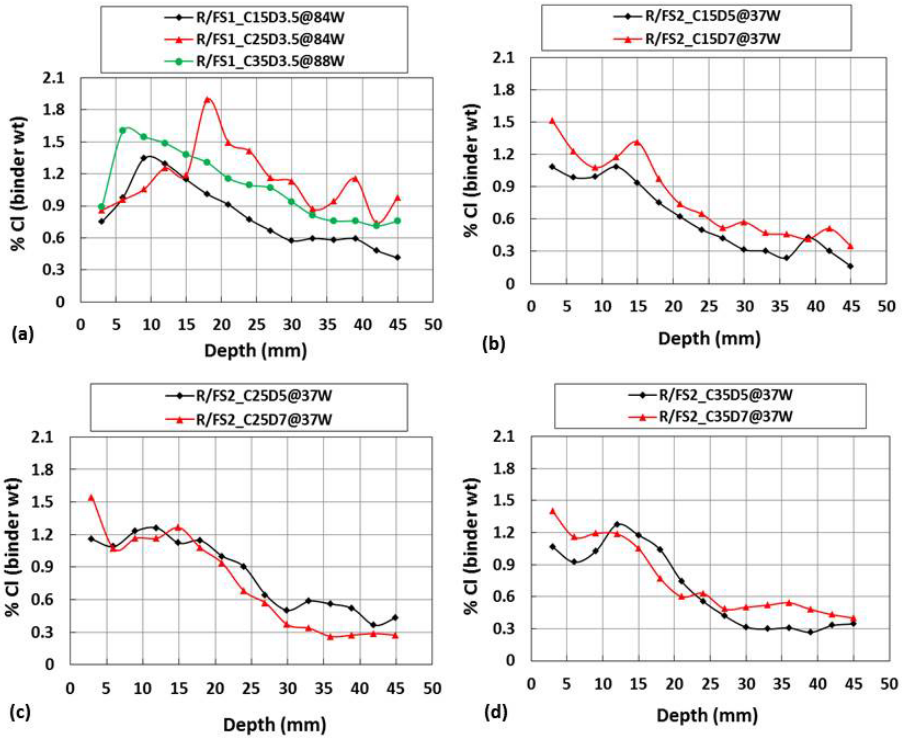

Figure 3.13: Total chloride profiles after different periods (84 weeks and 37 weeks) of cyclic wetting (3 days) - drying (4 days) by ponding with NaCl aqueous solution (Paul and Van Zijl 2016). Note that three cover depths of steel of 15, 25 and 35 mm (C15, C25, C35) and three levels of deflection (D35, D5 and D7 mm) were studied.

3.2.2.3 Corrosion in cracked R/SHCC

From the previous section it is clear that significant amounts of chloride are present at the level of the steel bars in R/SHCC, considered to be sufficient to cause corrosion initiation. For the same specimens used for chloride profiling (Figure 3.13), non-destructive corrosion rate measurements were performed at regular intervals during the exposure to cyclic wetting (3 days) and drying (four days) with NaCl aqueous solution. Finally, after the respective periods of exposure, the actual corrosion damage to the steel bars was determined by removing the bars from the specimens, cleaning and observation of distributed or pitting damage depths and areas. Reduced resistance of the bars were also determined by comparison of their tensile resistance with those of control steel bar specimens from the same batch that were not exposed to corrosion. A brief description of these main steps and the findings are presented here.

Coulostatic method

The Coulostatic measurement method has been applied by several researchers for corrosion in RC (eg. Gonzalez et al. 2001). At Stellenbosch University, laboratory equipment was developed by Mr Johan Müller, assisted by PhD-student Suvash Paul. The first simulation is illustrated in Figure 3.14, courtesy of Müller (2013a,b). The corrosion measurement strategy for the chloride-induced corrosion test specimens is schematised in Figure 3.15.

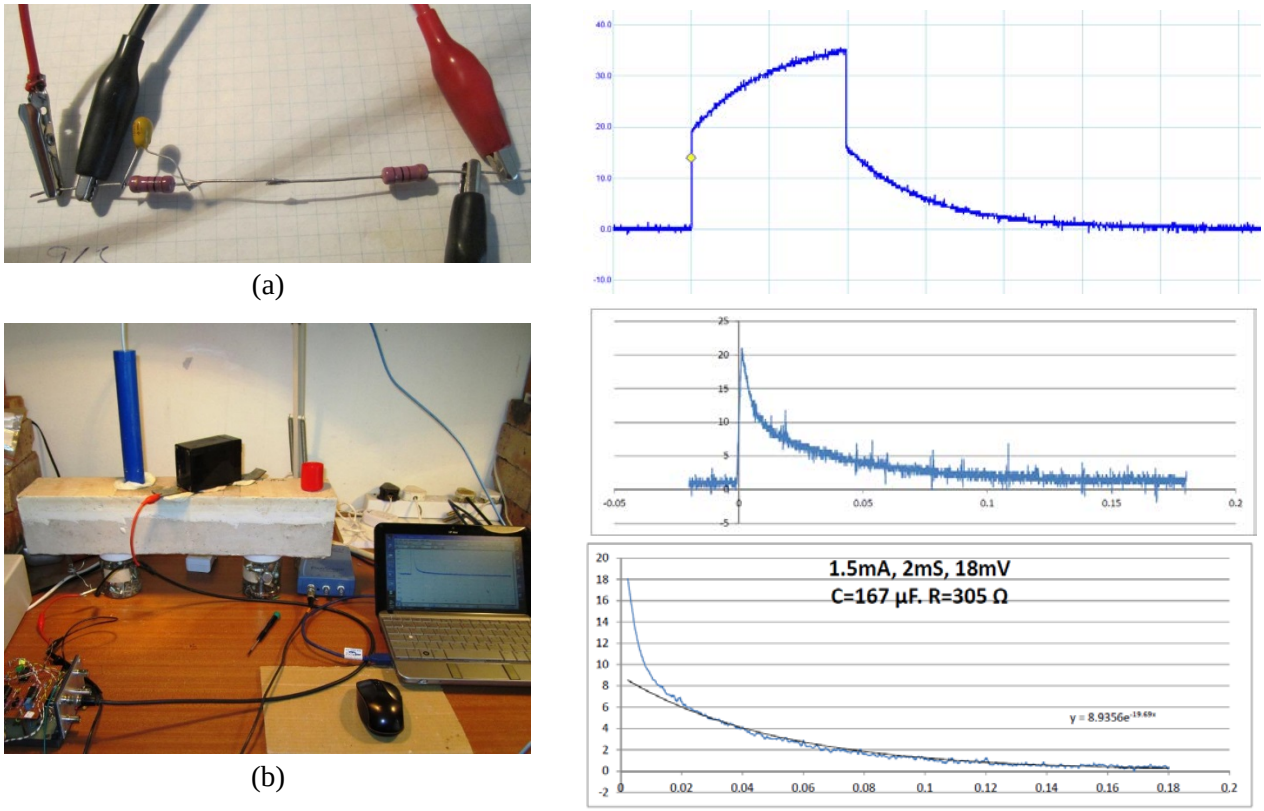

Figure 3.14: Development of Coulostatic corrosion measurement equipment, showing (a) Randles circuit and the voltage perturbation caused by an 0.2mA current pulse (Müller 2013a), subsequently tested on (b) an R/SHCC specimen, showing the perturbation and fitted exponential curve of the potential decay (Müller 2013b).

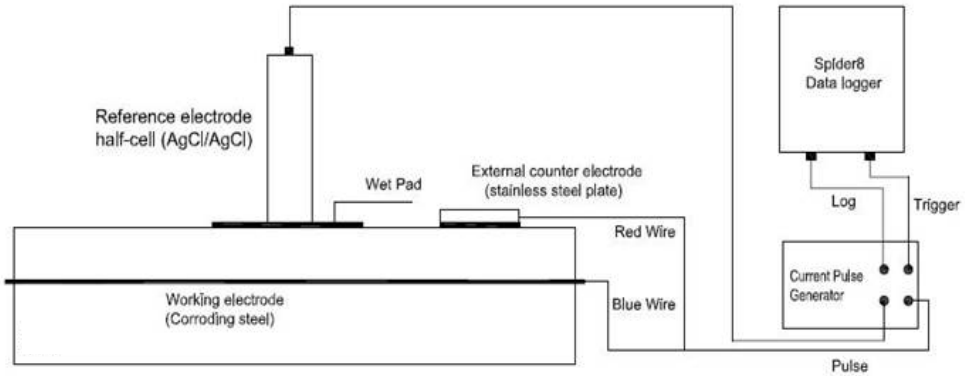

Figure 3.15: Corrosion rate measuring procedure using the Coulostatic technique (Paul and Van Zijl 2014).

The technique is described in detail by Paul and Van Zijl (2014) and in Paul (2015). The corrosion rate measurements are sensitive to temperature and moisture content. Time-integration of the corrosion rates enable more clear observation of corrosion trend. Paul and Van Zijl (2014) proposed the numerical integration of corrosion rate measurement *Vcorr* at time intervals t_i to obtain the total change in steel bar diameter $d_c(t)$ at time t due to corrosion from the following expression:

$$d_c(t) = d_{c0} + \int_0^t V_{corr}\,dt = d_{c0} + \sum_{i=1}^{N_t} \frac{1}{2}\left(V_{corr,i} + V_{corr,i-1}\right)\left(t_i - t_{i-1}\right) \qquad (3.1)$$

where allowance is made for an initial corrosion depth d_{co}, in cases where measurements start after a period of chloride-induced corrosion. Equation (3.1) was used to integrate the corrosion rates shown in Figure 3.16a, to produce the uniformly corroded depths shown in Figure 3.16b.

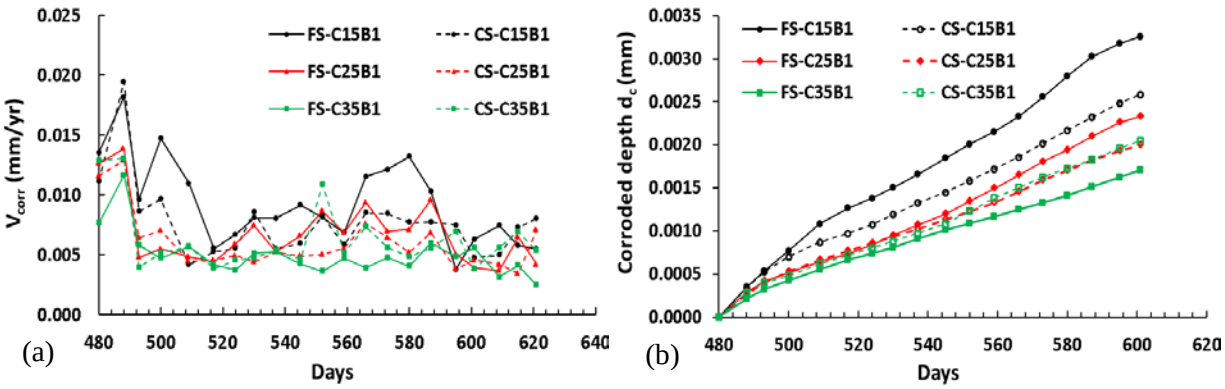

Figure 3.16: (a) Corrosion rate measurements in cracked R/SHCC specimens, and (b) time-integrated corrosion, assuming uniform corrosion over the full steel bar (Equation 3.1). The test parameters were three cover depths (C15, C25, C35 mm) and two sand types (FS – fine, CS – coarse), but a single steel reinforcing bar (B1) (Paul and Van Zijl 2014).

Parameter study: Cover depth

Various parameter studies were performed as reported by Paul and Van Zijl (2014, 2016), investigating the role of cover depth, average crack width and crack spacing. In Figure 3.17a, the computed corroded depths computed from Equation (3.1) are shown as function of the cover depths (15, 25 and 35 mm). It appears that a 15 mm cover leads to higher corrosion rate and total reduction in steel bar diameter than 25 and 35 mm covers for the SHCC types investigated. Note that the influence of cover depth, crack width and spacing (see for example Figures 3.7 and 3.9) on corrosion depth cannot be distinguished clearly. This led to the representation in Figure 3.17b,c, which shows the corroded depth as function of average crack width and spacing respectively, normalised by cover depth (C). A 15 mm cover depth causes a corrosion rate and thus corroded depth of about four times that with a 25 mm and 35 mm cover. A 35 mm cover is shown to bring no benefit in corrosion protection compared with a 25 mm cover.

Parameter study: Crack spacing

In Figure 3.12b, the inherent crack pattern on the tensile face of a typical B1 (single steel bar) R/SHCC specimen is shown, and in Figure 3.12c a specimen with five notches across the full tensile face of the specimen spaced 20 mm apart. By sawing the notches, crack spacing was indeed forced to be approximately that of the notch spacing. In this way, crack spacing was introduced as test parameter for corrosion in cracked R/SHCC. Specimens containing a single notch (N1), 3 notches at 40 mm spacing (N3) and 5 notches at 20 mm spacing (N5) were prepared and tested. An attempt was made to pre-crack the notched beams to equal crack widths in order to test the influence of crack spacing only. An LVDT was attached to the central 100 mm of each beam's tensile face to record the tensile deformation during tightening of the nuts onto the bolts at the beam ends shown in Figure 3.12a. Thereby, the horizontal deformation was controlled to 0.3 mm for N1 specimens, 0.9 mm for N3 and 1.5 mm for N5 specimens. A sample of results is presented in Figure 3.18. A higher corrosion depth is

found for a 40 mm crack spacing (N5) than for a 20 mm spacing (N3). It is acknowledged that the chloride-induced corrosion should be continued over a longer period to lead to more significant levels of corrosion. Also, the data pool must be extended, having tested only three beams of each specimen type. It is nevertheless postulated, and to an extent confirmed by the results shown in Figure 3.18, that the cathode to anode size in the electrochemical corrosion cell is reduced by a reduced crack spacing, whereby the corrosion rate is reduced.

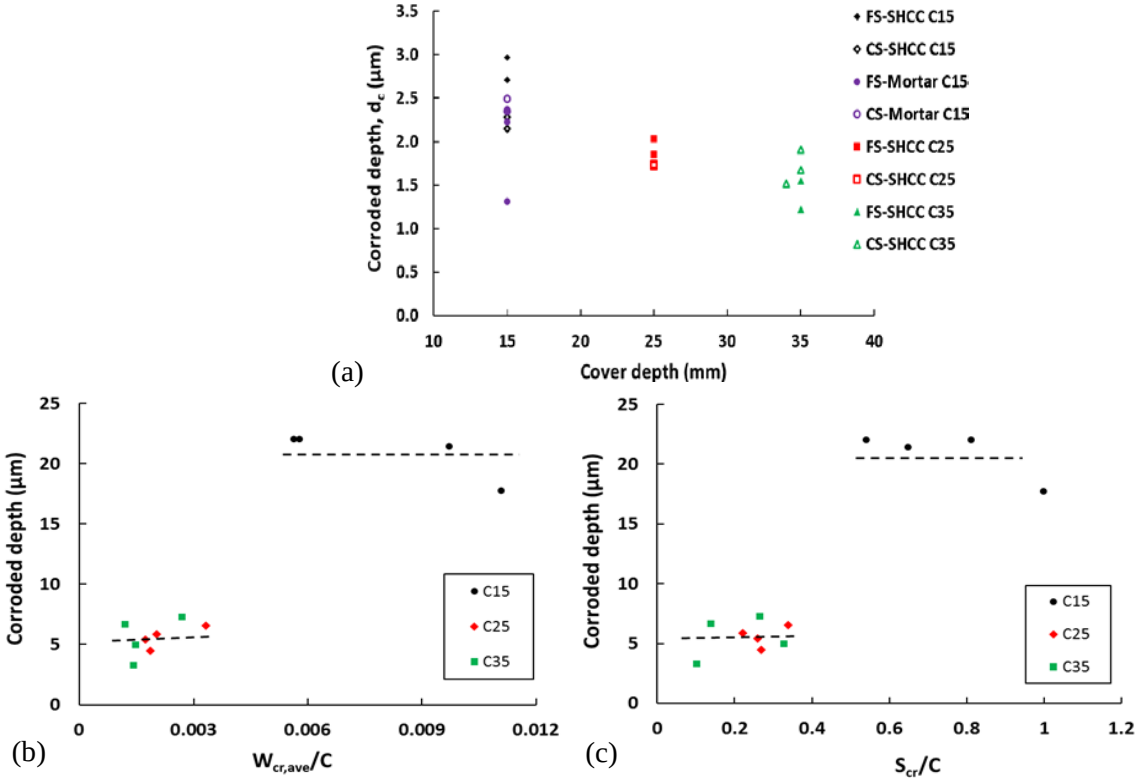

Figure 3.17: Corroded depths calculated with Equation (3.1) from corrosion rate measurements, shown as function of (a) cover depth, (b) average crack width normalised by cover depth (C) and (c) average crack spacing (S_{cr}) normalised by cover depth (Paul and Van Zijl 2014, 2016).

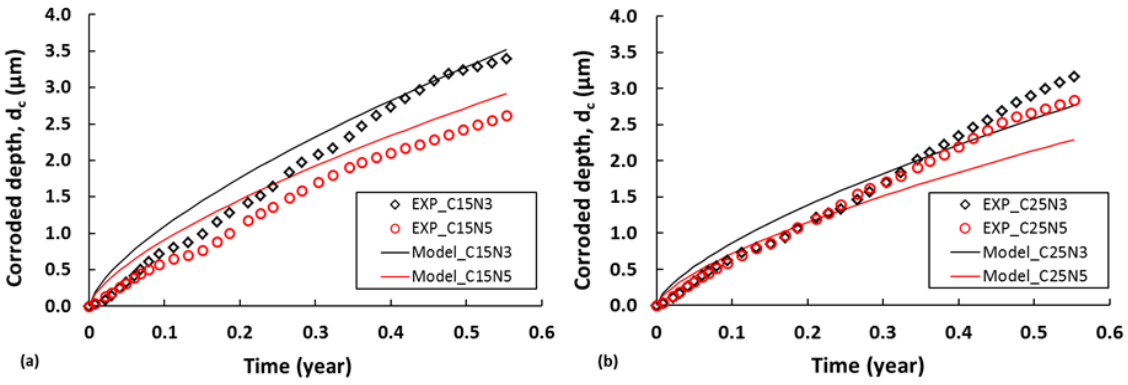

Figure 3.18: The influence of 20 mm versus 40 mm crack spacing on corroded depths in notched R/SHCC specimens N3 and N5 compared with the proposed expression (Equation 3.2) for chloride-induced corrosion rate in cracked R/SHCC, for (a) 15 mm and (b) 25 mm cover depth (Paul and Van Zijl 2016).

From the test results by Paul (2015) also reported in Paul and Van Zijl (2014, 2016), the following expression was developed for the corroded depth:

$$d_c(t) = \frac{0.35\delta_T \delta_{RH} W_{cr,ave} t^{\alpha_t} Cl_{free}^{\alpha_{cl}} S_{cr}^{\alpha_S}}{C^{\alpha_C}} \quad (3.2)$$

With time t (in years), $W_{cr,ave}$ the average crack width (in µm), Cl_{free} is the % of free chloride at the steel surface level (in % of binder mass), S_{cr} is the average crack spacing (mm) and C is the cover depth of the steel bar. Correction factors δ_T and δ_{RH} are introduced for temperature and relative humidity, both kept as 1.0 here for the specimens tested in a climate controlled room at 23±2 °C, and 55±5% RH. α_t, α_{cl}, α_S and α_C are the coefficients that depend on the ratio of wetting and drying periods, types of binder, range of maximum crack spacing and cover concrete. Here, the values of α_t, α_{cl}, α_S and α_C were determined to be 0.68, 0.5, 0.27 and 0.3 respectively, by fitting to measured data of Paul (2015). The solid lines in Figure 3.18 were computed from Equation (3.2) with these model parameters. Reasonable agreement is seen in the figure with measured data.

Actual steel bar corrosion damage

Figures 3.19a-c show X-ray computer tomography (CT) for observation of corrosion in the bar in a non-destructive manner. The steel bar was subsequently removed from the specimen, as also shown in Figure 3.19d. X-ray CT may be a suitable non-destructive method to quantify corrosion damage, due to sufficient difference in the steel bar, corrosion products and cement-based matrix densities. The reinforcing bars were removed from the remaining beams after the chloride exposure periods, for observation of the actual corrosion damage to the bars - Figure 3.20. After the accelerated chloride exposure (weekly wetting-drying cycles) for periods up to two years, insignificant damage was found in the steel bars. Bending of some bars occurred in the process of removal from the SHCC. In contrast to severely corroded reinforced concrete, where corrosion splitting and spalling of concrete may ease rebar removal, significant mechanical effort was required to remove the bars from the specimens.

To quantify actual damage, pitting depth was measured by a probe and dial gauge (Paul 2015). Figure 3.21 shows a trend of increased average pitting depth versus average crack spacing (Paul and Van Zijl 2016). Note that these are for the un-notched R/SHCC specimens.

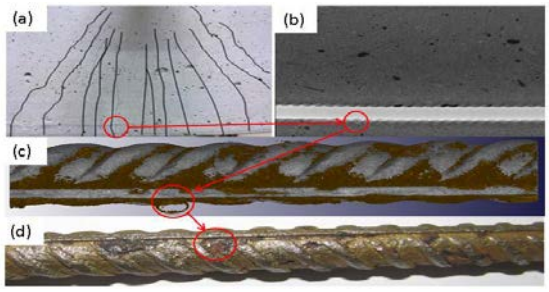

Figure 3.19: Corrosion inspection of R/FS-SHCC C15B1 steel (CT scan) method at 580 days (Paul and Van Zijl 2014).

Figure 3.20: Corroded steel bars after cleaning (Paul and Van Zijl 2014).

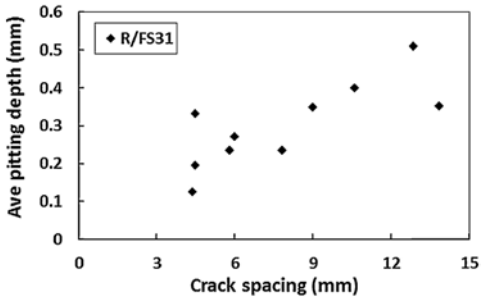

Figure 3.21: Average pitting depths versus average crack spacing in R/SHCC beam specimens (Paul and Van Zijl 2016).

Steel mass loss and final tensile resistance studies by Paul (2015) were inconclusive. A summary is given in Figure 3.22, where the estimated mass loss was calculated from the Coulostatic corrosion measurements and simple extension of Equation (3.1) for integration of mass loss. Note that mass loss measurement was done for the most recent test series of notched R/SHCC beams only, for which careful cleaning and weighing were done before specimen manufacturing, as well as after the accelerated chloride-induced corrosion over roughly 6 months. The maximum mass loss of less than 1 gram is about 0.3% of the original steel bar mass. If this is localised in an area of pitting corrosion, this may be significant, but such severe pitting was not observed. In the figure the single crack (notch N1) specimens did suffer the greatest actual mass loss for the 15 mm cover specimens (C15N1). This is not the case for the 25 mm cover, for which a reasonable explanation cannot be offered.

This research on corrosion in R/SHCC reported here has barely scratched the surface, considering the pool of data built over decades of dedicated research on corrosion in RC by comparison. It has nevertheless shed light on the relatively low corrosion rates in cracked R/SHCC compared with RC. Important mechanisms and parameters have been verified, albeit with limited data sets. Also, monitoring of corrosion in actual structures, in order to link accelerated exposure with actual corrosion rates are required in a next step. Clearly, the notion that corrosion initiation marks the end-of structural life is not realistic, should the potential durability of this strain-hardening construction material be exploited to the full. A design strategy should be based on predicted, reliable corrosion rates, and well-defined limit states. This is subject to continued research by the CDSI.

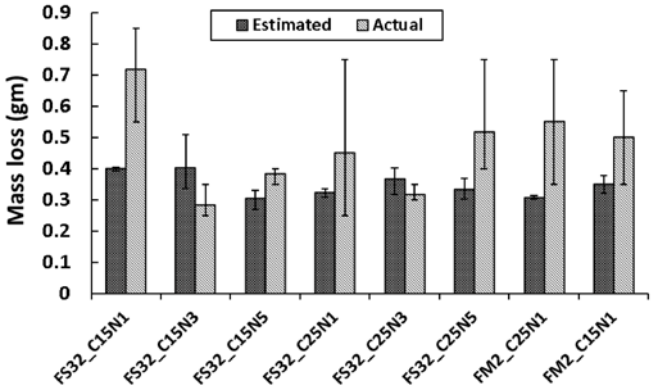

Figure 3.22: Steel reinforcing bar mass loss due to chloride-induced corrosion (Paul 2015).

3.3 Crack formation and ASR

Alkali silica reaction (ASR) is a well-known deterioration process in concrete, a reaction between certain forms of silica in aggregates with high alkaline pore solutions in concrete. The reaction product is lower in density, leading to expansion and build-up of internal pressure which eventually leads to cracking. Knowledge of ASR has been increasing over the past several decades, but the number of structures affected in South Africa and world-wide appears to increase.

3.3.1 Structural effects of ASR in RC structures

Three affected local structures are the Good Hope centre in Cape Town (Figure 3.23), the Danie Craven Stadium (Figure 3.24) in Coetzenburg, Stellenbosch, and the Kleinplaas dam in the Jonkershoek valley, Stellenbosch. The structures shown in Figure 3.23 and 3.24 have been repaired, but show continued ASR reaction and cracking. This is not unexpected, as it is usually not possible to stop or reduce the ASR affinity, i.e. the remaining ASR reaction potential, by the repair intervention. The strategy is usually to stop or slow the reaction down, by for instance sealing or water repellent treatment, as water is an essential ingredient for ASR.

Figure 3.23: Good Hope Centre, Cape Town, design by Studio Nervi, Italy in 1977 and constructed in 1978-1979. ASR was diagnosed in 1981 by Dr RE Oberholster (CSIR). Repairs were done, but recent photos shown here indicate significant ASR cracking of the main arch plinths.

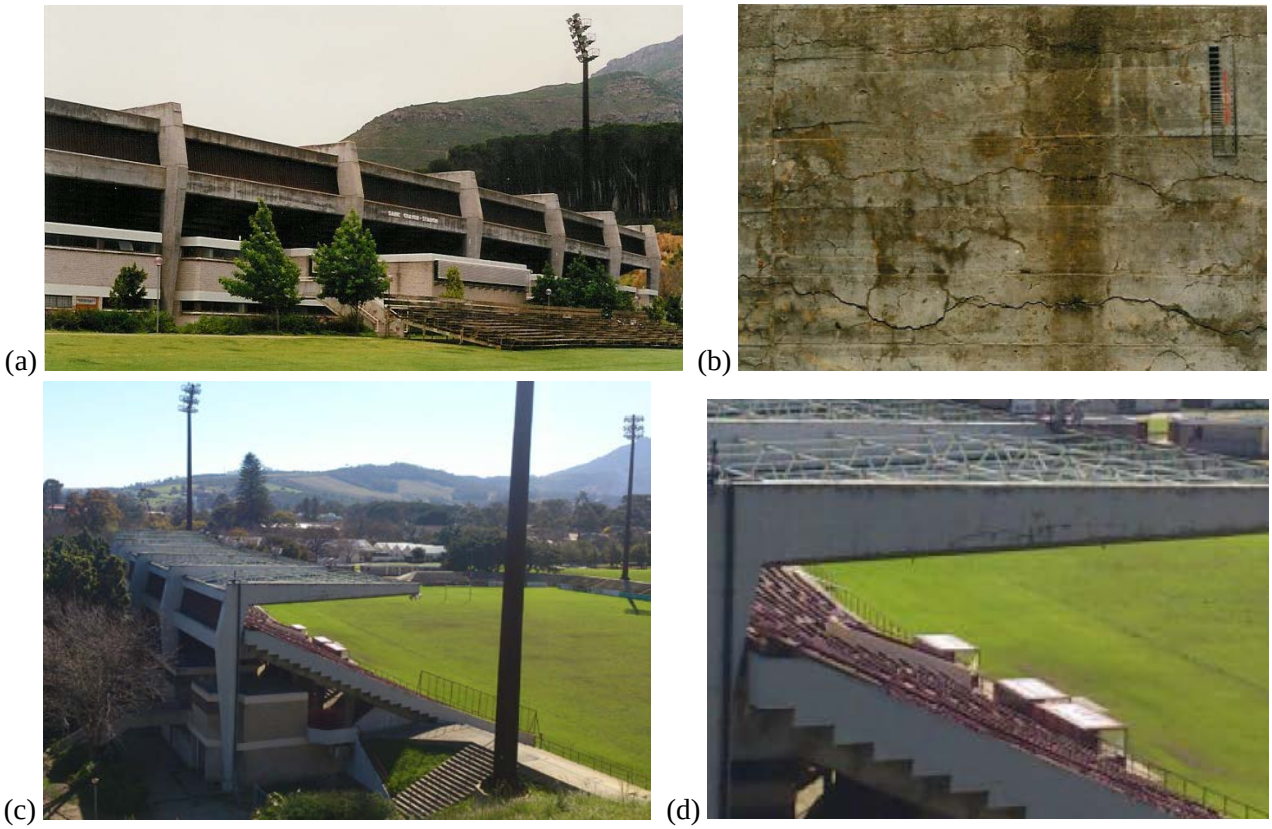

Figure 3.24: Danie Craven Stadium in Coetzenburg, Stellenbosch, showing (a) typical ASR cracking and stains, and (b) a close-up photo of ASR map cracking in one of the main cantilever beams when ASR was diagnosed in the structure (Oberholster 1990). After repairs in 1991 (c) a recent photo shows (d) reappearance of ASR cracks in places.

The results of ASR deterioration are unsightly cracking and discolouring, but also potentially significant loss of resistance, stiffness and vibration frequency. In a hypothetical study of the Danie Craven Stadium by de Villiers (2013), the dynamic response under crowd excitation was analysed. Considering a half sine dynamic force-time function caused by a single person jumping (Dazio 2013) with dynamic amplitude several times that of the person's weight, and incorporating crowd behaviour as proposed by Ellis and Ji (2004), the dynamic response of the structures was computed using the finite element model shown in Figure 3.25a. Cracking caused by ASR deterioration may reduce flexural stiffness of a structural element significantly. De Beer (2014) created artificial cracks in cantilever RC beams and monitored the flexural stiffness reduction, as well as the reduction in frequency associated with the first natural vibration mode. In a cantilever, the stiffness may be reduced to less than one fifth of the virgin stiffness. Considering a hypothetical case of severely deteriorated structural elements retaining only 30.8% of their virgin structural stiffness, a jumping crowd may cause accelerations of the stadium that may cause discomfort or even panic. Threshold accelerations associated with various degrees of human discomfort are given in Table 3.1 (Ellis and Ji 2004). Table 3.2 summarises the findings by De Beer (2014), that crowd jumping at 1.5 Hz may cause disturbing accelerations in the stadium, while simulated crowd jumping at 2.5 Hz, which is considered to be the upper limit for a crowd, causes accelerations that may cause panic. The deformed shape for the latter case is shown in Figure 3.25b. It is emphasized that the study assumed a hypothetical case of severe damage, which, from visual inspection in 2013-2014, has not realised. A thorough assessment of the current level and extent of ASR damage is advised.

Table 3.1: Acceleration comfort levels for humans occupying a stadium (Ellis and Ji 2004).

Measured acceleration	Human reaction
0-0.05g	Reasonable limit for passive person
0.05g-0.18g	Disturbing
0.18g-0.35g	Unacceptable
>0.35g	Probably causing panic

Table 3.2: Maximum accelerations for the case of a ASR deteriorated, full stadium under dynamic crowd load (De Beer 2014).

Jumping frequency (Hz)	% of original stiffness	Acceleration	Human comfort level
1.5 Hz	100%	0.042	No problem
	30.8%	0.068	Disturbing
2.5 Hz	100%	0.066	Disturbing
	30.8%	0.438	Panic

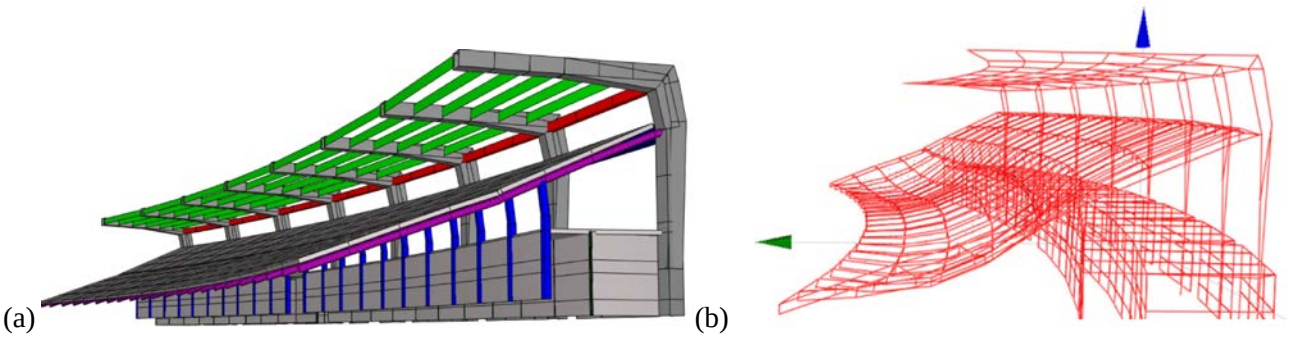

Figure 3.25: (a) Finite element model of the stadium structure (de Villiers 2013) and (b) shape of the dynamic deformation, with deformations enlarged for visualisation (De Beer 2014).

3.3.2 Mechanical cracks and ASR in plain concrete

ASR affects many structures world-wide. While guidelines for concrete mix design exist towards reduced risk of ASR in new structures (eg. Fulton 2009), guidelines for efficient treatment of affected structures are required. A research program was launched by the CDSI to study ASR of locally produced concrete, with aggregates and binders of the region. While developing insight in ASR susceptibility, swelling and deterioration of local concretes was an objective, a particular focus was on the combined condition of mechanically induced cracks and ASR exposure.

3.3.2.1 Developing a local test facility for ASR deterioration

Test equipment for accelerated ASR testing was developed by PhD-student Salhin Alaud in 2012-2013. They comprised stainless steel chambers insulated with wood panels as shown in Figure 3.26 for simulating exposure conditions according to ASTM C-1260 (Figure 3.26a) in hot (80 ^{o}C) sodium hydroxide (NaOH) aqueous solution, and according to ASTM C-1293 (Figure 3.26b) for submergence of concrete specimens in warm (38 ^{o}C) water. In each of the two chambers, partitions were made for two different conditions. In the chamber for hot exposure (Figure 3.26a), the separate partition was used for pure hot water, while the partitions in the

second device were used to test ASR deterioration under submerged conditions, as well as subject to high humidity (> 90%). In the latter warm test conditions, NaOH was mixed into the concrete specimens instead of into the water in the test chamber.

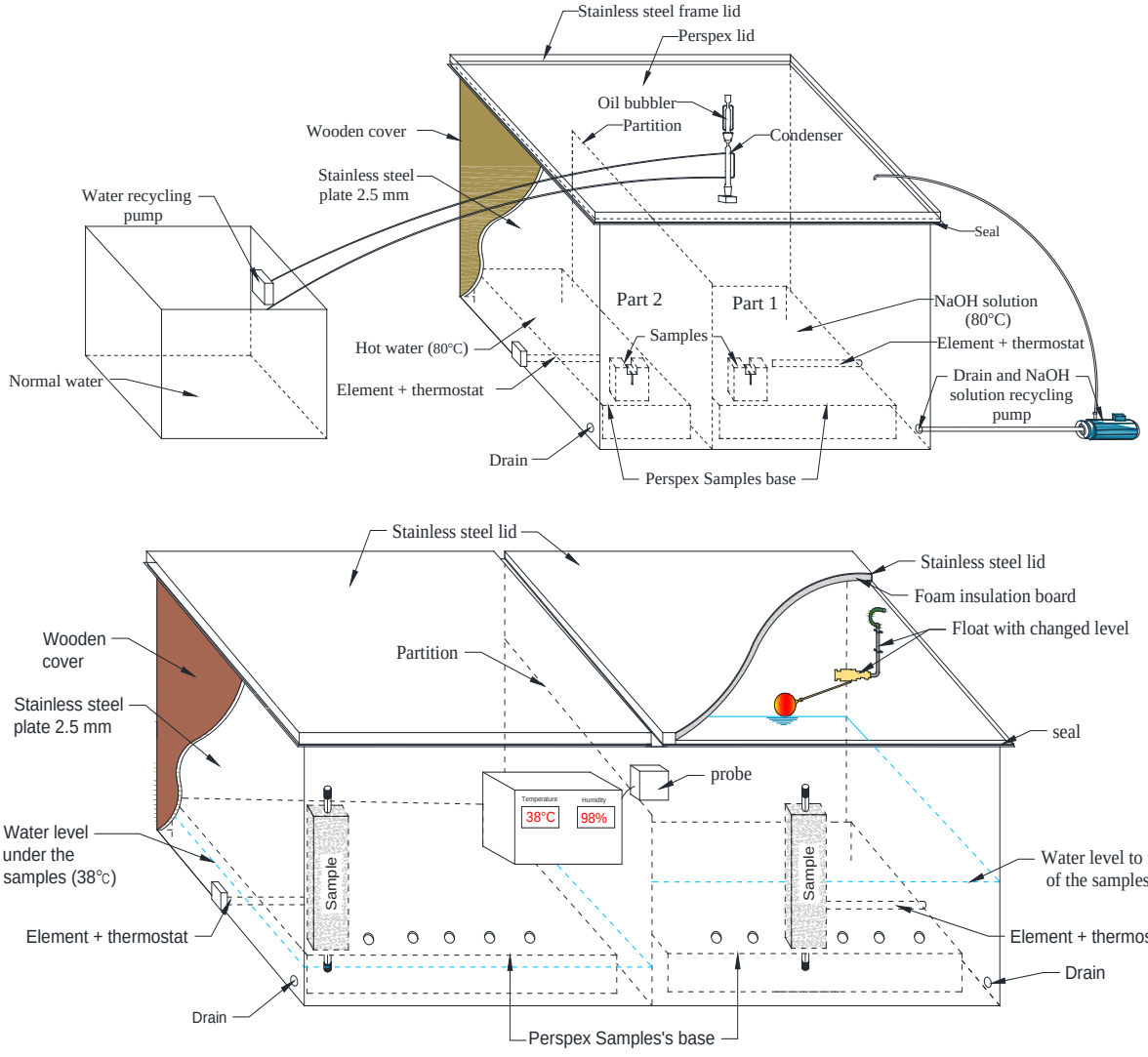

Figure 3.26: Accelerated ASR test chambers (a) with provision for a part containing hot (80 °C) water partitioned off from a part for hot (80 °C) NaOH aqueous solution according to ASTM C-1260, (b) with a part for warm water (38 °C) submergence of specimens according to ASTM C-1293 and a separate part for exposure to partial submergence and conditions of warm (38 °C) high humidity (>90%) (Alaud and Van Zijl 2016).

3.3.2.2 Characterising ASR deterioration in local concretes to the Western Cape region in South Africa

A test program was launched to characterise ASR in typical local concretes. Local coarse Greywacke (Gw) aggregate, known to be reactive, and a less reactive local Granite (Gr) aggregate were used in mixes, combined with natural silica sands from local sources, namely Philippi dune sand and Malmesbury sand. A CEM I 52.5N cement was used as binder, and blended in half of the specimens in a 50:50 mix with a ground granular Corex

slagment from a local steel manufacturing plant in the Western Cape. Corex slag is typically used in concrete mixes locally to reduce the alkalinity to reduce risk of ASR deterioration. The specimens are denoted by the abbreviations in Table 3.3, after the aggregate type, whether it contains Corex slag and the exposure (/w denoting submersion in water, and /H in high humidity (> 90%). These mixes were used to determine compressive strength and Young's modulus development in the various exposures in the test chambers. A control set was kept in the curing bath at 23±2 ^{o}C. The test program outline is given in Figure 3.27 and the main results are summarised in Figure 3.28 in terms of E-moduli and compressive strength as function of concrete age and exposure. It is acknowledged that these mechanical properties are often expressed as function of ASR swelling. Nevertheless, the results here confirm that compressive strength is less affected by ASR deterioration than the E-modulus. Also, the E-modulus of the specimens containing Greywacke, no Corex slagment and that were submerged in warm water was the most effected, confirming the reactivity of this aggregate, and the mitigation of ASR by replacement of cement with Corex slag. This is confirmed by the mapped cracking, which is most significant on the Gw/w specimens (Figure 3.29).

Table 3.3: Concrete mix ingredients and amounts (kg).

Series	Mix	Binder		Coarse aggregate		Fine aggregate		Water	NaOH
		CEM I 52.5	Corex slag	Granite	Greywacke	Philippi	Malmesbury		
Test Series 1	Gw	440	-	-	1000	-	815	184	-
	Gn	440	-	1000	-	815	-	220	-
	Gw-co	220	220	-	1000	-	815	202	-
	Gn-co	220	220	1000	-	815	-	226	-
Test Series 2	Gw/w Gw/H	440	-	-	1000	815	-	208	5.63
	Gn/w Gn/H	440	-	1000	-	815	-	212	5.63
	Gw-co/w Gw-co/H	220	220	-	1000	815	-	212	5.63
	Gn-co/w Gn-co/H	220	220	1000	-	815	-	216	5.63

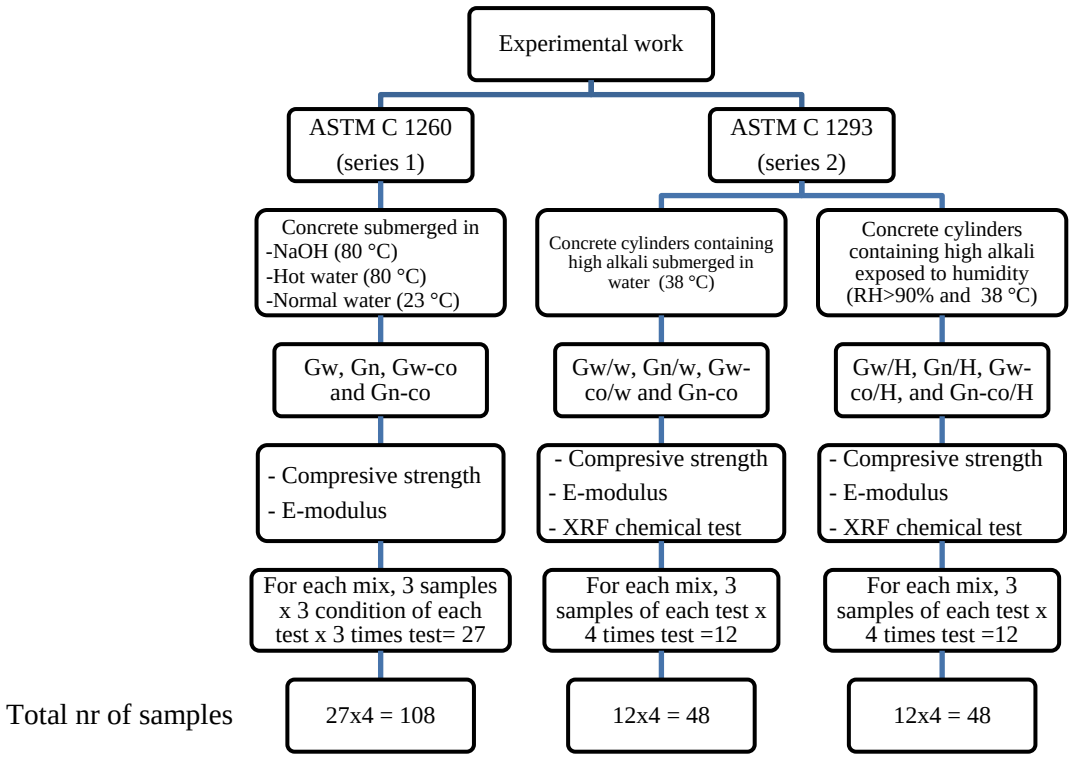

Figure 3.27: Test program for ASR deterioration of strength and E-modulus of local concretes (Alaud 2016).

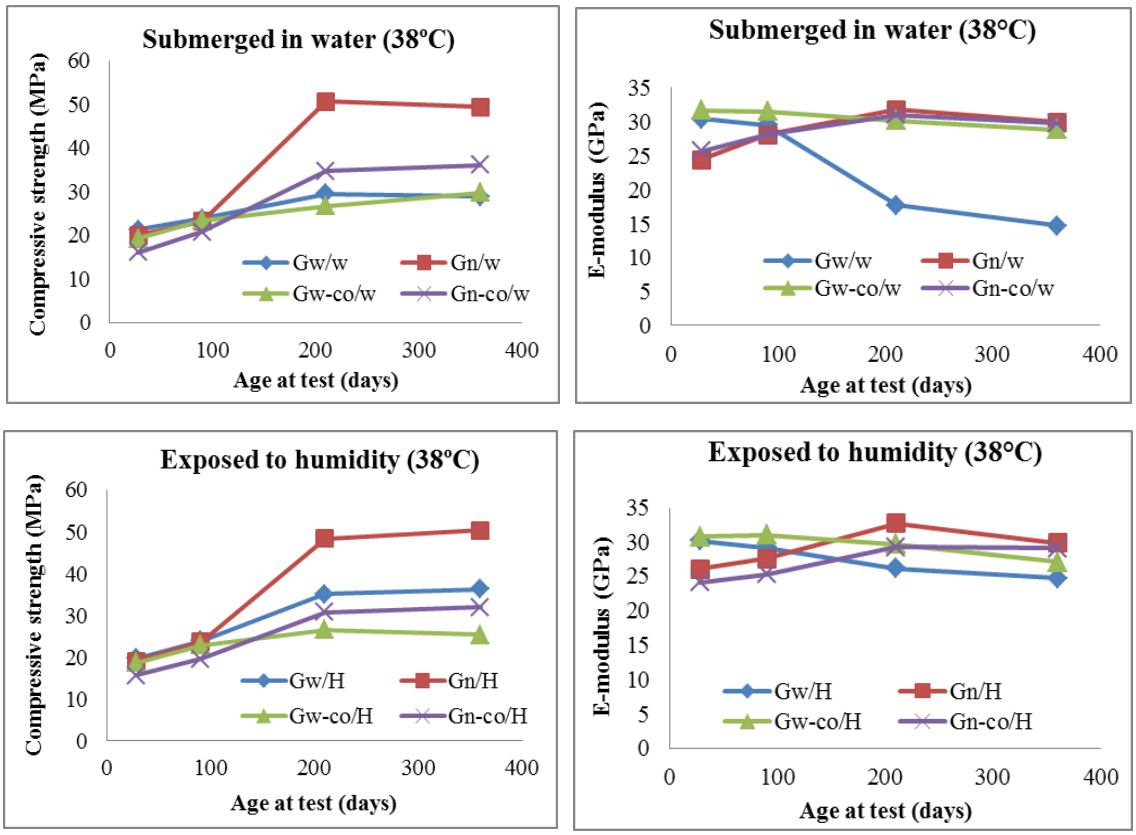

Figure 3.28: (Left) Compressive strength and (right) E-modulus development in time under various exposures (Alaud 2016).

Figure 3.29: Specimens after 1 year submerged in water at 38 ^{o}C (Alaud 2016).

3.3.2.3 Combined action of mechanical-induced cracks and ASR in concrete

To study the interaction of ASR deterioration with mechanically cracked specimens, a second experimental series was performed, as outlined in Figure 3.30, now only using the reactive Gw specimens, and those mitigated with Corex slag (Gw-co), tested in the hot (80 ^{o}C) water and NaOH solution (ASTM C-1260) chamber shown in Figure 3.26a. Wedge-splitting was executed to pre-crack specimens, on centrally slotted (30 mm wide by 20 mm deep) and notched (3 mm wide and 30 mm deep) cube specimens with 100 mm side lengths as shown in Figure 3.31. A closed-loop Instron materials testing machine (MTM) was used to perform the wedge splitting test, and to record the loading applied. Two LVDTs, one on each side of the notch as shown in Figure 3.30a, recorded the deformation, of which one controlled the crack mouth opening rate.

The specimens were placed in the chamber directly after stripping them from the steel moulds one day after casting. Half were placed in the hot water partition, and the other half in the hot NaOH solution partition. One month later, the specimens were removed for the wedge-splitting test, after which they were returned to their respective exposure conditions. High resolution photos were taken with a digimicro (dnt) camera with a magnification factor 35 before returning them to their hot submerged exposures. After subsequent weeks 1, 2, and 4 of submersion, the specimens were removed and photos carefully taken of the cracks in the same positions and with the exact same camera settings. After the 4th week, all the specimens were left outside the chamber in the laboratory for 1 week, after which photos were again taken, i.e. 5 weeks after pre-cracking.

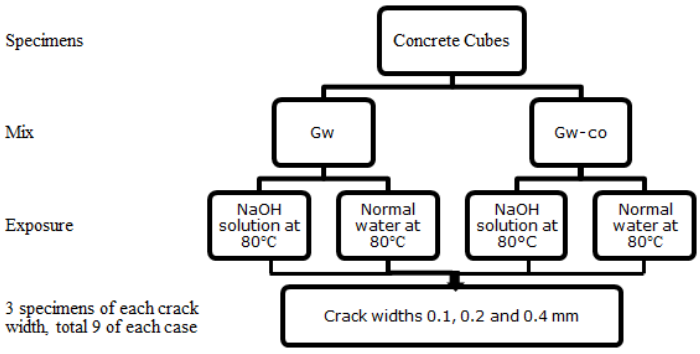

Figure 3.30: Test program for combined action of ASR and mechanical cracks in concrete (Alaud 2016).

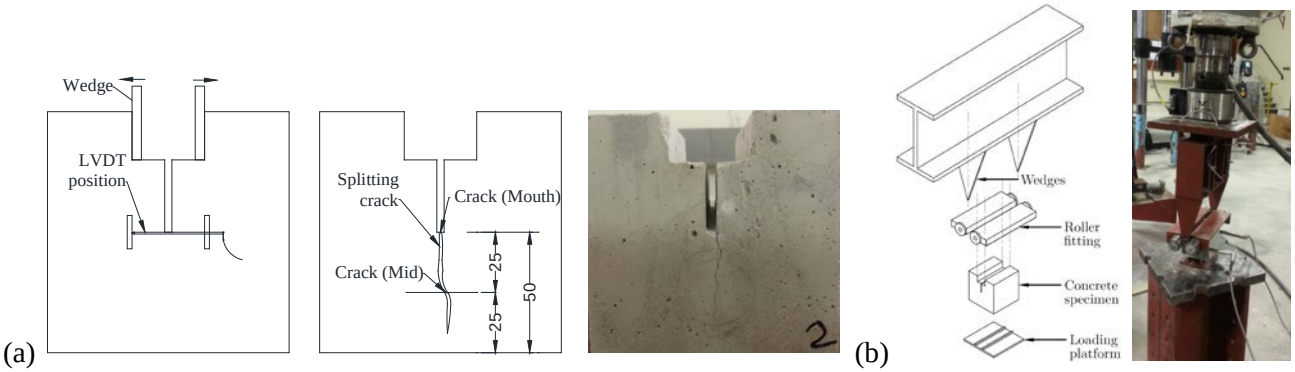

Figure 3.31: Wedge-splitting (a) specimens and (b) setup (Alaud and Van Zijl 2016).

From the photos, crack widths were carefully determined at the crack mouth and at mid-height, the positions shown in Figure 3.31. The results are shown in Figure 3.32 in terms of average crack width reduction for the two concrete types, subjected to hot NaOH and water. The results show that the crack widths were reduced due to concrete expansion. This reduction in crack width was more in the specimens immersed in hot NaOH solution, compared with those immersed in hot water, and most pronounced for the reactive Greywacke aggregate and no Corex slag (Gw/A, compared with Gw/w).

In Figure 3.33, the final crack reduction after 5 weeks is showed for each specimen, as function of the pre-crack width. Note that the pre-crack widths of 0.1, 0.2 and 0.4 mm were not achieved exactly, as reflected by the crack widths of up to more than 0.6 mm on the horizontal axis of Figure 3.33. More significant crack reduction is found for small crack widths, roughly less than 200 μm, than for wider cracks. Figure 3.34 shows an example series of photos of the same specimen, where partial closure of a secondary crack can be seen.

The largest crack closure occurs in the Greywacke mix without Corex slag in the hot NaOH solution. The crack closure is attributed to swelling due to thermal and hygral expansion, as well as ASR. The crack is a region of no or less restraint, where the overall dimensional change of the specimen causes the crack width to reduce. It is proposed that this reduction and even closure of a mechanically induced crack may be exploited in a repair strategy. It may be beneficial to allow such freedom within mechanical cracks as regions of ASR swelling which do not contribute to ASR-induced pressure build-up and cracking. However, cracks should not be allowed to act as pathways for deleterious gases and ions causing other deterioration processes. Larger cracks should be filled or sealed with a deformable material, while finer cracks could be impregnated with silane-solution for water repellence. Suitable repair materials and testing of this repair strategy are identified as research needs.

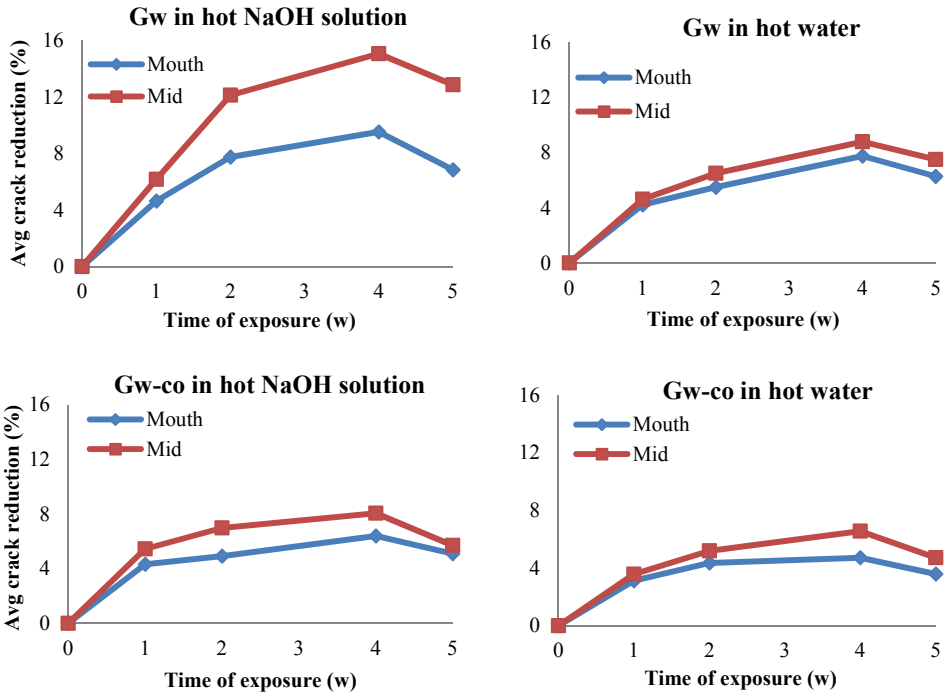

Figure 3.32: Average crack width reduction (Alaud and Van Zijl 2016).

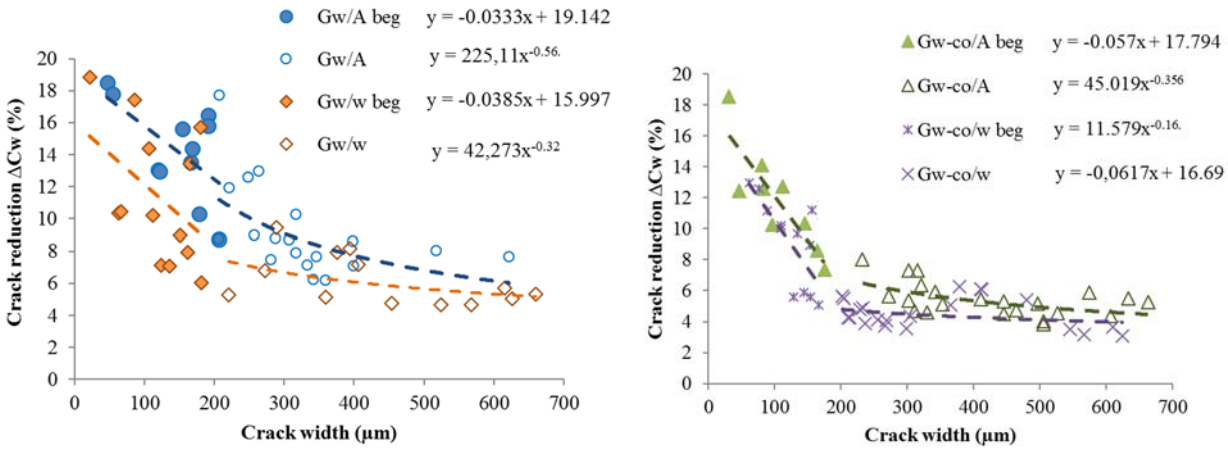

Figure 3.33: Average crack width reduction (Alaud and Van Zijl 2016).

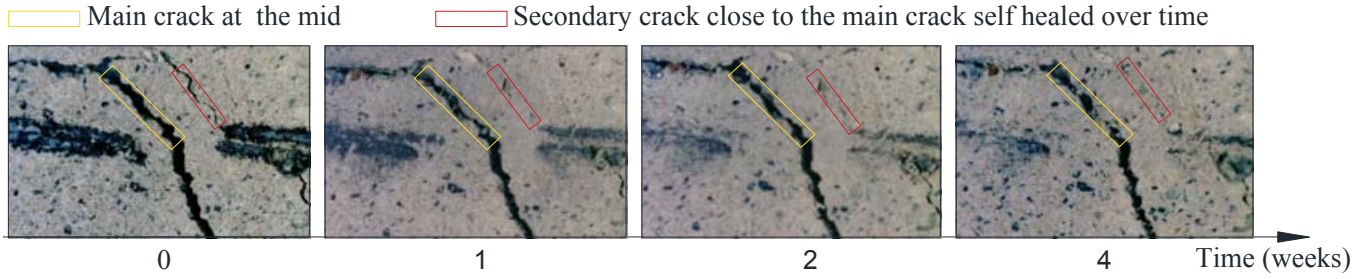

Figure 3.34: Photos of cracks after wedge-splitting (0) and after 1, 2 and 4 weeks in hot NaOH aqueous solution, showing a secondary crack closing completely (Alaud and Van Zijl 2016).

3.3.3 Mechanical cracking and ASR in RC

The combined effect of mechanically induced cracks and ASR was studied also for RC beams. Cracks were caused by cyclic tensile loading between 40 and 62 kN. The cyclic load-deformation response is shown in Figure 3.35. This loading range was chosen from monotonic test results, to ensure crack formation in each specimen. Specimen dimensions are shown in Figure 3.35. Each specimen contained a central 16 mm diameter bar. Thread was cut into the bar ends for attachment and mechanical tensile loading. To ensure crack formation at mid-height, the central 50 mm length of bar was machined down to 13 mm diameter. Deformation measurements were performed manually with a Marcator 1075R extensometer with resolution of 1 μm over 100 mm gauge lengths, of which target disc sets were attached on two opposite faces of each specimen as shown in Figure 3.35. An extensive test program was executed as outlined in Figure 3.36 and as described in detail by Alaud (2015).

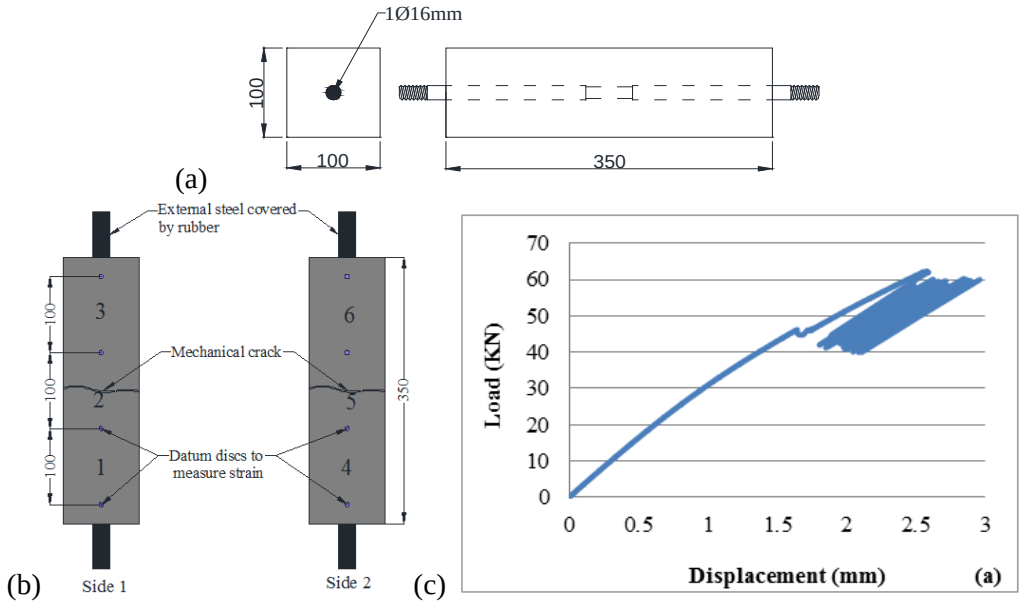

Figure 3.35: RC specimen (a) geometry, (b) gauge regions on two opposite faces and (c) typical cyclic loading-deformation response to the pre-cracking (Alaud 2016).

A subset of results of Series 2 is discussed here. Average strains measured on the (pre-)cracked and uncracked Gw and Gw-co specimens are summarised in Figure 3.37. Note that the deformations used for calculating the strains on (pre-)cracked specimens exclude the pre-crack, and thus reflect the deformations after the pre-cracking at an age of 4 weeks in Figures 3.37a,c. From the results it is clear that the deformation measured over the central, cracked gauge length in Figure 3.37a is less than the deformation on an uncracked specimen. This is ascribed to the crack removing the central restraint to continued ASR swelling, whereby the overall length change in the central region is reduced compared with an uncracked specimen. In Figure 3.37b the opposite trend is seen. The deformations shown there are for Gw specimens in the upper and lower gauge areas that do not include the crack. Here, the larger deformation in the pre-cracked specimens than in the uncracked specimens is ascribed to a higher reactivity caused by warm water reaching also the cracked surfaces. Reduced restraint by the steel bar on the swelling concrete in this region of the cracked specimen may also contribute to this larger deformation in the cracked specimens.

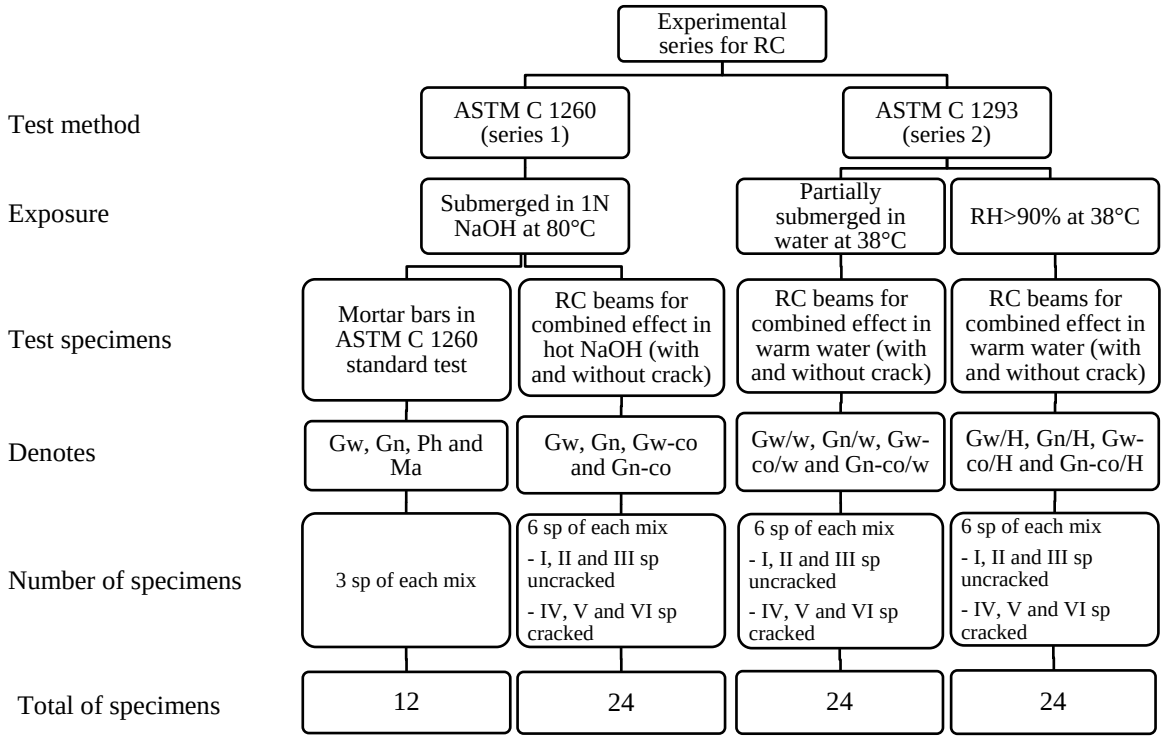

Figure 3.36: combined action of ASR and mechanical cracks in RC (Alaud 2016).

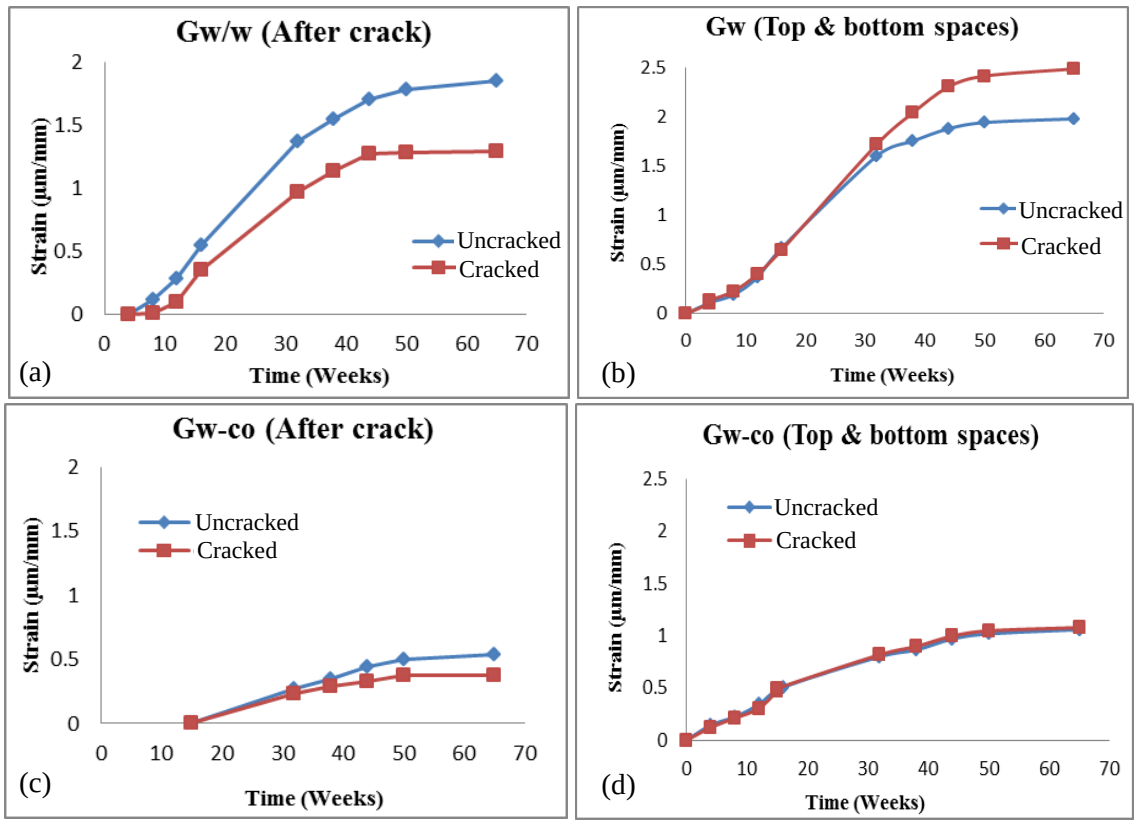

Figure 3.37: Average strains measured on Greywacke specimens in warm (38 ^{o}C) water measured over (a) the central, cracked gauge length under combined action of ASR and mechanical cracks in RC (Alaud 2016).

The mitigating effect of reduced alkalinity by inclusion of Corex slag is seen in Figures 3.37c,d. No or low reactivity and associated swelling is argued to lead to the relatively small difference in deformation between pre-cracked and uncracked specimens.

It is concluded that mechanical cracking may lead to increased reactivity due to the access of water to accelerate the ASR reaction. On the other hand, the crack provides space for pressure-free swelling. Crack measurements from high resolution photos in Figure 3.38 confirm that the width of mechanically induced pre-cracks reduce. In the figure an ASR crack running perpendicular to the mechanical crack can be seen to grow wider, near doubling from week 32 to week 65 of continued accelerated ASR exposure.

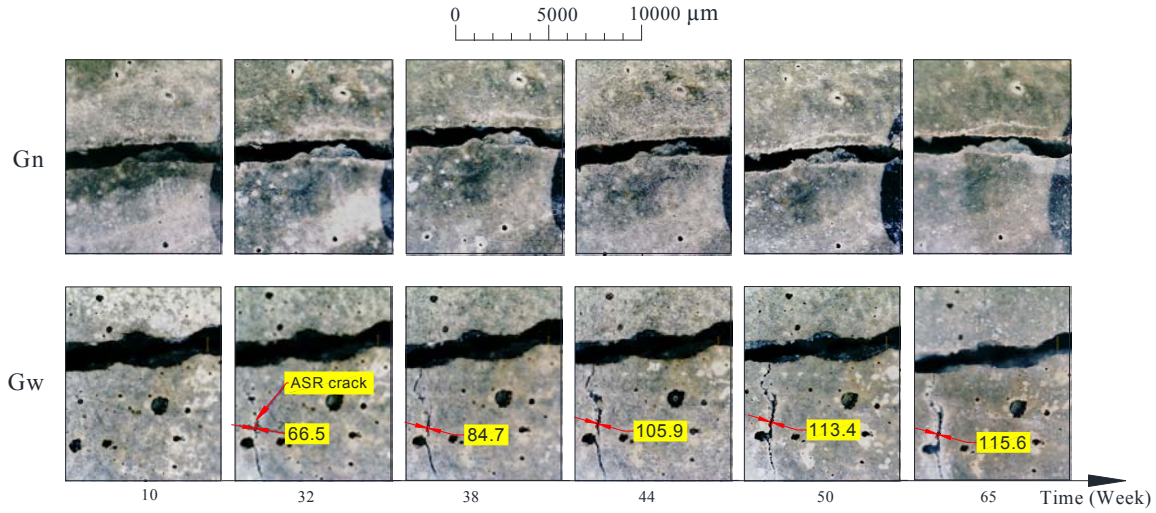

Figure 3.38: Reduction of the mechanical crack width in a steel bar reinforced Greywacke specimen (bottom), but relative insignificant reduction in a Granite aggregate specimen (top). Also shown is the initiation and increase in width of an ASR crack in the GW specimen (Alaud 2016).

3.4 Concluding remarks

The contributions on durability of recycled concrete aggregate, chloride-induced corrosion in R/SHCC, and ASR are topics of international research focus. In particular the work on R/SHCC was performed as contribution to the activities of RILEM TC 240-FDS, which the author chaired. This TC followed on TC 208-HFC to investigate actual deterioration processes in cracked SHCC. The results on chloride profiles in cracks in R/SHCC (Paul et al. 2016) are novel, and are included in Chapter 2 of the state-of-the-art report of TC 240-FDS (Van Zijl and Slowik 2016). Also, the monitoring of the subsequent corrosion damage to steel embedded in cracked SHCC, and the importance of crack spacing (Paul and Van Zijl 2016) are novel, and included in Chapter 9 of the STAR (Van Zijl and Slowik 2016). The low corrosion rate in finely cracked R/SHCC, despite sufficient amounts of chloride, oxygen and water present, remains to be formulated in durability design guidelines that accept gradual corrosion deterioration in R/SHCC, as opposed to the conservative approach where the initiation of corrosion is considered to be the end of structural life, or a signal for repair. The latter approach is due to the unpredictable, fast nature of macro-cell electrochemical corrosion in RC, as opposed to the low corrosion rates in R/SHCC due to the small cathode to anode ratios caused by fine crack spacing. This work is foreseen to continue, and the International Conference series SHCC, of which the author is co-founding member and Vice-President, is a suitable forum for the durability research community.

The results on crack formation and durability have raised international interest, reflected by keynote lectures by the author at the Australian Concrete Conference held in Melbourne in September 2015, at the Conference on Advances in Cement and Concrete Technology in Africa (ACCTA), held in Johannesburg in January 2013, SHCC2 in Rio de Janeiro in November 2011, and the ASMES International workshop on Basic Research on Concrete and Applications, held in July 2011 in Lausanne, Switzerland. This also led to invitations to present short seminars at the Department of Civil and Environmental Engineering in Nanyang, Singapore in June 2015, hosted by Dr En-Hua Yang, and in June 2010 at the Department of Civil Engineering in Gifu, Japan, hosted by Professor Keitetsu Rokugo.

Best paper awards were received for durability related research publications, the first for PhD student SC Paul (2015) at the Sustainable Construction Materials and Technologies Conference in Kyoto, Japan in August 2013, which led to the publication of the paper in the Advanced Concrete Technology Journal (Paul and Van Zijl 2013a), and the second (Van Zijl et al. 2016) was selected one of ten outstanding papers in 2015 by the Materials and Structures Board of Editors.

References

Alaud SM and Van Zijl GPAG 2014. Role of mechanical load and Alkali Silica Reaction in concrete, International Congress on Durability of Concrete ICDC, 4-6 December 2014, New Delhi, India.

Alaud SM and Van Zijl GPAG 2016a. Effects on concrete properties by ASR deterioration under different exposure conditions. SEMC, 5-7 September 2016, Cape Town, South Africa.

Alaud SM and Van Zijl GPAG 2016b. Role of pre-crack formation and Alkali Silica Reaction in concrete. 15th International Conference on Alkali Aggregate Reaction (15th ICAAR), 3-7 July 2016, Sao Paulo, Brazil.

ASCE 2005. Report card for America's Infrastructure, American Society of Civil Engineers, Washington, USA.

ASCE 2013. Report card for America's Infrastructure, American Society of Civil Engineers, Washington, USA.

ASTM C-1260 2007. ASTM, Standard Test Method for potential alkali reactivity of aggregates (Mortar-Bar Method, D), Annual Book of ASTM Standards, American Society for Testing and Materials.

Boshoff WP 2007. Time-dependant behaviour of Engineered Cement-based Composites. PhD dissertation, Stellenbosch University, South Africa.

Boshoff WP, Adendorff C and Van Zijl GPAG 2009. Creep of pre-cracked strain-hardening cement composites (SHCC), Proceedings of 8th International Conference on Creep, Shrinkage and Durability of Concrete and Concrete Structures (CONCREEP 8), Oct 2008, Ise-Shima, Japan, pp. 723-728

Boshoff WP, Altmann F, Adendorff CJ, Mechtcherine V 2015. A new approach for modelling the ingress of deleterious materials in cracked strain-hardening cement-based composites. Materials & Structures, published online June 2015.

De Beer 2014. The effect of stiffness reduction in reinforced concrete, due to alkali silica reaction, on a stadium's vibration response. BEng final year report, Stellenbosch University.

De Villiers 2013. Vibration response of a stadium, affected by alkali silica reaction, to dynamic excitations with consideration for human comfort. BEng final year report, Stellenbosch University.

ELLIS BR, JI T 2004. The response of structures to dynamic crowd loads - Digest 426. BRE Centre for Structural and Geotechnical Engineering.

Fulton 2009. Fulton's concrete Technology, 9th edition, Cement and Concrete Institute, South Africa.

Gonzalez JA, Cobo A, Gonzalez MN, Feliu 2011. On-site determination of corrosion rate in reinforced concrete structures by use of galvanostatic pulses, Corrosion Science 43,611-625.

Lepech M, Li VC 2005. Water permeability of cracked cementitious composites. In: Proceedings of ICF11, Turin, Italy, Mar. 2005, pp 113–130.

Miyazato S, Hiraishi Y 2005. Transport properties and steel corrosion in ductile fiber reinforced cement composites. In: Proceedings of ICF11, March 2005, Turin, Italy.

Miyazato A, Hiraishi Y 2013. Durability against steel corrosion of HPFRCC with bending cracks, Journal of Advanced Concrete Technology 11, 135-144.

Müller J 2013a. Corrosion measurements, unpublished document, Stellenbosch University, South Africa.

Müller J 2013b. Corrosion measurements 2, unpublished document, Stellenbosch University, South Africa.

OBERHOLSTER B. 1990. Verslag oor die inspeksie van die betonwerk van die Danie Craven Stadion, Stellenbosch, vir Alkali-Silikareaksie en aanbevelings insake die rehabilitasie daarvan. Report on the inspection of concrete works of the Danie Craven Stadion, Stellenbosch for ASR and recommendations regarding the rehabilitation (report in Afrikaans). CSIR, South Africa.

Paul SC 2015. The role of cracks and chlorides in corrosion of R/SHCC. PhD dissertation, Stellenbosch University, South Africa.

Paul SC, Van Zijl GPAG 2016. Chloride-induced corrosion modelling of cracked reinforced SHCC. Archives of Civil and Mechanical Engineering (ACME) 16: 734-742, DOI 10.1016/j.acme.2016.04.016.

Paul SC, Van Zijl GPAG, Babafemi J, Ming Jen TAN 2016. Chloride ingress in cracked and uncracked specimens made from strain-hardening cement-based composite (SHCC). Construction and Building Materials 114, 232-240.

Paul SC, Van Zijl GPAG 2014. Crack formation and chloride induced corrosion in reinforced strain-hardening cement-based composite (R/SHCC), Journal of Advanced Concrete Technology 12 (Sept 2014) 340-351.

Paul SC, Van Zijl GPAG 2013a. Mechanically induced cracking behaviour in fine and coarse sand strain-hardening cement based composites (SHCC) at different load levels. Journal of Advanced Concrete Technology 11, 301-311

Paul SC, Van Zijl GPAG 2013b. Durability index test performance of recycled concrete aggregate mixed with natural aggregate. International Journal of Advanced Civil Engineering and Architecture Research 2(1) 53-64.

Paul SC, Van Zijl GPAG 2013c. Mechanical and durability properties of recycled concrete Aggregate for normal strength structural concrete, International Journal of Sustainable Construction Engineering & Technology 4(1) 89-103.

RILEM TC 178-TMC 2002a. Testing and modelling chloride penetration in concrete, Analysis of total chloride content in concrete, Materials and Structures 35, 583-585.

RILEM TC 178-TMC 2002b. Testing and modelling chloride penetration in concrete, Analysis of water soluble chloride content in concrete, Materials and Structures 35, 586-588.

Sahmaran M, Li M, Li VC 2007. Transport properties of engineered cementitious composites under chloride exposure. ACI Mater J 104(6) 604–611.

Van Zijl GPAG 2011. On ingress into strain-hardening cement-based composites (SHCC), International Journal for Restoration of Buildings and Monuments 17(6) 1-12.

Van Zijl GPAG, Boshoff WP 2009. Mechanisms of creep in fibre-reinforced strain-hardening cement composites (SHCC), Proceedings of 8th International Conference on Creep, Shrinkage and Durability of Concrete and Concrete Structures (CONCREEP 8), Oct 2008, Ise-Shima, Japan, pp. 753-759.

Van Zijl GPAG, Paul SC 2016. Crack distribution linked to chloride-induced corrosion in R/SHCC. Paper ID No. 201, BEFIB, 19-21 September 2016, Vancouver, Canada.

Van Zijl GPAG, Slowik V (eds.) 2016. A framework for durability design with strain-hardening fibre-reinforced cement-based composites (SHCC), State-of-the-art report, Rilem TC 240-FDS, Springer Publishers.

Van Zijl GPAG, Wittmann FH 2010. On durability of SHCC, Journal of Advanced Concrete Technology 8(3) 261-271.

Van Zijl GPAG, Wittmann FH (eds.) 2011. Durability of Strain-Hardening Fibre-Reinforced Cement-Based composites (SHCC), State-of-the-art report, Rilem TC 208 HFC, SC 2, Springer Publishers, ISBN-13: 978-94-007-0337-7

Van Zijl GPAG, Wittmann FH, Oh BH, Kabele P, Toledo Filho RD, Fairbairn EMR, Slowik V, Ogawa A, Hoshiro H, Mechtcherine V, Altmann F, Lepech MD 2012. Durability of strain-hardening cement-based composites (SHCC), Materials and Structures 45(10) 1447-1463.

Van Zijl GPAG, Wittmann, FH, Toledo Filho RD, Slowik V, Mihashi H 2016. Comparative testing of crack formation in SHCC. International Journal Materials and Structures 49(4) 1175-1189.

Wagner C 2016. Durability related properties of strain-hardening cement-based repair layers on cracked concrete substrate. PhD thesis (in German), TU Dresden

Wagner C, Slowik V 2011. On the water permeability of cracked strain-hardening cement-based composites. In: Proc. 2nd Int. RILEM Conf. on Strain-Hardening Cementitious Composites (SHCC2-Rio). 12-14 December 2011, Rio de Janeiro, Brazil. Rio de Janeiro, Brazil, 12-14 Dezember. Bagneux, France: RILEM Publications (RILEM proceedings, PRO 81), S. 181–188.

Wittmann FH, Van Zijl GPAG 2006. Task Group B – Durability of SHCC Conclusions. In: Proceedings Rilem International Workshop on High Performance Fiber Reinforced Cement-Based Composites (HPFRCC) in Structural Applications, May 22-27, Honolulu, Hawaii, pp. 109 – 114.

Wittmann FH, Wang P, Zhang P, Zhao, T, Betzung F 2011. Capillary absorption and chloride penetration in neat and water repellent SHCC under imposed strain. In proceeding of 2nd international RILEM Conference on Strain-Hardening Cementitious Composites, Brazil, pp.165-172.

Zhang P, Wittmann FH, Zhao TJ, Lehmann EH, Tian Vontobel P 2010. Observation and quantification of water penetration into strain-hardening cement-based composites (SHCC) with multiple cracks by means of neutron radiography. Nucl Instrum Methods Phys Res A 620, 414–420.

Chapter 4 Renovation and retrofitting towards extended structural life span

4.1 Introduction

Historical masonry buildings and structures across the world are the subject of significant research programs and interventions to save these structures for future generations. Such historical buildings may be renovated or retrofitted to extend their service lives for centuries, well beyond typical 30, 50 or even 100 year design service life of infrastructure. This is justified by their cultural heritage and social value, but in cases also cost-efficiency. In contradiction, structural damage within the life span may prematurely end their service. Unreinforced masonry structures are susceptible to damage in seismic events. This has led to post-event repairs and retrofitting of masonry buildings. In earthquake regions, owners and local authorities should pro-actively reinforce masonry or other structures to acceptable levels of structural reliability in the event of an earthquake. Various retrofitting strategies exist for masonry structures, of which the most usual is connecting walls by metal ties to facilitate global structural response to avoid low-frequency, brittle response and collapse of individual walls. Apart from well-connected structural parts, ductile in-plane shearing resistance of walls is required to withstand cyclic lateral base acceleration.

Knowledge of mechanical behaviour of masonry was crucial in the assessment of retrofitting strategies for unreinforced load-bearing masonry structures (ULM). The author's PhD (Van Zijl 2000) laid a foundation in computational strategies, including time-dependent phenomena of shrinkage, relaxation and creep. Experimental characterisation and verification of masonry mechanical behaviour in compression was to a large extent performed by Vermeltfoort (2005) in the Pieter van Musschenbroek laboratory of Eindhoven University of Technology, with continued collaboration in characterising masonry behaviour (Vermeltfoort et al. 2007a,b).

This chapter describes retrofitting strategies for firstly the renovation of a historical Dutch building 'De Adelaar' to prevent or control restrained shrinkage crack formation in the masonry façades. The work was not performed in isolation by the author, but the project team included an Architect, Leo Verhoef Associate-Professor in the Faculty of Architecture, TUD, Casper Groot, Associate professor in masonry structures in the Faculty of Civil Engineering, TUD and his colleague Peter de Vries. The renovation proposal of converting the 'Adelaar', an old and deteriorated soap factory warehouse in Amsterdam to an office building was prepared by Leo Verhoef. Physical experimental validation of the retrofitting strategy was led by Dr Caspar Groot, assisted by Peter de Vries, while the author led the retrofitting strategy through computational modelling and analysis.

A second retrofitting strategy is proposed by the author for unreinforced masonry buildings in the Western Cape. Regions of the Western Cape Province of South Africa experience light to moderate seismic events (SANS10160 2011). Low to medium-rise unreinforced load bearing masonry (ULM) buildings, of which typical examples are shown in Figure 4.2, were erected here before seismic resistance became a standardized requirement in 1989. These buildings are expected to perform poorly in seismic events. The author has launched a research project to develop an overlay retrofitting strategy to enhance seismic resistance of ULM structures. As overlay material, strain-hardening cement-based composites (SHCC) has recently been proposed (Van Zijl and De Beer 2016a). By appropriate retrofitting design, this multiple cracking material is foreseen to change the brittle ULM response into a ductile composite response to seismic excitation.

Figure 4.1: Damage in De Adelaar, a historical Dutch masonry building, due to restrained shrinkage by reinforced concrete frame.

(a)  (b) 

Figure 4.2: Typical unreinforced load bearing (a) clay brick and (b) concrete block masonry residential buildings in the Western Cape, South Africa.

Finally, studies were performed on repair or retrofitting strategies for reinforced concrete with CFRP strips and with an SHCC overlay. A test was designed for cyclic de-bonding characterisation of CFRP from concrete substrates by Badenhorst (2012), who also performed finite element analyses to study the cyclic debonding of the CFRP strips. Stander (2007) and Van Zijl and Stander (2009) reported experimental results on interfacial bond characterisation of an SHCC overlay on a concrete substrate. These results have been simulated by Lukovic (2016) and are incorporated in *Chapter 8: Behaviour of bonded SHCC overlay systems* (Luković 2016) of the state-of-the-art report of RILEM TC 240-FDS (Van Zijl and Slowik 2016). In the next sections the retrofitting strategies for masonry are elaborated in greater detail.

4.2 Renovation of ‘De Adelaar’

Historical buildings with traditional unreinforced load bearing masonry (ULM) walls, combined with a concrete inside structure are prone to damage caused by differences in thermal and moisture-induced expansion and movement. Daily and seasonal changes in the façade temperature relative to the inside bearing structure can lead to vertical cracks in the brickwork. Renovation of a historic Dutch building, 'De Adelaar' (Figure 4.1) was proposed to transform the deteriorated old soap factory into an office building. The building was constructed in 1906 and has been declared as a monument by Dutch authorities. A retrofitting intervention was proposed, to prevent or control cracks in the masonry façades.

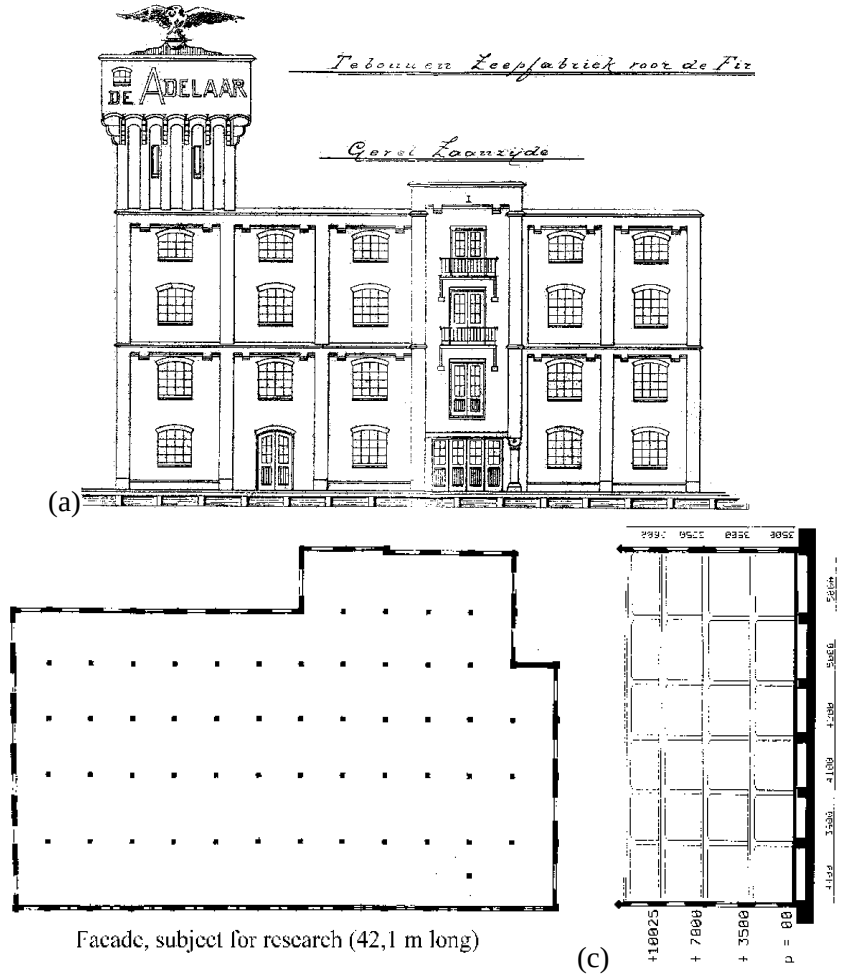

Figure 4.3: 'De Adelaar' soap factory (a) façade facing the river Zaan, (b) plan showing outer unreinforced masonry walls and inner RC column grid and (c) elevation showing the RC floor and roof slabs.

4.2.1 Masonry cracking due to restrained shrinkage

The visible cracking in the façade (Figure 4.1) was postulated to have been caused by restrained shrinkage of the masonry (Van Zijl and Verhoef 2001). Being a soap factory at the beginning of the previous century, no air condition was supplied in the building. Nevertheless, temperature differences between the exterior and interior could have reached 32 ^{o}C in winter. Thereby, the exterior masonry would shrink due to thermal cooling while the interior RC floors resting on the masonry walls would not shrink, or shrink less. Through floor weight, frictional resistance restrained the masonry shrinkage, whereby tensile strength was exceeded, causing cracking in the masonry. This is most notable at discontinuities, i.e. at window openings.

To demonstrate that restrained shrinkage could indeed be the mechanism of the cracking, finite element analyses were performed of a typical, individual storey façade wall part, as shown in Figure 4.4. The wall was modelled as a homogeneous continuum, and anisotropic multi-surface plasticity as proposed by Lourenço et al. (1998), modified Van Zijl et al. (2001a,b) to incorporate bulk creep and rate dependence for regularisation of localisation. For details of the plane stress modelling approach, masonry material model parameters, see Van Zijl and Verhoef (2001). Table 4.1 summarises the typical clay brick masonry parameters used, notably incorporation of lower tensile strength perpendicular to bed joints (f_{ty}) than parallel to bed joints (f_{tx}).

Due to uncertainty of the restraint by connecting walls, extreme cases of fully restrained and unrestrained conditions were considered, see Figure 4.5. To evaluate the effect of movement joints in the façade in limiting cracking, this was computationally evaluated (Figure 4.5 c, d). The results are summarised in Figure 4.6 in terms of the maximum computed crack width in the wall for these boundary conditions (Figure 4.6a). It can be seen that for a wall restrained by a cross wall, the crack opens at a temperature drop of about 5 ^{o}C, and opens to a maximum of more than 0.25 mm at 32 ^{o}C. Clearly, wide and unsightly cracking arises despite a dilatation or movement joint, which rules this out as a measure of sufficiently limiting crack widths in the façade.

The results of sensitivity studies to the masonry fracture energy, tensile strength and resisting (non-shrinking) floor stiffness are shown in Figures 4.6 b-d. The low floor stiffness resembles timber flooring. Notably, historical masonry buildings with timber floors are less prone to cracks in the façade.

Table 4.1 Model parameters.

	E (GPa)	φ_c	ν	f_{tx} (MPa)	f_{ty} (MPa)	α (^{o}C^{-1})	ρ (kg/m^3)
Masonry wall:	5	2	0.2	0.4	0.2	7x10^{-6}	1900
Concrete floor:	30	0	0.2	∞	∞	12x10^{-6}	2400

E = Young's Modulus

v = Poisson's ratio

φ_c = creep coefficient (after 100 days)

ρ = mass density

f_{tx} = tensile strength parallel to bed joints

f_{ty} = tensile strength perpendicular to bed joints

α = thermal expansion coefficient

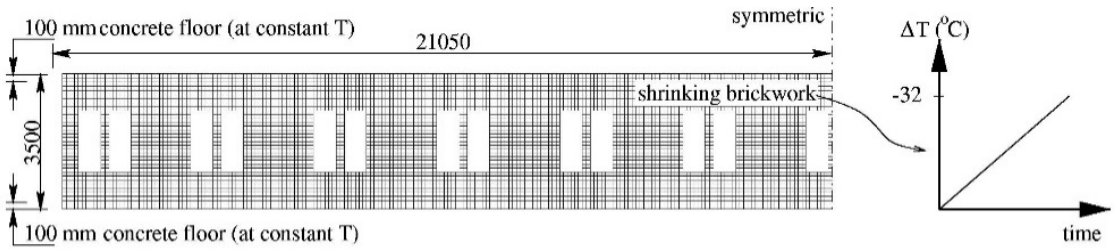

Figure 4.4: Schematisation of 'De Adelaar' wall for FEA. Dimensions in mm.

(a) Boundary 1

(b) Boundary 2

(c) No movement joint

(d) Movement joint

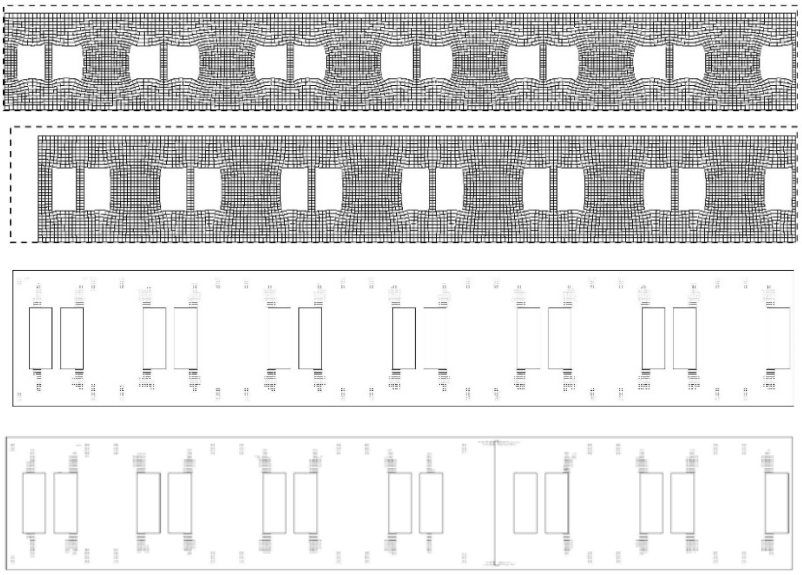

Figure 4.5: Illustration of FE analysis results of thermal cooling deformation (a) restricted by cross walls and (b) with no restraint; smeared crack size and orientation indicated at integration points (c) with no dilation/movement joint in the wall and (d) with a movement joint included.

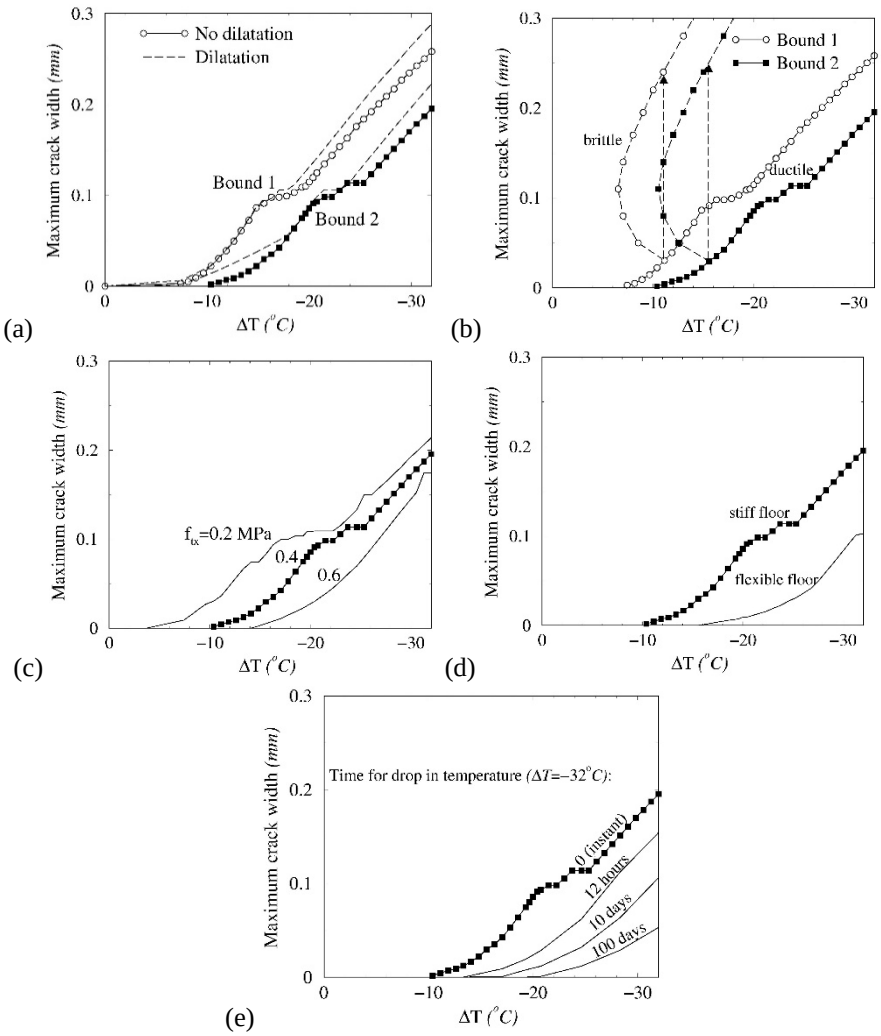

Figure 4.6. Maximum crack width development sensitivity to (a) boundary type 1 and 2, (b) masonry fracture energy, (c) tensile strength, (d) floor stiffness and (e) rate of cooling.

4.2.2 Validation of masonry wall cracking due to restrained shrinkage

Van Zijl et al. (2004) performed a restrained shrinkage physical simulation. Due to the specimen size, instead of thermal cooling of the masonry wall, heating of the 'restraint' was performed. A set-up was chosen comprising of two aluminium beams framing a brickwork wall of 220 mm thickness and overall measurements of 1.28 m (height) by 2.0 m (length), shown in Figure 4.7. In the middle of the brickwork an opening was left to weaken the wall, as an imitation of a window, and to introduce cracking in the brickwork. The masonry comprised typical Dutch soft mud (Rijswaard) bricks and a mortar mix of 1:1:6 (cement:lime:sand) by weight. The wall was built in a climate room at 20 ^{o}C and 70% relative humidity. It was allowed to cure for 4 weeks before the test was performed.

The lower beam was supported by a central, steel bearing block, as well as four cylindrical bearings to allow free horizontal translation upon heating of the beams. The beams were glued to the masonry with a cement-based glue, instead of an epoxy, which has deteriorating stiffness with increased temperature. The beam surfaces were roughened beforehand to produce interlocking with the glue to prevent shear-slipping. This was done to impose the worse-case scenario of full interlocking between the structural elements to maximize the restraint to differential dimensional change.

To prevent excessive bending of the beams and simulate top weight, an average compressive pre-stress of 0.7 MPa was applied to the masonry by six pairs of steel rods, V1-V6 in Figure 4.7. Force transducers monitored the pre-stressing force continuously, showing negligible relaxation over a period of 12 h before the main experiment.

Inverse restrained shrinkage was induced in the wall by heating the aluminium beams. Heated water was pumped through copper pipes, Figure 4.7 (left), in contact with both vertical surfaces of each beam, Figure 4.7 (right). A total of 21 thermocouples along the length and depth of each beam monitored the temperature. By altering the water flow rate, the upper and lower beam temperature could be controlled to a difference of within 1 ^{o}C throughout the experiment. Also, a negligible thermal gradient arose in the beam length, as well as through the depth, due to the high heat conductivity of aluminium and the low thermal rate applied, Figure 4.8. Two thermocouples were placed in the wall in the first layer (M1) in contact with the beam, as well as the third layer (M2) to monitor masonry heating. During the 3 hour test period the first layer warmed by 13 ^{o}C, but the third layer an insignificant 2 ^{o}C.

The resulting cracks observed in the masonry wall in the experiment, and those from computational analyses are shown in Figure 4.9. While symmetry was assumed in the FE model, as reflected by the symmetrical computed crack patterns (Figure 4.9b), the actual cracks arose dominantly one one side (Figure 4.9a). This is due to imperfections in the materials and bricklaying, despite best practice and making use of the services of a professional bricklayer. However, the initial symmetrical cracks at both sides of the opening in the wall model changed to a single crack in the wall centre at advanced stage of the simulation (Figure 4.9c). Good agreement was nevertheless found between the development of the crack width in the physical experiment, with that in the FE model, as shown in Figure 4.10.

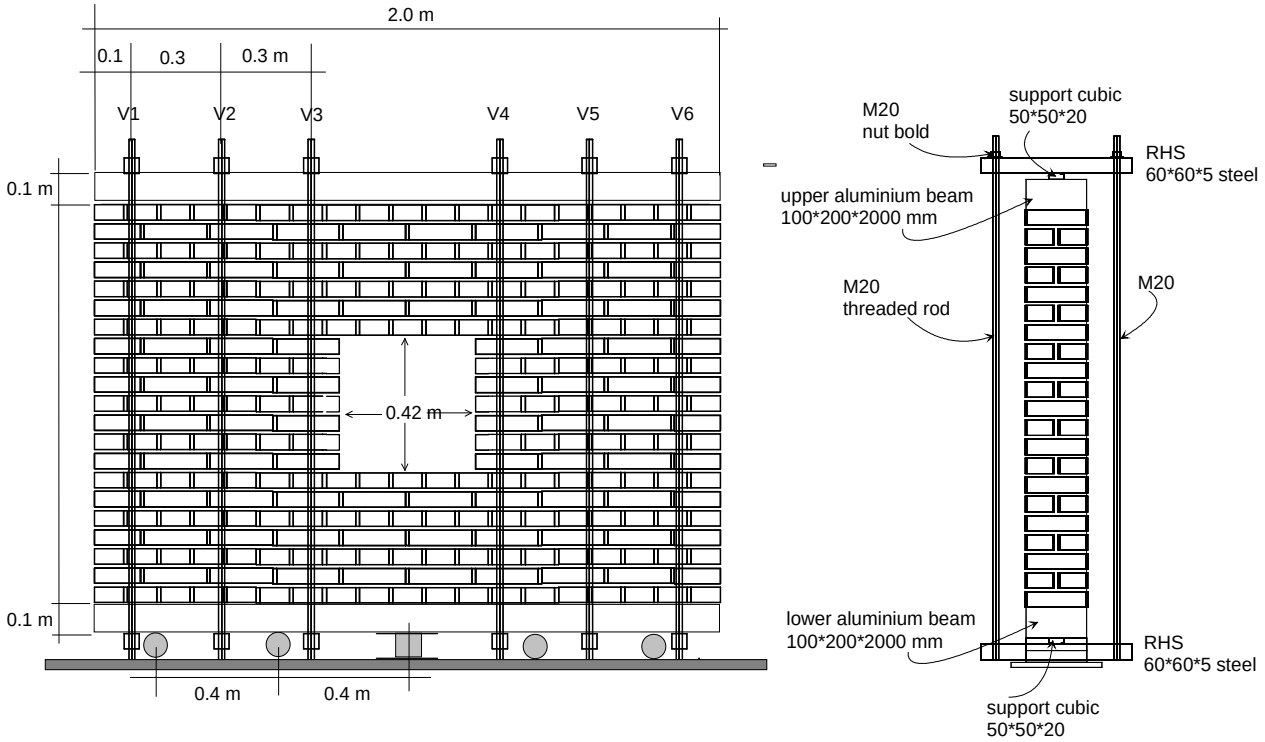

Figure 4.7: Restrained shrinkage masonry wall experimental set-up.

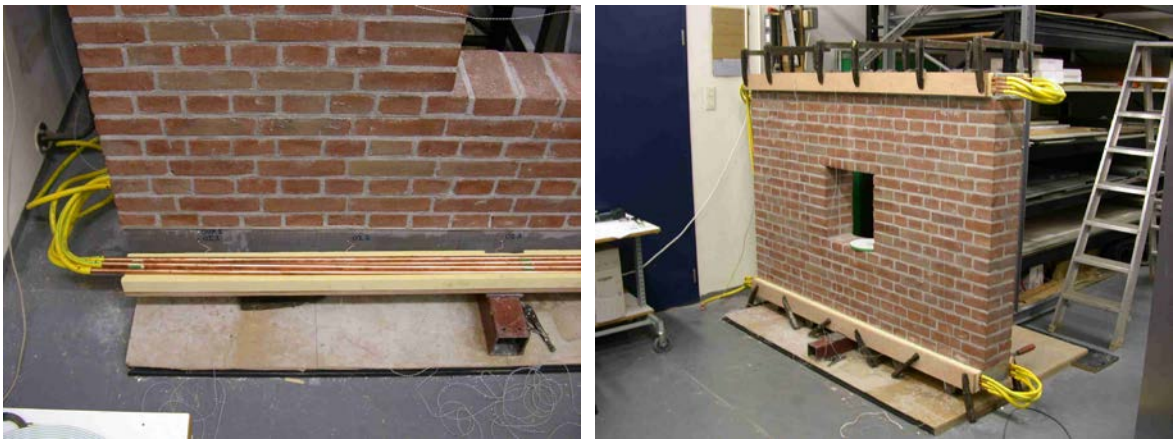

Figure 4.8: Heating of aluminium beams by warm water flow through copper pipes (Van Zijl et al. 2004).

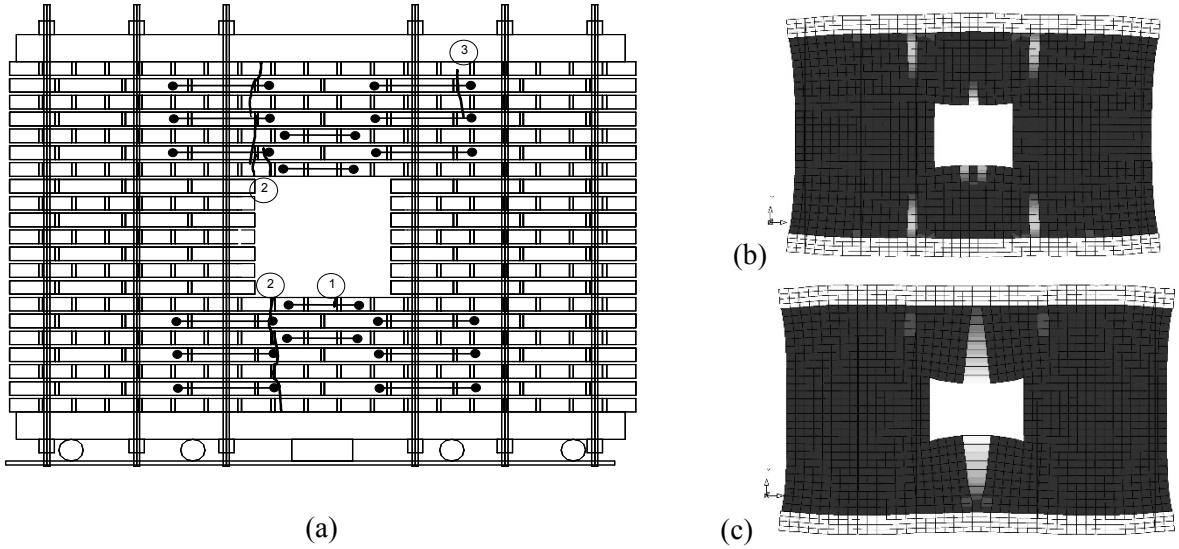

Figure 4.9. Cracks (a) observed in masonry wall, and (b) predicted in phase 1 and (c) phase 2 (Van Zijl et al. 2004).

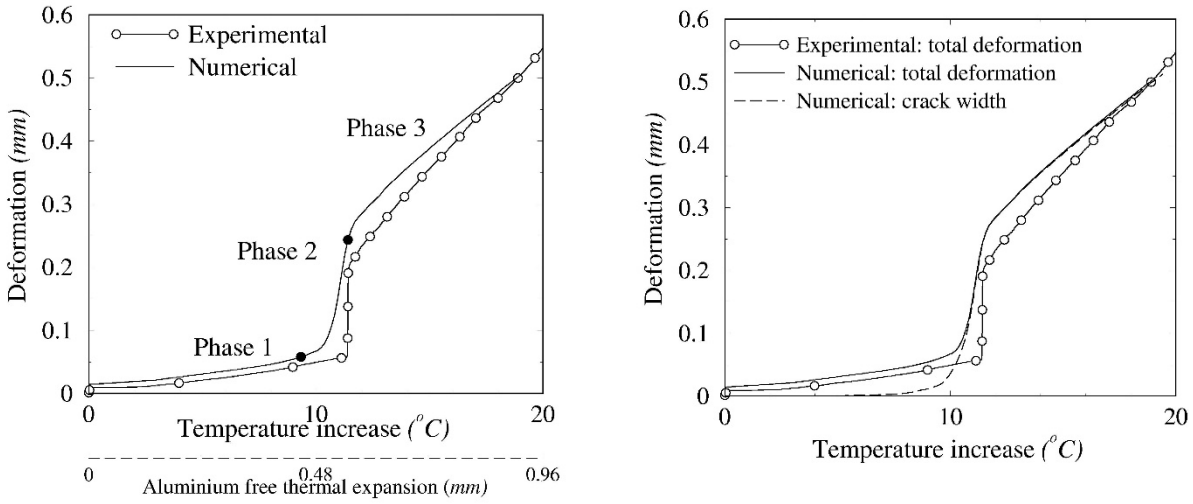

Figure 4.10: FEA predicted and measured deformation and crack width development (Van Zijl et al. 2004).

4.2.3 Renovation strategy, validation and modelling

Having proven the mechanism of cracking, a strategy was proposed to limit the crack widths. Application of carbon fibre reinforced polymer (CFRP) sheets to the interior face of the masonry walls was proposed and evaluated computationally and physically (Van Zijl and De Vries 2005). This was done by repairing the cracked wall of the previous section, applying the CFRP strips to the wall surface, and re-testing the wall.

Three cracked layers above and below the opening respectively were repaired, retaining a small cracked part in the upper left part above the opening, as well as in the lower left part below the opening – see Figure 4.11a. The wall was left to cure in the climate room at 20 ºC and 70% relative humidity where it was originally built and where the initial, unreinforced wall experiment was performed. The repaired region was kept moist for the first 48 hours to allow optimal curing. In total, 23 days were allowed between the repair and the ensuing restrained shrinkage physical experiment of the repaired and retrofitted wall. Two weeks after the repair, four SIKA

CARBODUR S 1012 CFRP strips of 100 mm wide, 1.2 mm thick and 2 m long were glued to the rear side of the wall, Figure 4.11b. Standard procedure was followed to apply the strips. Firstly, the wall parts where the strips were to be placed were brush-cleaned. Simultaneously, the CFRP strips where de-greased. Next, the two-component SikaDur 30-Normal epoxy was applied to a thickness of up to 5 mm, due to the wall rear side unevenness. Finally, each strip was placed manually and evened out with a hand-held roller. To test the adhesion, 8 aluminium cylinders were glued to the wall, as well as to separate, loose bricks. After 24 hours the cylinders were pulled off with standard equipment, leading to failure of the masonry/brick surface in each case. During the 3-week preparation period between the previous experiment on the unreinforced masonry and the current experiment, the pre-stress level in the wall relaxed by approximately 5-6%. Shortly before commencing with the heating of the beams to introduce the restrained shrinkage action to the reinforced wall, the pre-stress level of -0.7 MPa was restored. Subsequently, the deformation measurement devices were activated and heating of the beams was started.

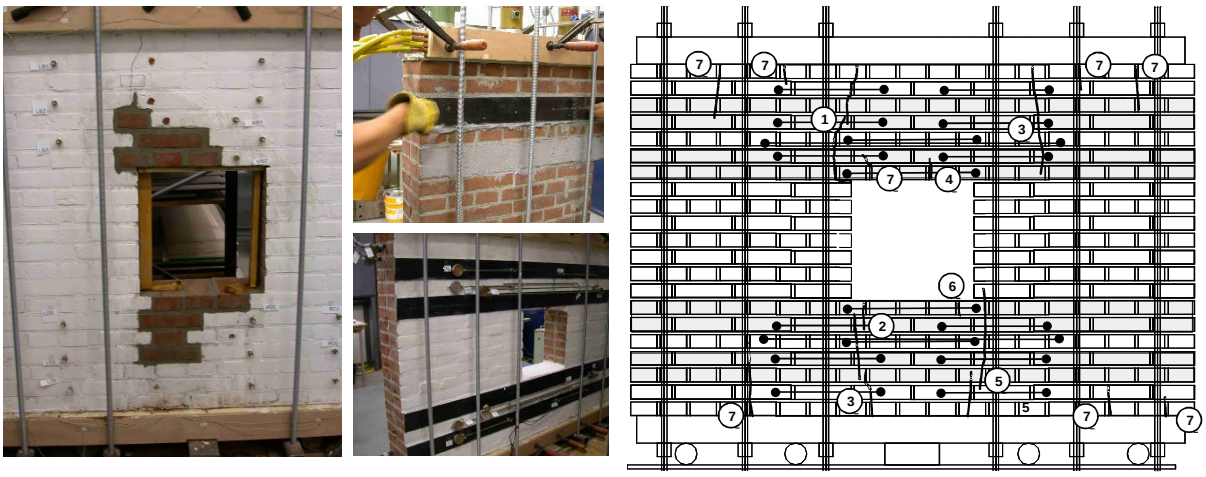

Figure 4.11: (a) Masonry wall repair, (b) CFRP strip application and (c) cracking upon re-testing (Van Zijl and de Vries 2005).

Upon re-testing, eight cracks arose in the upper part, and seven cracks in the lower part of the wall. The widest crack, marked 1 in Figure 4.11c was the one left partially unrepaired in the upper part of the wall after the previous experiment. This crack propagated further, starting at a temperature increase of about 10 ^{o}C and followed the repair line. Crack (2) arose at 12.5 ^{o}C, two cracks marked (3) at 18 ^{o}C, crack (4) at 22 ^{o}C, followed shortly afterwards by crack (5). At 27.5-29 ^{o}C the cracks marked (6) and (7) initiated. No slip occurred between the beams and the wall or between the CFRP strips and the wall.

The CFRP strips were modelled by four node plane stress elements, each overlapping two rows of the elements representing the wall, as shown in Figure 4.12. This ignores eccentricity of the strips, which were applied on one side of the wall only. The material properties for the CFRP are shown in Table 4.2. To capture CFRP delamination, plane interface elements were placed between the rows of CFRP elements and the coinciding wall elements. An interface material law, which limits the bond strength, as well as the shear-slip resistance (Van Zijl 2000), was employed for this glued connection, with parameters shown in Table 4.2. The bond strength f_t was based on the average resistance measured by pull-off tests of steel cylinders glued to the masonry with the same epoxy. In each test the brick and/or mortar joint skin was severed, leaving the glue joint in-tact. No data

for the shearing resistance τ_u was available, but a lower limit of the bond strength (1.0 MPa) was assumed, along with a conservative friction coefficient of 0.1. The employed fracture energy for bonding and shearing toughness $\boldsymbol{G_f^I}$, $\boldsymbol{G_f^{II}}$ respectively are considered to be lower bound values.

Although the first cracks arose by propagation of the cracks left from the first experiment on the unreinforced wall, no attempt was made to simulate the pre-damage. This could be considered by modelling no-tension interface elements in that region. The estimation and inclusion of the current state of masonry, especially historical masonry, in modelling strategies, are nevertheless important issues for consideration. The wall and beam self-weight was applied in an initial step, followed by a step for the pre-stressing of the steel bars to produce an average pre-compression of 0.7 MPa in the wall. Subsequently, the temperature of the aluminium beams was increased at a rate of about 7 ^{o}C.h^{-1}.

Table 4.2: Model parameters employed.

Aluminium	Steel	Epoxy	Masonry	CFRP
E=70 GPa	E=210 Gpa	k_n=3035 N. mm^{-3}	E=4 GPa	E=165 GPa
ν=0.25	ν=0.25	k_s=1265 N. mm^{-3}	ν=0.2	ν=0.2
α_T=24.10^{-6}	-	-	-	-
ρ=2700 kg.m^{-3}	ρ=7850 kg.m^{-3}	ρ=900 kg.m^{-3}	ρ=1900 kg.m^{-3}	ρ=1900 kg.m^{-3}
		f_t =1.0 N.mm^{-2}	f_{tx} =0.5 N.mm^{-2}	f_t =1500 MPa
		τ_u = 1.0 - 0.1σ	f_{fy} =0.25 N.mm^{-2}	
		G_f^I = 0.02 N.mm^{-1}	g_{fx} =0.0007 N.mm^{-2}	
		G_f^{II} = 0.05 N.mm^{-1}	g_{fy} =0.00035 N.mm^{-2}	
			m = 100 000 N.s.mm^{-2}	

E=elasticity modulus, m=cracking viscosity, G_f^I =mode I fracture energy
ν=Poisson's ratio, f_t=tensile strength, G_f^{II}=mode II fracture energy
k_n=interface normal stiffness, f_{tx}=tensile strength parallel to bed joints, g_{fx}=fracture energy ass. with f_{tx}
k_s=interface shear stiffness, f_{fy}=tensile strength perpendicular to bed joints, g_{ty}=fracture energy ass. with f_{ty}
ρ=density, τ_u=shear strength,
α_T=thermal exp. coefficient, σ=normal stress (tension positive).

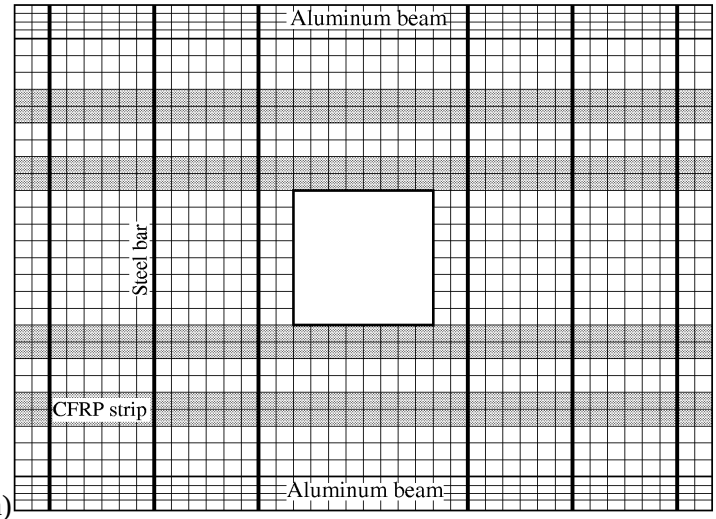

(a)

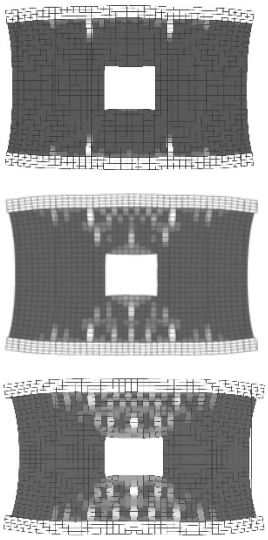

(b)

Figure 4.12: (a) FE model of CFRP retrofitted wall. (b) Computed crack control by CFRP reinforcement in masonry walls, showing plastic strain contours on the deformed wall at various elevated temperatures.

The computed wall deformation at different stages of the test are shown in Figure 4.12. Cracks initiated at about 9 ^{o}C in the same regions as in the unreinforced wall, but were bridged by the CFRP strips, causing several more cracks to initiate and grow upon further heating. Thereby, the maximum crack width was predicted to be limited to less than 0.15 mm, as shown in Figure 4.13. The predicted distributed cracking is confirmed to some extent by the observed crack pattern in the laboratory experiment. The location of individual cracks is not of concern, determined by amongst others material imperfection, which was not considered. More important is that several, densely spaced cracks are predicted, verified by the experimental observation. However, bending of the wall, with subsequent larger crack widths on the unreinforced, outer side, was observed in the experiments. The maximum width (at the extreme elevated temperature of 29 ^{o}C) of an accessible crack in the wall opening was measured as being 0.1 mm on the reinforced side, but 0.3 mm on the front surface. This out-of-plane bending was ignored by the computational model, leading to the underestimation of the maximum crack widths, Figure 4.13. Nevertheless, reasonable agreement is found and, importantly, despite the dominating cracks in the weakened area from the first experiment, the CFRP-reinforcement sufficiently controlled their widths, by transferring stress to nearby masonry, leading to a dense crack pattern. The maximum width of 0.4 mm measured at 29 ^{o}C at the initially damaged region on the outer surface is a concern, calling for more stringent repair of damaged masonry before applying eccentric, external CFRP reinforcement. Alternatively, CFRP-strips must be applied on both wall faces to limit cracks to fine widths to retain aesthetical appeal.

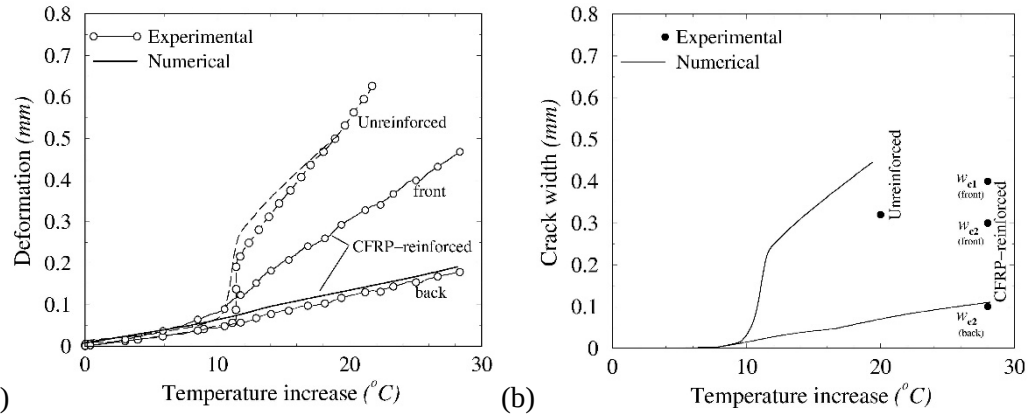

Figure 4.13: (a) Predicted and measured deformations in left upper region where the largest crack arose. (b) Predicted and measured crack widths.

4.3 Retrofitting towards enhanced seismic resistance

Another retrofitting strategy has been proposed (De Beer and Van Zijl 2016, Van Zijl and De Beer 2016a,b), in this case for seismic resistance of residential infrastructure. Regions of the Western Cape Province of South Africa experience light to moderate seismic events (SANS10160, 2011). Low to medium-rise ULM buildings were erected here before seismic resistance became a standardized requirement in 1989. These buildings are expected to perform poorly in seismic events. Stellenbosch University has launched a research project to develop an overlay retrofitting strategy to enhance seismic resistance of ULM structures. As overlay material, SHCC has recently been adapted for shotcrete application (De Beer and Van Zijl 2016). Material development was done to produce a shotcrete version which has appropriate open time, i.e. time for application before initial set, which can be pumped with standard, locally available shotcrete equipment at a reasonable pressure without segregation, and sprayed onto masonry without significant rebound, run-off and waste. Sufficient adhesion of the fresh SHCC to the masonry is required, as is appropriately quick viscosity build-up to enable typical required overlay depths of up to 60 mm to be produced. Such large thicknesses may be required to reinforce several leafs

thick walls, while typical depths of 10 to 30 mm may suffice for the intended application in low to medium rise buildings. The spraying application of SHCC to a masonry wall in the Structures Laboratory of Stellenbosch University is shown in Figure 4.14.

In-plane shear is a dominant mode in seismic excitation. In designing the retrofitting strategy, masonry shear wall mechanics (eg. Van Zij et al. 2001, Vermeltfoort et al. 1993, van der Pluijm 1992, 1998) and SHCC mechanical behaviour are incorporated. Coulomb-friction captures the shearing action along masonry joints well. A computational model with multi-surface limits shown in Figure 4.15a was proposed to capture masonry shear-slip along joints. Softening simulates the loss of chemical/mechanical adhesion to purely frictional resistance under normal pressure. Dilatant volume increase in masonry during inelastic shear-slip (see Figure 4.15b) was shown and characterised by van der Pluijm (1992, 1998). This is incorporated computationally by incorporating a dilatancy coefficient Ψ which varies with confining pressure σ, shear-slip distance δ_{vp}, formulated as (Van Zijl 2004a,b):

$$\Psi = \begin{cases} 0 & \sigma < \sigma_u \\ \Psi_0 \left[1 - \dfrac{\sigma}{\sigma_u} \right] e^{-\delta v_p} & \sigma_u \le \sigma < 0 \\ \Psi_0 e^{-\delta v_p} & \sigma_u \ge 0 \end{cases} \tag{4.1}$$

with a limiting pressure σ_u at which the volume growth is arrested due to high-pressure smoothening of the interfacial roughness. The numerical model is shown to be in reasonable agreement with experimental dilatancy in Figure 4.15b. This dilatant volume increase must be borne in mind to accurately reflect shear wall behaviour in experimental procedures. Should this volume increase be restricted or prevented, significant wedging will occur and lead to increased shearing resistance and possible altered failure modes.

Multiple cracking, the main characteristic of SHCC, has been shown also in shear response (Van Zijl and Shang 2007), as described in Section 2.1. This holds potential for improved ductility of masonry walls, should the retrofitting strategy succeed in mobilising such multiple cracking and the associated high energy dissipation. SHCC shearing response was shown in shear tests (Figure 2.4). Significantly higher ultimate shear strength than direct tensile strength was observed (Figure 2.4b). This is ascribed to principal stress rotation, which is enabled by the sustained tensile stress beyond the appearance of first cracks. Figure 2.5 illustrates the diagonal tensile-compressive stresses arising under shear, and principal stress rotation and crack alignment, allowing increased shearing resistance. This section describes the development of SHCC that can be sprayed onto masonry, as well as the design and verification of multiple cracking SHCC overlays for improved in-plane shearing resistance and ductility.

Figure 4.14: Spray-application of SHCC to a masonry wall, showing from left to right standard commercially available shotcrete equipment, spraying through a nozzle which supplies circumferential pressure to the SHCC material, trowelling for the surface finish and thickness.

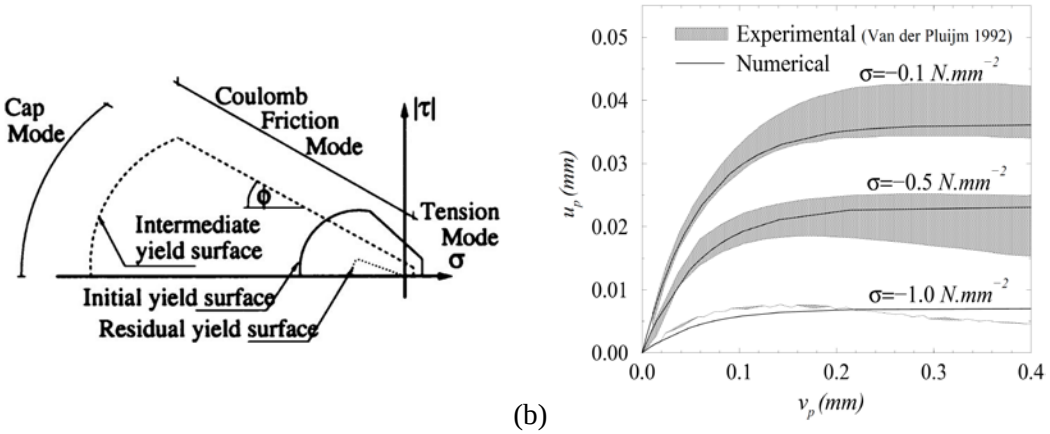

(a) (b)

Figure 4.15: Constitutive model for masonry interfacial shear, including (a) Coulomb friction shear with tensile and compressive limits and capturing (b) experimental observation of dilatancy by Van der Pluijm (1992) of clay brick masonry (Van Zijl 2004).

4.3.1 Bonded SHCC overlay material development

The SHCC mix ingredients, as adapted for sprayability, are summarised in Table 4.3. Polyvinyl-alcohol (PVA) fibres were used, with length of 8 mm, diameter 40 μm, tensile strength and Young's Modulus of 1.6 GPa and 40 GPa respectively. To characterise the SHCC, compressive and uniaxial tensile tests were performed according to recent RILEM recommendations (Van Zijl et al. 2016). Dumbbell specimens with gauge area cross-section of 40x80 mm (*d* x *w* in Figure 4.16a) over a central 108 mm length were cast in moulds, protected, stripped after 1 day, water cured at 23±2 ^{o}C, and tested at the age of 14 days. The tensile stress-strain responses shown in Figure 4.18 for the 140% specimens, denoting the fly-ash to cement percentage ratio, are typical for this mix. To compare the sprayed SHCC properties, dumbbell specimens were also sprayed into the moulds, curing and testing them exactly as the cast specimens. In this way, an average ultimate tensile strength of 3.0 MPa (coefficient of variation 0.072) was determined for cast specimens, compared with an ultimate strength of 2.08 MPa (CoV 0.006) for the sprayed specimens. A loss in tensile ductility was also found, with the ultimate tensile strain of 3.2% (CoV 0.336) and 2.1% (CoV 0.266) for cast and sprayed SHCC respectively. The 2% strain is considered sufficient for the application, and no further optimisation of the spray mix was undertaken.

Table 4.3: SHCC ingredient materials and proportions in kg/m^3.

Cement	Fly-ash	CAC	Sand	Water	VMA*	SP†	V_f ‡
420	620	21	540	365	0.8	2.2	0.02

* Viscous Modifying Agent
† Superplastiser
‡ Fibre volume fraction

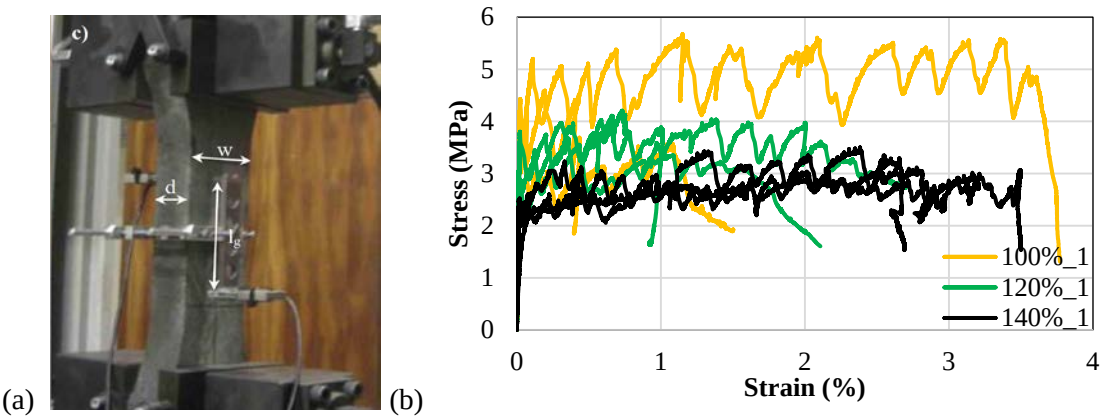

Figure 4.16: (a) Dumbbell type specimens and tensile test setup. (b) Direct tensile stress-strain results.

4.3.2 Characterisation of masonry bond

The Coulomb-friction model parameters of masonry joint friction coefficient and adhesion were characterized by performing Triplet tests according to BS EN 1062-3 in a 2 MN Instron MTM. Masonry specimens consisting of three clay bricks joined by two 10 mm mortar joints were prepared. Baked clay bricks from local industry for load-bearing masonry walling in the Western Cape were used together with a Class I cement-based mortar. The bricks were pre-wetted to ensure an acceptably low water absorption rate from the fresh mortar. Eighteen specimens were prepared, of which six each were tested with 0, -0.3 MPa and -0.6 MPa normal stress. The normal stress could be maintained throughout the triplet tests, by the large coil springs seen in Figure 4.19a, whereby dilatant volume increase could be accommodated without significant change in normal force, which was continuously monitored by a load cell also seen in Figure 6a. From the results, the joint interface adhesion (c_j) was determined to be 0.28 MPa, and the friction coefficient Φ to be 1.08. The triplet test specimen and setup is shown in Figure 4.17a, showing the typical smooth front (left) and grooved rear (right; 5 mm deep by 12 mm wide) face of the clay bricks.

The triplet tests were also performed on five specimens onto which 30 mm SHCC overlays had been sprayed on both faces. After building these five masonry triplet specimens, they were air cured at 24±2˚C and relative humidity of 65±5% for seven days. Then, 30 mm overlays were sprayed onto both faces and troweled flat. The specimens were left to set for 24 hours in the laboratory, after which they were wrapped in plastic foil and kept in the same conditions for a further 13 days until testing. The tests were also performed in the 2 MN Instron MTM. As planned, these specimens failed by de-bonding of the overlay. At the failure load, the masonry joint resistance had already been reached and softened, so that it could be neglected in determining the average bond strength of the SHCC-masonry interface. The average bond strength was calculated to be 2.30 MPa (CoV 0.293). Note that no distinction was made between the smooth face and the grooved face bond. So, the bond reflects an average value.

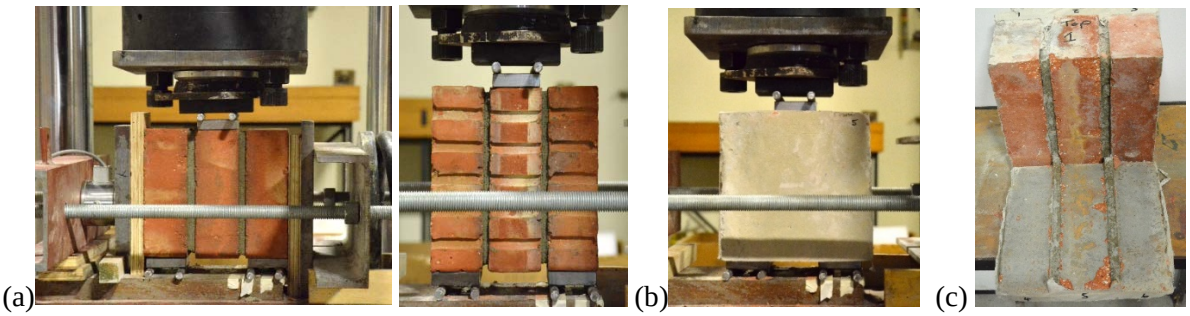

Figure 4.17: Triplet test configuration for triplet specimens (a) with no overlay showing the smooth front and grooved back face, and (b) with 30 mm overlays on both faces. (c) De-bonded overlays from triplet tests to characterise interfacial bond strength.

4.3.3 Failure mode design and verification

Two failure modes are foreseen, namely multiple crack formation in the shear zone of the SHCC overlay (Figure 4.18: Mode 1) and debonding (Figure 4.18: Mode 2). To exploit the SHCC energy dissipation, Mode 1 is preferred. This will also lead to a thinner overlay required, whereby material and, importantly in seismic excitation, mass is reduced.

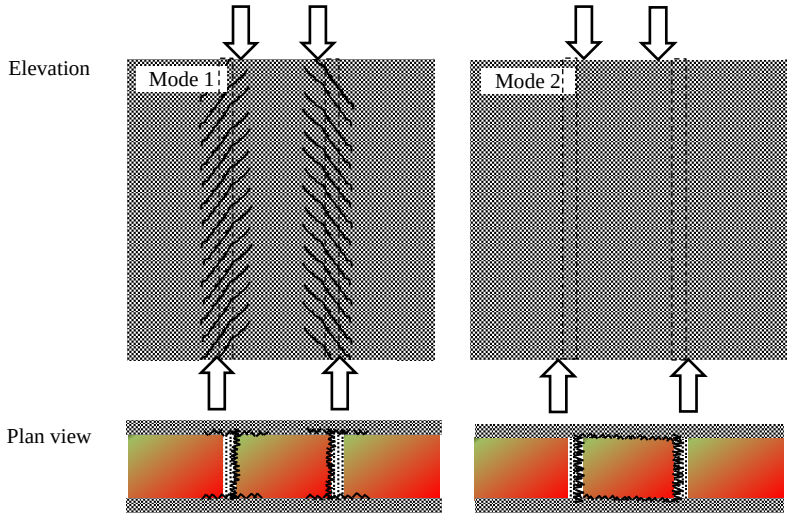

Figure 4.18: Failure modes illustrated on masonry triplet specimens with SHCC overlays.

Considering the paths of failure shown in Figure 4.18, and geometrical parameters of brick element height h_b, width w_b, mortar joint thickness t_b, SHCC thickness t_s, SHCC shear resistance τ_s and the masonry-SHCC interfacial bond τ_b, the shear force required for failure Mode 1 and 2 can be expressed as follows:

$$F_{\text{mode}1} = 4\tau_s h_b t_s + 2h_b w_b \left(c_j - \Phi\sigma\right) \tag{4.2}$$

$$F_{\text{mode}2} = 2h_b t_b \tau_b + 2h_b w_b \left(c_j - \Phi\sigma\right) \tag{4.3}$$

From Equations (2, 3) the threshold SHCC overlay thickness for mode 1 to occur, can be derived

$$t_s < \frac{t_b \tau_b}{2\tau_s} \tag{4.4}$$

To verify the failure modes and an overlay design procedure, a larger triplet test was performed. These specimens each comprised nine clay bricks, attached with eight 10 mm thick mortar joints, as shown in Figure 4.21. Apart from control specimens without overlays, two overlay thicknesses were chosen; thin, 10 mm overlays and 30 mm overlays, in both cases sprayed onto both faces of the masonry specimens. Using Equation (4.4), with parameters h_b, w_b, t_b equal to 222 mm, 105 mm and 70 mm respectively, c_j = 0.28 MPa from Section 4.2.2, τ_b = 2.3 MPa from Section 3 and τ_s is the SHCC ultimate shear resistance. Considering the latter to be 50% more than the ultimate tensile resistance (Van Zijl and Shang 2007), Equation (4.4) demands that the overlay thickness should be less than 25 mm for Mode 1 failure. So, 10 mm overlays were applied by spraying onto both faces of one set of three triplet specimens to ensure that Mode 1 would dominate, and two specimens were prepared with 30 mm overlays to ensure Mode 2 debonding. The test setup is shown in Figure 4.19a, debonding failure confirmed in the 30 mm overlays (Figure 4.19b), and multiple crack formation in the SHCC in the shear region confirmed in Figure 8c. Note the eventual crack localisation (Figure 4.19c centre), and that larger delaminated overlay remained on the smooth face than on the brick grooved face, where the higher interfacial bond caused a more vertical shear crack localisation, and failure directly next to the shear plane. The force versus shearing displacement responses are shown in Figure 4.20.

4.3.4 Free and restrained drying shrinkage of SHCC

Shrinkage of SHCC, restrained by a relatively dimensional stable masonry substrate, may cause partial debonding of the SHCC, increasing the likelihood of Mode 2 failure (see Figure 4.18). For the specimens described in Sections 4.3.2 and 4.3.3, shrinkage of the overlay was prevented by wrapping of the triplet test specimens. However, in practical retrofitting applications the SHCC overlay will be subjected to drying shrinkage. Free and restrained shrinkage tests were performed to quantify the drying shrinkage of the SHCC. For free shrinkage, SHCC was sprayed into steel moulds of dimension 100 mm x 100 mm and length 500 mm. After 24h, the specimens were stripped and Demac targets were attached at a 100 mm gauge length as shown in Figure 4.21 (top, left). The specimens were left unsealed in a climate room at 24±2˚C and relative humidity of 65±5%. A hand-held Demac extensometer was used to measure the length change. Four samples were used with two measurements on each sample.

For the restrained shrinkage tests, the masonry substrate served as restraint to the shrinking bonded SHCC overlay. Masonry wall parts were prepared by constructing four masonry wall parts, two each of the two brick arrangements shown in Figure 4.21 (top right). Two of these wall parts represent a vertical section of a masonry wall, due to the brick layout. The other two wall parts represent a horizontal part of a masonry wall, with typical running bond. An SHCC overlay was sprayed onto each of the four wall parts. Due to the larger number of mortar joints of the ‘vertical’ masonry substrates, it is foreseen that these vertical walls present less restraint to shrinkage of the bonded SHCC overlay. The specimen dimensions were 1030 mm by 220 mm. They were left in laboratory conditions to cure for seven days and provide stiff restraint to the SHCC overlay. SHCC overlays of 30 mm thickness were sprayed onto one side of each sample and left to harden for 24 hours before LVDT’s were attached as shown in Figure 4.21 (top, right) to measure deformation on the outer face of the SHCC over a gauge length of 500 mm. These specimens were kept in a similar climate as the free shrinkage specimens. The shrinkage development over 56 days of drying is shown in Figure 10c. After 56 days the average shrinkage

strain of the free specimens was 675 micro strain. This is a relatively low shrinkage compared with other researchers (eg. Boshoff 2007). The restrained shrinkage at the surface after 56 days was in the range 567.5 to 623.7 micro strain, with a higher strain measured for the vertical arrangement of bricks. No cracks were observed, in the overlays.

(a)

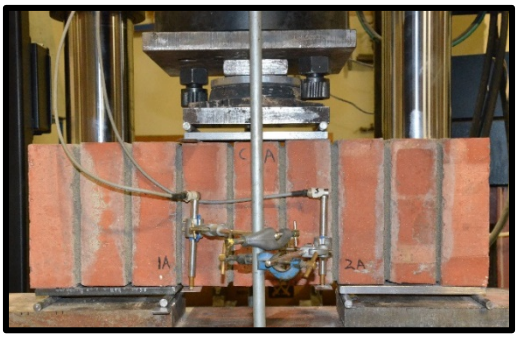

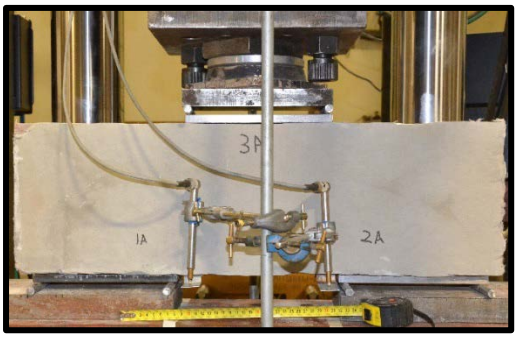

(b) De-bonding for 30 mm SHCC overlay

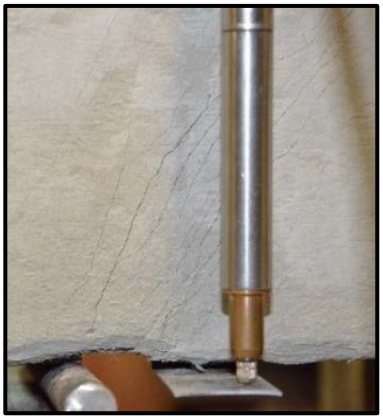

(c) Multiple shear cracking along shear plane in 10 mm SHCC overlay

Figure 4.19: (a) Large triplet test setup of control and overlayed specimens, showing (b) de-bonding along the masonry-overlay interface for 30 mm overlays and (c) (from left to right) multiple shear crack formation in 10 mm overlays, localisation and larger de-bonded region on the (rear) smooth brick face than on the (front) grooved brick face.

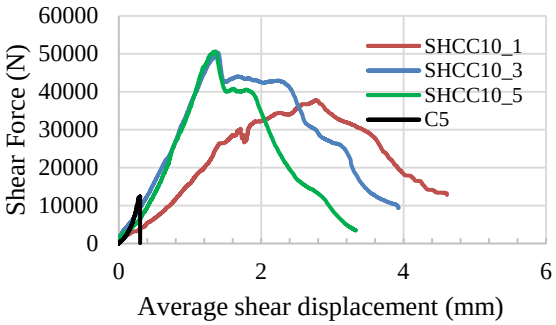

Triplet specimen	Shear force (kN)	Shear stress (MPa)
Masonry (3)	11.6 (0.537)	0.29
10 mm overlay (3)	46.21 (0.159)	5.06
30 mm overlay (2)	58.14 (0.038)	-
(No. of specimens)	(Coefficient of variation)	

Figure 4.20: Large triplet specimen responses for 10 mm overlays, and tabularised average resistances for control, 10mm overlay and 30 mm overlay specimens.

4.3.5 Validation: Shear wall test

Validation of the overlay strategy is currently performed in the structures laboratory of Stellenbosch University (Van Zijl and De Beer 2016b). A preliminary report is given in this section. Up to now, three masonry shear walls of 935 x 1150 mm (height x width) were tested. Two were control walls, the first a single leaf masonry wall of 110 mm thick, and the second a double leaf wall of 220 mm thickness. The third wall was 110 mm thick, onto which a 30 mm overlay was sprayed on one face at the masonry age of 30 days, having cured in laboratory conditions. The SHCC overlay was not protected from drying shrinkage, but kept in laboratory conditions until the time of testing, when the overlay was 50 days old. No visible cracking arose, but after spraying water onto the surface, fine cracks could be observed as darker lines on the photo in Figure 4.21d.

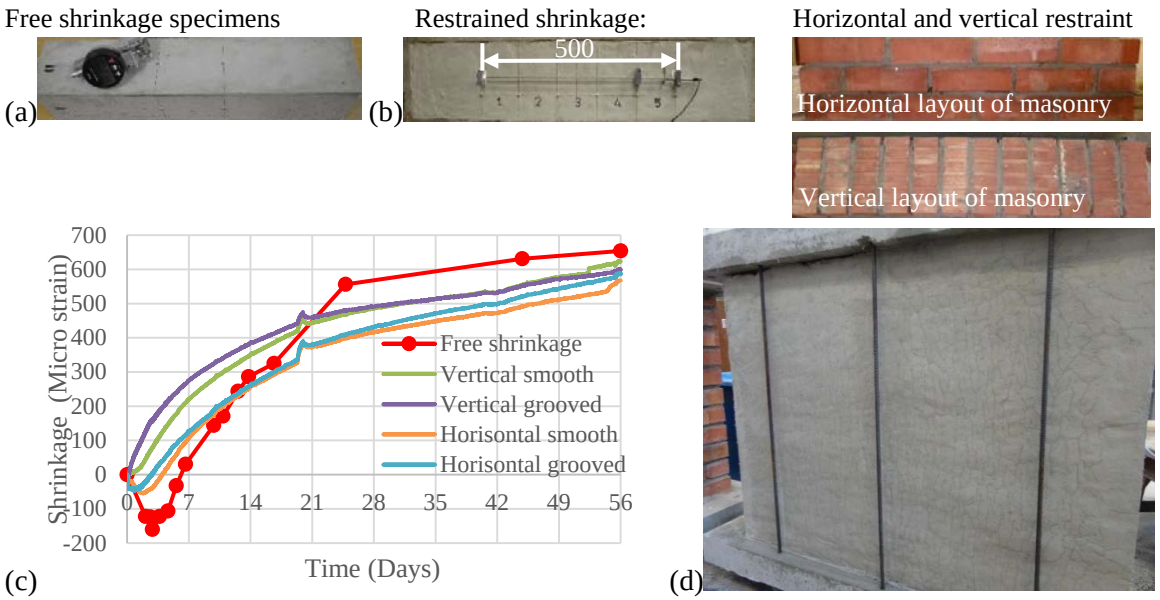

Figure 4.21: Drying shrinkage measurement on (a) free shrinking SHCC specimens, and on (b) restrained SHCC overlays, showing (c) the shrinkage strain development in time and (d) fine shrinkage cracks on the large shear wall overlay.

Each wall was built onto reinforced concrete beam, and another placed on the top. The two beams were subsequently tied with three threaded rods on each side, as seen in Figure 4.21d. On the day of testing, the walls were placed in a specially designed A-frame, bolted to the strong floor in the laboratory. An illustration of the setup is given in Figure 4.22.

The test results of the first three specimens are shown in Figure 4.23. Diagonal cracks have been highlighted in white on the two control walls, and in black on the wall with overlay. The horizontal load-displacement responses are shown on the graph in Figure 4.25d. The horizontal displacement is the difference between LVDT measurements on the wall top and the wall bottom, to subtract overall shift of the wall during the test. It is clear that significantly increased shearing load and ductility is brought about by the SHCC overlay. Multiple cracks are successfully induced in the overlay. From this result, it appears that a thinner than 30 mm overlay may be selected, whereby multiple diagonal cracks might arise earlier without impairing the ductility.

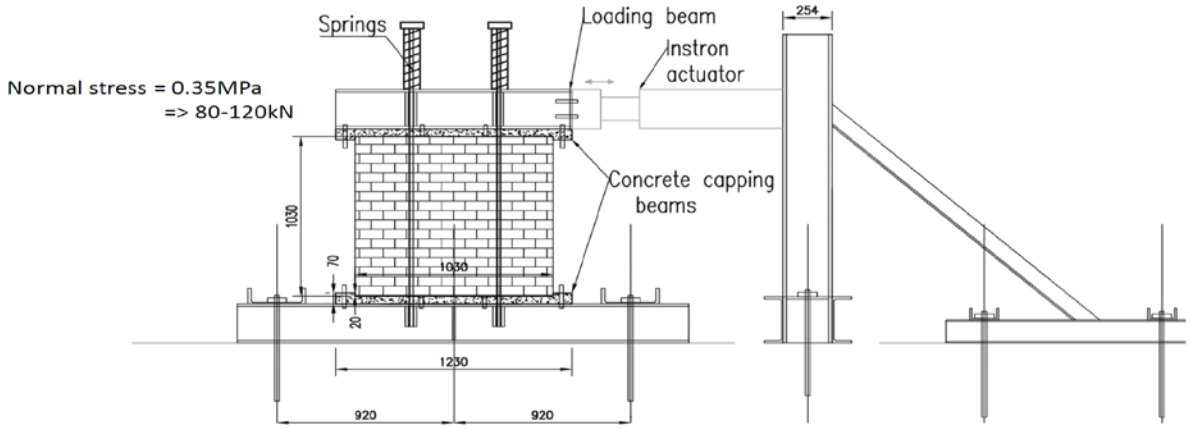

Figure 4.22: Shear wall test setup shown schematically. (Dimensions in mm.)

4.4 Concluding remarks

The retrofitting strategies presented in this chapter were enabled by thorough understanding of the mechanical behaviour of the substrate masonry and concrete, the retrofitting materials CFRP and SHCC, and the interfaces between them. Appropriate constitutive models for these construction materials and the interfaces between overlay and substrate were developed and characterised. Retrofitting for crack-control and increased seismic resistance have been the respective objectives of the strategies reported in this chapter, but are not limiting.

The results of SHCC bonded overlay by Van Zijl and Stander (2009) have been included in Chapter 8 of the STAR TC 240-FDS (Van Zijl and Slowik 2016). International interest in the retrofitting strategies is evident. The author received the best paper award for the retrofitting strategy towards renovating the 'Adelaar' building (Van Zijl and Verhoef 2001) at the 9th Canadian Masonry Symposium in Fredericton, Canada in June 2001. Dr Jens-Peter Ulfkjaer of Aarhus University has invited the author to visit the group to advise on the development of a retrofitting strategy for masonry buildings in Denmark, after the recent collapse of a masonry façade there. The author was also visiting professor in the Department of Civil and Geosciences of Delft University of Technology in August-September 2016, hosted by Professor Jan Rots. His group is involved in investigating the recent emergence of seismic activity in the Groningen province of the Netherlands due to gas extraction. The author was invited to present a seminar to the group on retrofitting of masonry walls for seismic resistance.

References

Badenhorst AJ 2012. Debonding of external carbon fibre reinforced polymer plates from reinforced concrete structures by cyclic loading effects. MScEng-thesis, Stellenbosch University, South Africa.

Badenhorst AJ, Van Zijl GPAG 2016. Cyclic debonding of carbon fibre reinforced polymer strips from reinforced concrete. Concrete / Beton, Journal of the Concrete Society of Southern Africa.

Boshoff, W 2007. Time-Dependant Behaviour of Engineered Cement-Based Composites. PhD dissertation, Stellenbosch University, South Africa.

Boshoff WP and Van Zijl, GPAG 2007. A computational model for strain-hardening fibre-reinforced cement-based composites. J SAICE, 49(2) 24-31.

British Standard BS EN 1052-3 2002. Method of test for masonry- Part 3 Determination of initial shear strength. BSI British standards.

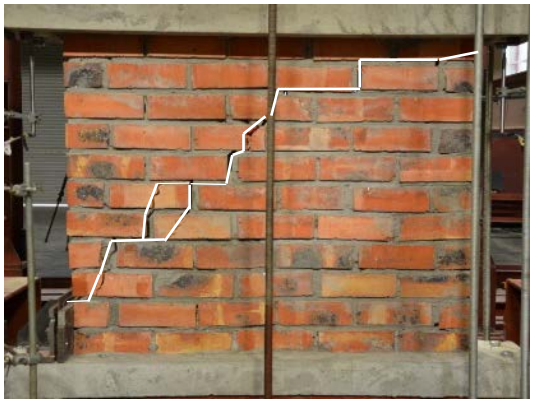

(a) Control wall, t = 110 mm

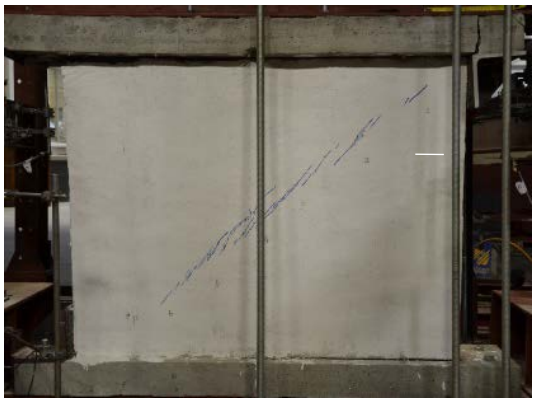

(b) 110 mm wall with 30 mm SHCC overlay

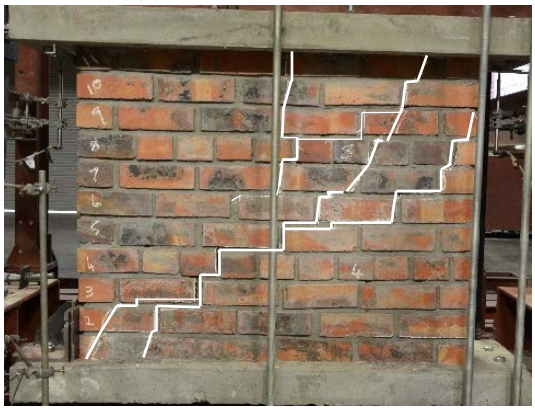

(c) Control wall, t = 220 mm

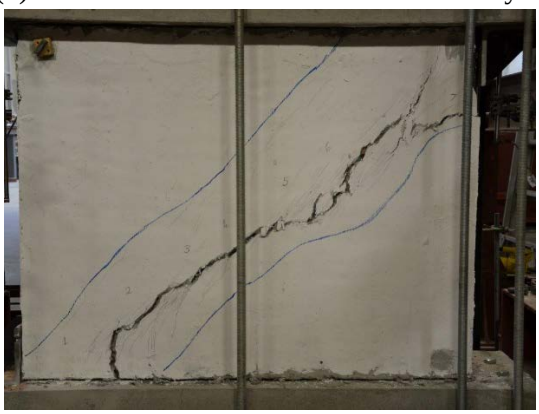

(d) 220 mm wall with 15 mm SHCC overlay

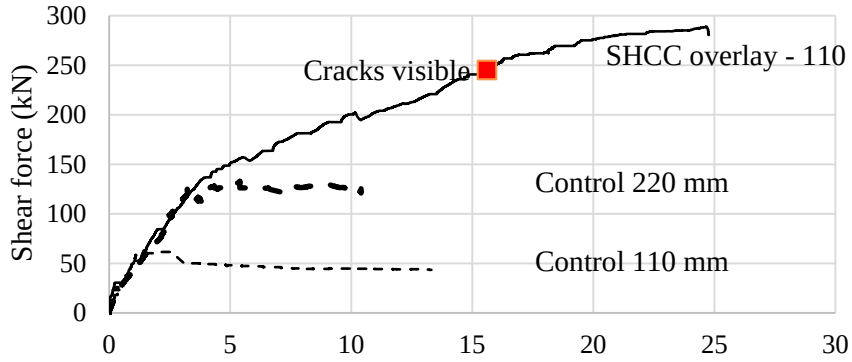

(e)

Figure 4.23: Failure patterns after the shear tests drawn in white on (a) single leaf (110 mm thick) reference wall, (b) single leaf with 30 mm SHCC overlay and (c) double leaf (220 mm thick) reference wall, (d) double leaf with 15 mm SHCC overlay, as well as (e) the corresponding shear force – displacement responses.

De Beer L and Van Zijl GPAG 2016. SHCC overlay as retrofitting strategy for load bearing masonry seismic resistance. In: Proceedings of BEFIB, Paper ID 117, 19-21 September 2016, Vancouver, Canada.

Li VC, Wang S, Wu C 2001. Tensile strain-hardening behavior of PVA-ECC, ACI Materials Journal 98 (6) 483–492.

Lin, Yi-Wei 2014. Strengthening of structures using ECC shotcrete. PhD dissertation, University of Auckland, New Zeeland.

Lourenço PB, Rots JG and Blaauwendraad J (1998). Continuum model for masonry: parameter estimation and validation. J. ASCE J. Struct. Eng., June, 642-652.

Lukovic M 2016. Influence of interface and SHCC properties on the performance of repair systems. PhD dissertation, Deflt University of Technology, The Netherlands.

SANS 10249. 2012. Masonry walling. Pretoria: SABS Standards Division, South Africa.

SANS 10160-4. 2011. Basis of structural design and actions for buildings and industrial structures. Part 4: Seismic actions and general requirements for buildings. Pretoria: SABS Standards Division, South Africa.

Slowik V, Luković M, Wagner C, Van Zijl GPAG 2016. Behaviour of bonded SHCC overlay systems, Chapter 8 of A framework for durability design with strain-hardening fibre-reinforced cement-based composites (eds. GPAG Van Zijl, V Slowik), State-of–the-art-report of RILEM Technical Committee 240-FDS, SPRINGER.

Stander H 2007. Experimental and computational characterisation of SHCC-Concrete interfacial bond. MScEng-thesis, Stellenbosch University, South Africa.

Van der Pluijm, R 1992. Deformation controlled shear tests on masonry. Rep. BI-92-104, TNO Building and Construction, Delft, The Netherlands (in Dutch).

Van der Pluijm R 1998. Overview of deformation controlled combined tensile and shear tests. Rep. TUE/CCO/98.20, Eindhoven Univ. of Technology, Eindhoven, The Netherlands.

Van Zijl, GPAG 2000. Computational modelling of masonry creep and shrinkage. PhD dissertation, Delft Univ. of Techn., The Netherlands.

Van Zijl GPAG 2004a. Modeling Masonry Shear-Compression: Role of Dilatancy Highlighted. Journal of Engineering Mechanics 130(11): 1289-1296.

Van Zijl GPAG 2004b. Masonry shear response characterization. Masonry International, Journal of the British Masonry Society, 17(1), 26-32.

Van Zijl GPAG 2007. Improved mechanical performance: Shear behaviour of strain-hardening cement-based composites (SHCC). Cement and concrete reseach 37:1241-1247.

Van Zijl GPAG 2009. Constitutive model for fibre-reinforced strain-hardening cement composites (SHCC), Concrete / Beton, Journal of the Concrete Society of Southern Africa, November 2009, No124: 8-15.

Van Zijl GPAG 2010. Computational modeling of strain-hardening cement composites (SHCC), International Conference on Advanced Concrete Materials, 17-19 November 2009, Stellenbosch, South Africa, pp. 263-270

Van Zijl GPAG, De Beer L 2016a. An SHCC overlay retrofitting strategy for unreinforced load-bearing masonry, Proceedings of 9th International Conference on Fracture Mechanics of Concrete and Concrete Structures - FRAMCOS-9, V. Saouma, J Bolander, E Landis (Eds), 29 May-2 June 2016, Berkeley, USA.

Van Zijl GPAG, De Beer L 2016b. Retrofitting unreinforced load-bearing masonry with a sprayed SHCC overlay, Proceedings of FIB 2016 Symposium, 21-23 November 2016, Cape Town, South Africa.

Van Zijl GPAG, De Borst R and Rots JG, 2001a. The role of crack rate dependence in the long-term behaviour of cementitious materials. Int. J. Solids and Structures, 38(30-31), 5063-5079.

Van Zijl GPAG, De Borst R and Rots JG, 2001b. A numerical model for the time-dependent cracking of cementitious materials. Int. J. Numerical Methods in Engineering, 52(7), 637-654. DOI: 10.1002/nme.211

Van Zijl GPAG and De Vries PA 2005. Masonry wall crack control with CFRP. ASCE Journal of Composites for Construction, 9(1), 84-89.

Van Zijl GPAG, De Vries PA and Vermeltfoort AT 2004. Masonry wall damage by restraint to shrinkage. ASCE Journal of Structural Engineering. 130(7), 1075-1086.

Van Zijl GPAG, Rots JG, Vermeltfoort AT 2001. Modelling of shear-compression in Masonry. CDROM-Proc. 9th Canadian Masonry Symposium, PH Bischoff, JL Dawe AB, Schriver and AJ Valsangkar, eds., Fredericton, Canada.

Van Zijl GPAG, Slowik V (eds.) 2016. A framework for durability design with strain-hardening fibre-reinforced cement-based composites (SHCC), State-of-the-art report, Rilem TC 240-FDS, Springer Publishers.

Van Zijl GPAG, Stander H 2009. SHCC repair overlays for RC: Interfacial bond characterization and modeling, CDROM Proc. International Conference on Concrete Repair, Rehabilitation and Retrofitting (ICCRRR 2008), University of Cape Town, South Africa, pp. 995-1003.

Van Zijl GPAG, Verhoef LGW 2001. Computational assessment of renovation intervention in a historic masonry building. CDROM-Proc. 9th Canadian Masonry Symposium, eds. P.H. Bischoff, J.L. Dawe, A.B. Schriver and A.J. Valsangkar.

Van Zijl GPAG and Verhoef LGW 2003. Double Sided Restrengthening of Historic Brickwork with Rods and Strips of Carbon Fibre Reinforced Plastic (CFRP). Int J Restoration of Buildings and Monuments, 9(4), pp. 435-453.

Van Zijl GPAG, Wittmann FH, Toledo Filho RD, Slowik V, Mihashi H 2016. Comparative testing of crack formation in strain-hardening cement-based composites (SHCC). Materials and Structures, 49(4) 1175-1189.

Verhoef LGW and Van Zijl GPAG 2002. Re-strengthening of brickwork to reduce crack width. Advances in Engineering Software, 33, 49-57.

Vermeltfoort AT 2005. Brick-mortar interaction in masonry under compression. PhD dissertation, Eindhoven University of Technology, Eindhoven, The Netherlands.

Vermeltfoort AT, Martens DRW and Van Zijl GPAG 2007a. Laser speckle (ESPI) observation of brick-mortar interface behaviour under compression. Canadian J Civil Engineering, November 2007, 34(11) 1467-1474.

Vermeltfoort AT, Martens DRW and Van Zijl GPAG 2007b. Brick-mortar interface effects in masonry under compression. Canadian J Civil Engineering, November 2007, 34(11) 1475- 1485.

Vermeltfoort AT, Raijmakers TMJ and Janssen HJM 1993. Shear tests on masonry walls.

Visser G 2009. FRP external reinforcement of bridges in SA, MEng-thesis, Stellenbosch University, South Africa.

Chapter 5 Sustainable energy harvesting structures

5.1 Introduction

The southern African region has abundant wind and solar radiation, and technologies to efficiently harvest them are emerging. More than 90% of South African power demand is currently met by coal-fired power stations. The introduction of the Renewable Energy Independent Power Producer Program (REIPPP) in August 2011 was a significant step towards the envisaged reduction of South Africa's emissions by 34% by 2020, and 42% by 2025.

Experimental wind turbines were erected in 2002-2003, but the REIPPP has led to the construction of operational wind farms in South Africa. For the three rounds of REIPPP tender bids, the wind energy unit price dropped from 114c per kWh to 74c per kWh. Whilst this indicates the competitive nature and rapid technology development in the relatively short time span, local content remains a concern, comprising typically civil works on wind farms, foundation design to tight specification, and construction assembly. Until recently, steel support towers have been fully imported. Two local steel tower factories have started producing towers, the first in Coega in the Eastern Cape in early 2014 delivering towers of 80 to 120 m tall, and the second in Atlantis in the Western Cape delivered the first 99 m tall towers in October 2015. Also, post-tensioned concrete towers have recently been introduced in local wind farms with pre-casting of the RC elements and road-transportation to site.

The structural design of support towers for South African wind farms has without exception been done by foreign partners. A challenge lies in the special nature of wind turbine support structures and the extremely high number of load cycles they experience due to wind turbulence, the turbine rotation, and the aerodynamic interaction with the support tower when a blade passes it. In the typical wind turbine design life span of 20 years, it experiences roughly a hundred million (10^8) load cycles, which exceeds existing characterised fatigue results. No design standard for wind turbine structures yet exists. Design guidelines have been proposed, for instance the DNV/Risø (2002) and IEC 61400-1:2005. Two Masters projects were launched to investigate appropriate design guidelines for local conditions. Additional objectives were comparison of the material cost for tall (80, 100 and 120 m) post-tensioned concrete, steel and hybrid towers and their foundations (Way 2014, Way and Van Zijl 2015), and understanding the influence of various local founding conditions and cracking of a tall (100 m) RC tower on the tower vibration frequencies (Van Zyl 2014, Van Zyl and Van Zijl 2015).

The solar chimney power plant (SCPP) concept offers an alternative for solar thermal energy capture. A collaborative project "The Solar Chimney: Research on structural and flow characteristics" was sponsored by the Volkswagen Stiftung, Hannover over the period 2003 to 2007. Together with the author, the project investigators were Professor Reinhard Harte of Bergische Universität Wuppertal in Germany, and of Stellenbosch University Professors Detlev Kröger and Theo von Backström of the Department of Mechanical Engineering. While Professor Harte and the author focussed on structural aspects, the colleagues from Mechanical Engineering were responsible for flow and performance characteristics, and appropriate turbine systems and layout. A reference case of a 1500 m tall tower, and 7000 m diameter collector structure, with power generating capacity suggested to be 400 MW was considered, although other configurations were studied for their power output. Arid regions in Upington and other Northern Cape regions of South Africa were considered for a SCPP.

Three PhDs were awarded from this project. Under the author's supervision, Dr Cobus van Dyk defined and analysed structural options for the inlet guide vanes supporting the 1500 m tall chimney (van Dyk 2004). He subsequently assessed technology development requirements for this radical innovation (Van Dyk 2008, Van Zijl and van Dyk 2009), with its structural height exceeding existing tallest building by a significant margin. Emeritus-Professor Johan Retief provided co-supervision on structural reliability, and Emeritus-Professor Gideon de Wet on systems engineering. Dr Thomas Fluri (2008) proposed a turbine layout and optimised power conversion units under supervision of Professor von Backström. Under supervision of the late Professor Detlev Kröger, Dr Hannes Pretorius (2007) studied the output performance towards optimising and controlling the solar chimney plant, considering various alternative collector roof layouts, size, reflectivity and emissivity, as well as soil or rock type for heat storage and the influence of crops grown under the collector. Supporting studies were performed on damping of the vibration modes and wind loading simulations (Rousseau 2005, Rousseau and Van Zijl 2007), as well as wind flow characteristics around cylindrical towers and the stabilising role of vertical ribs (Alberti 2006, Alberti and Van Zijl 2007). Due to the high Reynolds number regime expected for the tall chimney structure, wind tunnel studies were performed in the large facilities of Shimizu Corporation, Tokyo in collaboration with Professor Yukio Tamura to shed light on the stabilising influence of vertical ribs around the cylindrical tower circumference (Kikuchi et al. 2007a).

The Solar Chimney project led to further collaboration with wind-engineering specialist Emeritus-Professor Hans-Jürgen Niemann and Emeritus-Professor Wilfried Krätzig, a specialist in shell structures and cooling tower design. Through this collaborative project, structural design and construction methods, multiple turbines as opposed to a single large one, as well as performance of the plant and its control towards base line power production were brought to an advanced level (Von Backström et al. 2008). A cost model was developed by the research team (Fluri et al. 2008), concluding that previous cost estimates by Schlaich et al. (2004) likely underestimated the cost. Despite these research and publication efforts, as well as approaches to regional power utilities by the research team and its wider network of collaborators, the concept has not been accepted for implementation. Internationally, attempts to raise capital to construct a solar chimney plant continue. In this chapter, aspects of the contributions by the author and his team at the CDSI towards the SCPP are described.

5.2 The solar chimney wind loading

Wind excitation of the tall chimney tower is the dominant action acting on the SCPP. Figure 5.1 shows the schematic and artist's impression of a SCPP. Tower heights in the range 500-1500 were considered by the research team, with the 1500 m tall tower clearly exceeding existing building heights by a significant margin. Wind speeds at such height, combined with the tower diameter of 160 m will cause wind flow with Reynolds numbers in the transcritical range, i.e. $R_e > 5 \times 10^6$. Wind tunnels did not exist that could generate such high Re numbers, and this range is beyond the currently characterised flow regimes. Uncertainties are the drag coefficient required for toppling-over design consideration, and whether alternate vortex shedding occurs in this regime, leading to potentially destructive lateral vibration and resonance of the tower.

Alberti (2006) postulated that nature holds a potential mitigating solution. The Saguaro Cactus (Figure 5.2a) reaches heights of 8 to over 15 m, with diameters 0.3 to over 0.8 m, leading to slenderness ratios (height / diameter) in the range 12 to 23 for taller species, and 5 to 12 for those shorter than 4.5 m. This includes a slenderness ratio comparable with the SCPP chimney of approximately nine. The Saguaro Cactus is exposed to extreme wind conditions of $R_e = 10^6$ (Talley and Mungal 2002), but has adapted to withstand these wind forces

despite a relatively shallow root system. The ribbed circumference, with rib protrusion height to cylinder diameter of roughly 0.07, is postulated to be a key mechanism of changing flow patterns around the Cactus.

This nature-inspired mitigation measure was subjected to experimental verification, with two alternative rib configurations shown in Figure 5.2c together with the control, smooth cylinder (Alberti 2006). Based on the wind tunnel size and blockage ratio of no more than 5%, the models were 1000 mm high with a 300 mm outer diameter Perspex pipe as cylindrical core. V-shaped Perspex strips were added to create the 21 mm high vertical ribs as shown in Figure 5.2c, simulating the typical Cactus rib height to shaft diameter ratio of (21 / 300 =) 0.07. Pressure taps were placed every 8° around the circumference of the cylinder in three rows at heights of 400 mm, 500 mm and 600 mm from the base – see Figure 5.2b. In the ribbed models, the pressure taps were placed in the valley between the vertical ribs. For full details, the reader is referred to Alberti (2006).

Through collaboration with Professor Tamura, the models were tested in a large wind tunnel of the Shimuza Corporation in Tokyo. The facility has a fan of 4 m diameter, which generates wind speed of maximum 35 m/s and test section of 3.5 m wide, 2.5 m high and 20 m long. Unfortunately vibrations occurred at high fan speeds, limiting the test regime to a maximum of 25 m/s, and a range of $9.9 \times 10^4 < R_e < 5.6 \times 10^5$.

Only main results are highlighted. Firstly, a stabilising effect by the ribs is observed in the results summarised in Figure 5.3. For the smooth cylinder, external pressures (C_p) show transitions from symmetrical distribution around the circumference at lower wind speeds (10, 15, 16 m/s) to asymmetrical pressures at intermediate wind speeds (17, 18 m/s), and back to a symmetrical distribution at higher wind speeds (19, 20, 25 m/s). This does not occur with the ribbed cylinders (Figure 5.3d,e). Secondly, the high suction ($C_p < -2$) that will lead to an oval deformed shape of the circular cross-section of the tower, is roughly halved ($C_p \approx -1$) in both ribbed cylinders.

The instability in wind pressures, and in particular the asymmetrical pressure distributions around the cylinder circumference is argued to indicate likelihood of alternate vortex shedding, which may cause lateral oscillation. In the tested regime, this was shown to be mitigated by the ribs. The structural design, constructability and cost estimate of such ribs were not performed, but present a potential solution for realising the SCPP. Also, the transcritical regime of R_e numbers could not be reached in the wind tunnel, and the stabilising effect of the ribs remains to be verified in this regime.

(a) 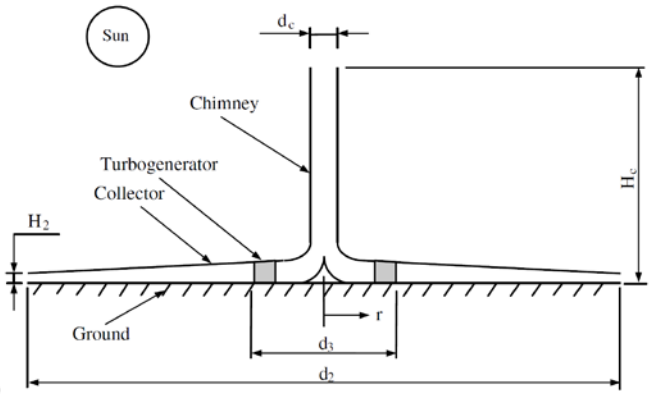

(b) 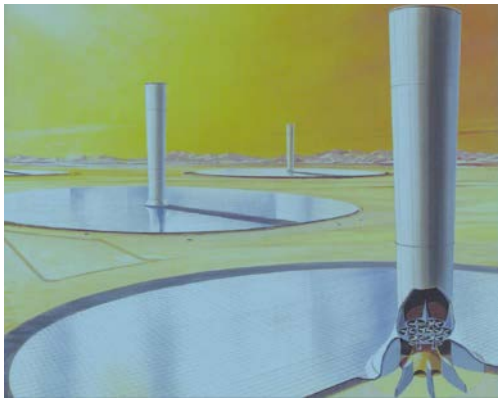

Figure 5.1: (a) Schematic representation and (b) an artist's impression (Schlaich 1995) of a SCPP.

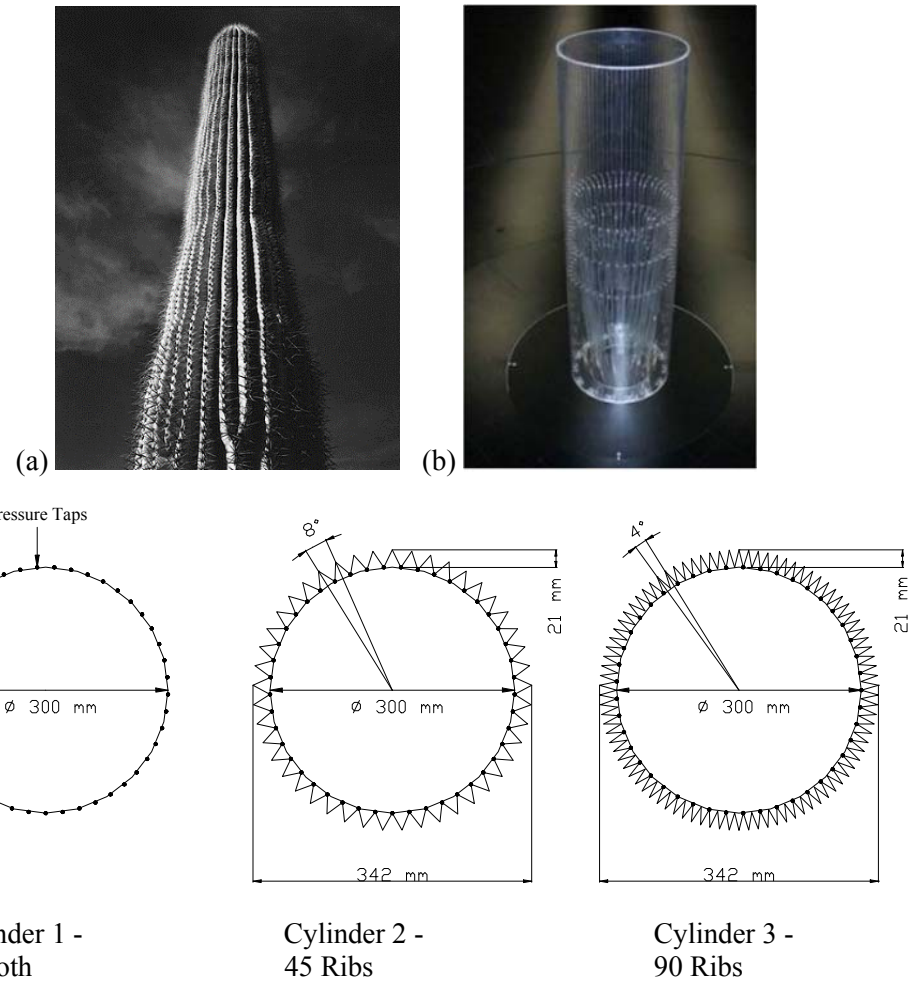

Figure 5.2: (a) The Saguaro Cactus ribbed structure (Talley and Mungal 2002), (b) wind tunnel test model without ribs, showing internal and pressure gauges, (c) schematic of three cylinder models tested, with height 1000 mm (Alberti and Van Zijl 2007).

While ovalisation and lateral vibration were addressed in the above experimental procedures and results, the internal pressures in an open cylinder such as the solar chimney, and the overall drag coefficient was not measured. Two further wind tunnel test series were performed in the wind tunnel of the Department of Mechanical Engineering, Stellenbosch University. This facility has a 90 m/s wind speed capacity but a test space of only 1.425 m wide, 1.0 m high and 1.9 m long. To keep within the 5% blockage limit, small cylindrical models were manufactured, shown in Figure 5.4 for determination of the drag coefficient. Once again the transcritical regime could not be reached, with the test range limit to $9.9 \times 10^4 < R_e < 5.6 \times 10^5$.

The model was attached to a one directional load cell balance, which was designed to read the total horizontal drag force on the cylinder. From this force (F_d) the drag coefficient (C_d) was calculated from

$$C_D = \frac{F_D}{\frac{1}{2}\rho v^2 A} \tag{5.1}$$

with ρ the air density, v the wind speed and A the frontal area of the cylinder. Hereby, the drag coefficients shown in Figure 5.5 were calculated, confirming stabilisation of also the drag coefficient by the ribs.

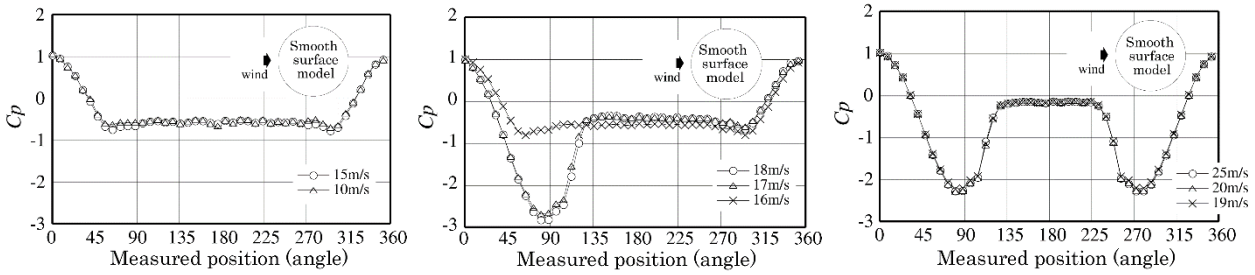

Cylinder 1 – Smooth: (a) 10, 15m/s (b) 16, 17 and 18m/s (c) 19, 20 and 25m/s

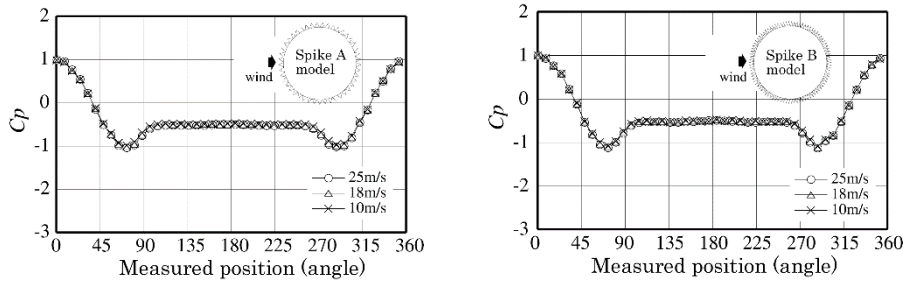

(d) Cylinder 2 - 45 ribs (e) Cylinder 3 model - 90 ribs

Figure 5.3: External pressures coefficients (C_p) measured in Cylinder 1–smooth for wind speeds (a) 10, 15 m/s (b) 16, 17 and 18 m/s (c) 19, 20, 25 m/s. The pressures on the ribbed cylinders with (d) 45 ribs and (e) 90 ribs (Kikuchi et al. 2007a).

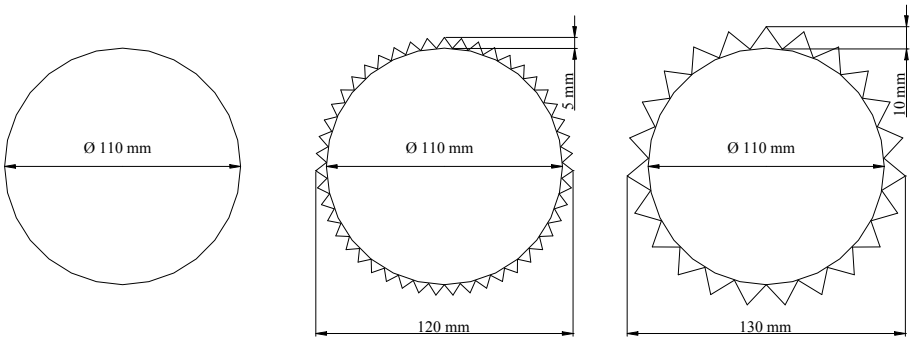

Cylinder 1 - Smooth | Cylinder 2 - Small Ribs | Cylinder 3 - Large Ribs

Figure 5.4: Three cylinder models of height 285 mm used in wind tunnel tests to determine the drag coefficient (Alberti 2006).

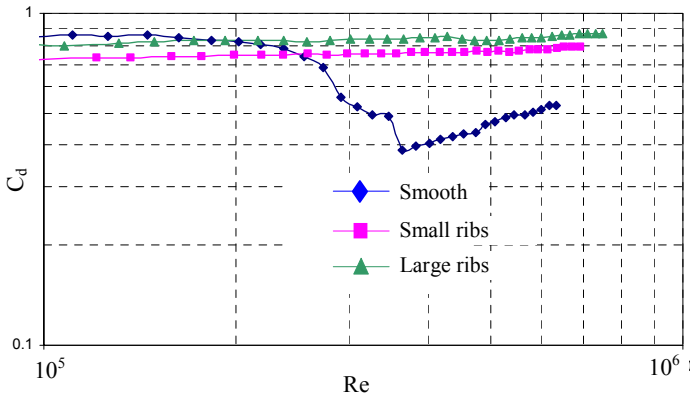

Figure 5.5: Drag coefficients measured on cylinder models (Alberti 2006, Alberti and Van Zijl 2007).

The third experimental series was performed in the wind tunnel at Stellenbosch University to measure external (C_p) and internal (C_{pi}) pressures along the cylinder circumference at various heights close to the open top end, to inform the structural design of the tower, but also the thermodynamic performance evaluation of the SCPP. The details are reported by Alberti (2006) and summarised by (Alberti and Van Zijl 2007). An important finding was that the internal pressure (suction) was reduced from C_{pi} = -0.8 for no internal, upward flow in the cylinder to C_{pi} = -0.1 for upward air flow in the cylinder similar to that expected in the SCPP (Alberti and Van Zijl 2007).

5.3 Structural behaviour and design aspects

The inlet guide vanes direct the horizontal air flow under the collector (Figure 5.1), into the tower towards the turbine(s), as illustrated in Figure 5.6a. Van Dyk (2004) proposed to exploit these structures for transmitting vertical forces from the tower to the base, as illustrated in Figure 5.6b. A further transition to the tower shell is required to avoid excessive stress concentrations. Three geometries, of which discretised geometries for finite element analysis are shown in Figure 5.7. It was shown that the alternative transitions did not influence the natural frequencies of the overall tower structure, with the first global modal frequency equal for the three solutions at 0.1 Hz. Option (iii) in Figure 5.7b was calculated to be the cheapest option (Van Dyk 2004).

For the vibrational analyses, various structural matters were investigated and finally implemented in the model by van Dyk (2004), including the wheel spoke stiffener concept proposed by Schlaich et al. (2004) to prevent or limit excessive ovalisation of the tower, an optimised wall thickness and steel reinforcement without significant internal air flow losses, as described in more detail by Van Dyk (2008)[1]. Rousseau (2005) studied the dynamic response of the 1500 m tall tower. The first six natural vibration modes are illustrated in Figure 5.8, showing the dominant first mode (at 0.1 Hz), and the phenomenon of ovalisation (Mode 2). He further considered three simplified configurations of wind action schematised in Figure 5.9 for dynamic wind loading cases. In particular, load inversions simulate winds generated by temperature inversions and thunder storms typical for Upington or other Northern Cape regions of South Africa.

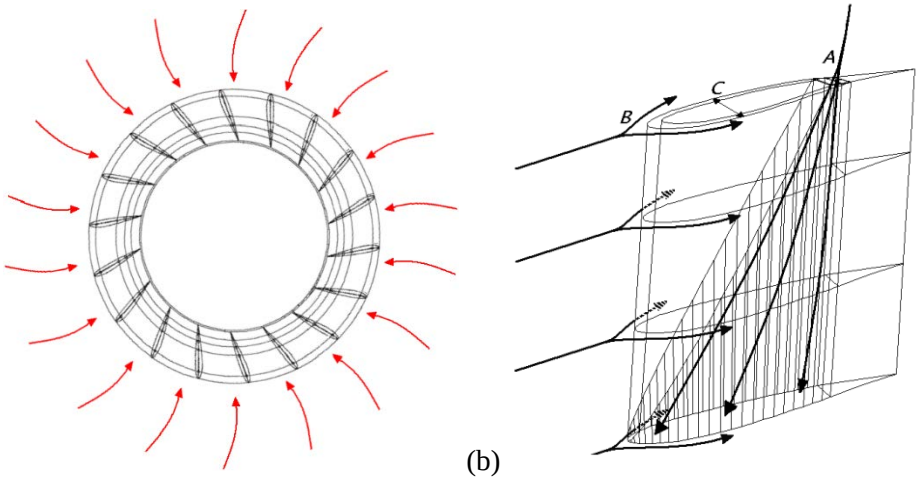

(a) (b)

Figure 5.6: Illustration of the inlet guide vanes (a) aerodynamic function to swirl air flow into the tower in case of a single turbine and (b) structural function of force transmission from the tower to the base (Van Dyk 2004, Van Dyk and Van Zijl 2004).

[1]The contributions of BEng(Civil) final year projects performed by Michael Lumby (2003) on optimising the Solar Chimney wall thickness and steel reinforcement, and by Eliz-Mari Lourens (2004) on the ring stiffeners are acknowledged.

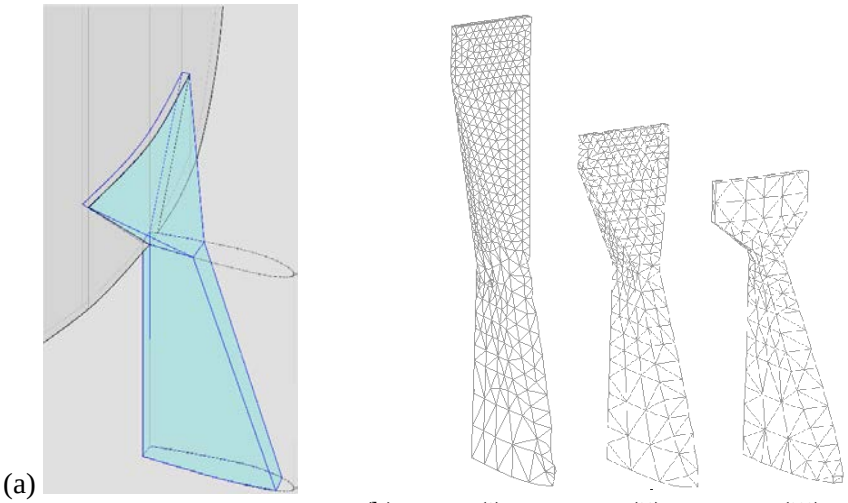

Figure 5.7: (a) Illustration of bearing support within an inlet guide vane, and (b) three alternative solutions investigated (Van Dyk and Van Zijl 2004).

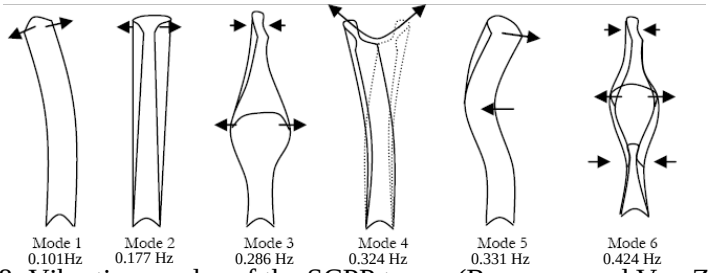

Figure 5.8: Vibration modes of the SCPP tower (Rousseau and Van Zijl 2006).

In absence of physical measurements of damping on such a tall structure, Rousseau and Van Zijl (2006) estimated a damping factor by extrapolation of measured damping values of various towers and chimneys. The result suggested a relatively low damping in the range 1.4 – 1.9% (of critical damping) for a structure with natural frequency of 0.1 Hz. The frequency response for these simplified wind load cases is shown in Figure 5.9 for a wind amplitude of 42.5 m/s. Of significance is whether load cases that excite particular higher vibration modes lead to higher vibration amplitudes than the typical Mode 1 unidirectional wind load used in static push-over analyses. At the frequency of 0.33 Hz (Mode 5, Figure 5.8), Load Cases 2 and 3 indeed are seen in Figure 5.9 to cause significantly higher amplitudes than Load Case 1, due to the excitation of the particular mode shape. However, the highest amplification of longitudinal excitation of the tower occurs at 0.1 Hz.

Alternate vortex shedding may lead to lateral or across wind vibration. In absence of mitigating measures such as vertical ribs suggested in Section 5.2.1, agreement between a vibrational mode of the tower and the frequency of vortex shedding should be avoided. This is expressed by the Strouhal number S_t and the critical wind speed V_{crit} from:

$$V_{crit} = f \frac{D}{S_t} \tag{5.2}$$

with f the tower natural frequency and D the tower diameter. A Strouhal number of 0.22 has been suggested by van Dyk (2008) for the transcritical flow regime, based on ESDU (1998). This is adjusted for three-dimensional

effects along the tower height. Base on Equation (5.2) the critical wind speeds exceed the maximum wind velocities expected over the tower height (van Dyk 2008).

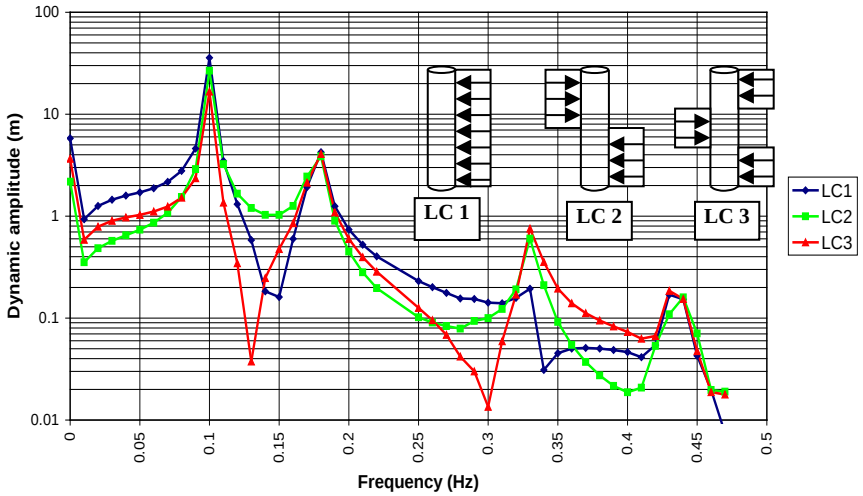

Figure 5.9: (a) Simplified wind load cases and (b) corresponding frequency response of the solar chimney (Rousseau 2005, Rousseau and Van Zijl 2006).

5.4 Systems engineering and technology management towards realising the SCPP

Due to the perceived immaturity of the SCPP technology, Cobus van Dyk (2008) proposed that the technology development be managed along principles of systems engineering and technology management. In incremental innovation, experience and capacities in familiar fields are exploited, but radical innovation is required for the 1500 m tall SCPP which exceeds existing structural heights by a significant margin (Figure 5.10), is required to deliver base line power generation despite day-night and seasonal cycles, and for a power conversion system of this scale. A systems-based strategy framework was developed, supervised in particular by Professor Gideon van Dyk on this topic, to identify critical technology elements and uncertainties for decision making towards resource allocation for research and development.

A radical innovation methodology (RIM) was developed, consisting of five stages, namely (i) setting up a reference case based on current technology and insight, (ii) systems breakdown into functional systems to identify technology elements, (iii) evaluation and comparison of alternatives and their impact on system performance, (iv) identification and isolation of critical technologies and assessment of the risk involved associated with the research and development to bring these technologies to the required performance level, and (v) formulating a strategy for each technology (Van Dyk 2008). The five phases are illustrated in Figure 5.11.

With the RIM applied to the SCPP tower specifically, three technologies critical for development were identified, namely reconfiguration of the tower wall thickness, a parabolic hyperboloid geometry and tower circumferential stiffeners. They are listed in Table 5.1 as the top three of ten identified technologies for development. The reference case of the SCPP tower (stage one of the RIM) is shown in Figure 5.12, for the power production capacity of 200 MW[2].

[2] Pretorius (2007) reports daily and seasonal variations to power generation, and control measures to mitigate the variations.

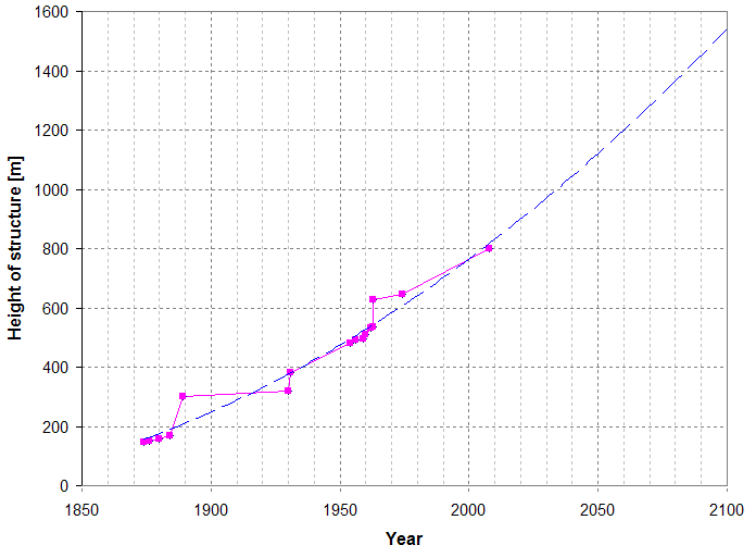

Figure 5.10: Extrapolation trend of tallest man-made structures (van Dyk 2008).

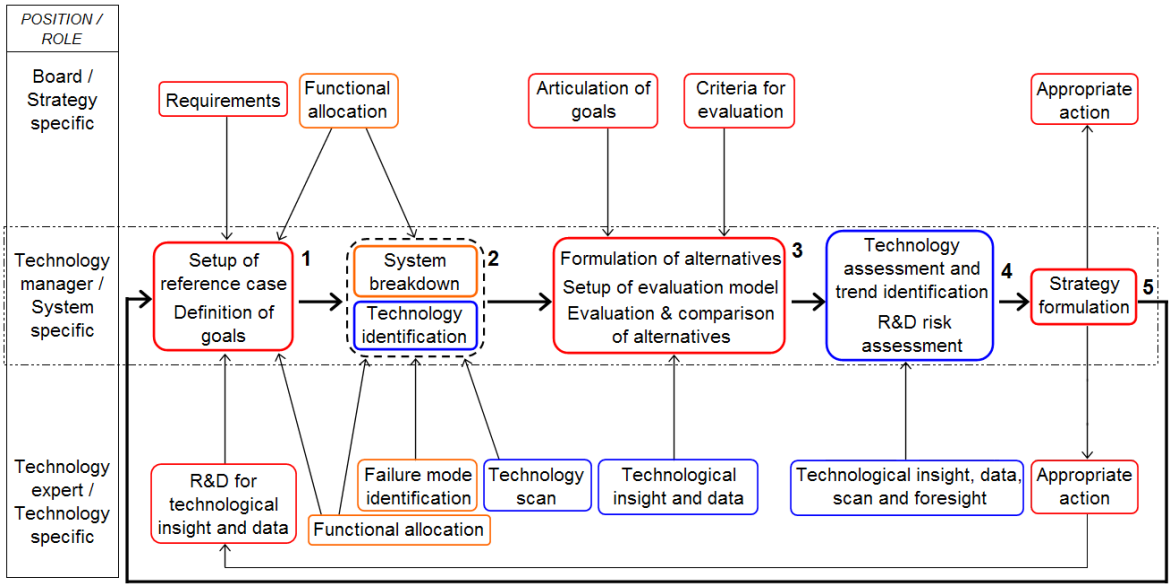

Figure 5.11: Graphical representation of the RIM (Van Dyk 2008).

Table 5.1: Research priorities based on technology position analysis in the RIM (van Dyk 2008).

Rank	R&D topic	Motivation
1	Incorporation of wall thickness re-configuration and investigation for mitigating adverse dynamic response.	Very significant mitigation of buckling with moderate reduction of LEC at very low R&D risk.
2	Incorporation of parabolic hyperboloid geometry and investigation for mitigating adverse dynamic response.	Very significant LEC reduction at low R&D risk.
3	Incorporation of more circumferential stiffeners, given the concept is proven.	Moderate mitigation of buckling at low R&D risk.
4	Wind velocity extrapolation profile characterisation, decreasing uncertainty in wind action model.	Moderate impact on buckling mitigation at moderate R&D risk.
5	Investigation to region's surface roughness characteristics in the area of the proposed site of construction.	Low to moderate impact on buckling mitigation at moderate R&D risk.
6	Investigation of mitigating adverse structural behaviour in increased chimney height.	Significant impact on LEC reduction at high R&D risk.
7	Investigation of mitigating adverse structural behaviour in flaring chimney.	Low to moderate impact on LEC reduction at moderate R&D risk.
8	Remain in touch with developments/breakthroughs in cable staying, external damping and directional design technology.	Further introductory/familiarizing investigations may prove productive toward identifying this field as a potential priority area.
9	Remain in touch with developments/breakthroughs in concrete material characteristics.	Although very high risk R&D, significant breakthroughs may impact significantly on structural integrity.
10	Further investigation to realise Saguaro Cactus geometry in order to mitigate adverse dynamic response.	Low to moderate impact on buckling (lower limit) at moderate to high R&D risk.

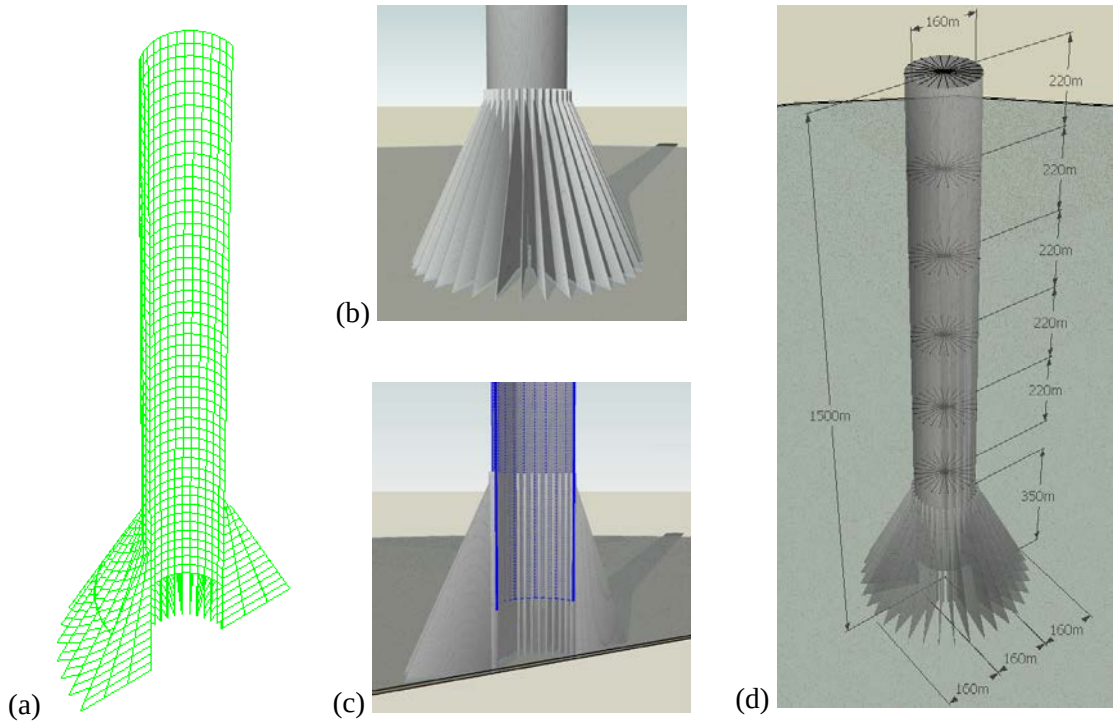

Figure 5.12: Illustration of the Solar Chimney (a) FE model, (b) transfer section, (c) chimney wall and (d) overall configuration (Van Dyk 2008).

5.5 Current status

The research project developed solutions regarding structural realisation of the large tower, power generation and control through various collector roof layouts and material, for day-night and seasonal generation capacity, and turbine and power unit layout. This motivated the extended research team to propose a pre-feasibility study of a SCPP to the Namibian power utility in February 2007. This was not accepted. Subsequently, structural design and refinement was performed for various tower sizes (500, 1000, 1500 m) by the Structural Division Germany of the Solar Chimney Competence Network (SCCN). The SCCN consisted of the research team, strengthened by Professors Krätzig, Niemann and Höffer of Bochum. A collaborative paper on the "State and recent advances in research and design of Solar Chimney Power Plant Technology" was published by the SCCN (Von Backström et al. 2008). Figure 5.13 shows the layout of three tower heights. It must be noted that these designs were prepared by the Structural Division Germany in parallel with the late stages of the SCPP research project, incorporating the optimised multiple turbine layout proposed by Fluri (2008).

A detailed cost model was developed by the research team for large scale SCCPs, including the cost of the tower, collector and the power conversion units (Fluri et al. 2009). Higher cost was found than previous estimates in the literature, both for the investment and levelised electricity cost (LEC). This was ascribed to higher actual plant cost, but also lower power production than previous estimates. Carbon credits were shown to significantly reduce LEC.

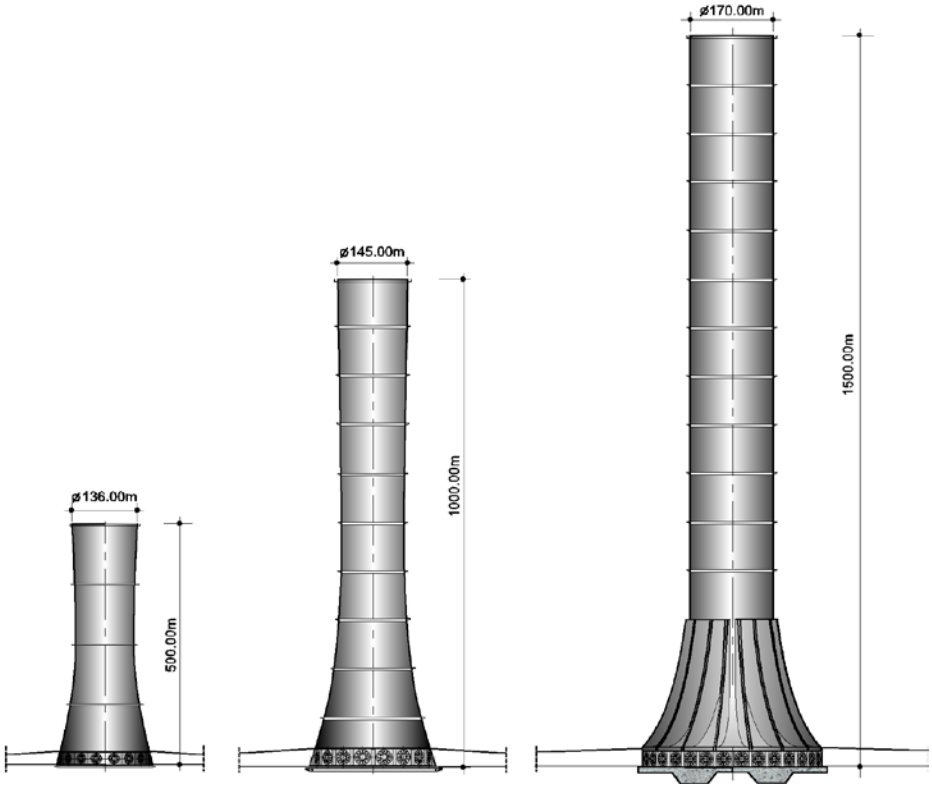

Figure 5.13: Variants of the Solar Chimney towers (Von Backström et al. 2008).

5.6 Concluding remarks

Whilst the SCPP concept has not been brought to application in actual solar energy capturing power plants, it is argued that the technology development through this research project by the team and collaborating international experts in the extended SCCN, has brought the level to the verge of implementation. The large capital investment may be the stumbling block, together with the large structural size. Raising capital for the construction of a SCPP is a continuing quest by lobby groups, with latest reports of German Consultancy company Schlaich, Bergermann and Partner collaborating with Hyperion Energy to build a 200 MW SCPP with a 1000 m tower and 10 000 m diameter collector in Western Australia, and EnviroMission collaborating with Apollo Development to build 200 MW capacity SCPPs in West Texas (NG 2014).

An international conference series Solar Updraft Tower Power Technology was launched by the collaborators, and the author served as Scientific Committee member. The conference was hosted by Ruhr-Universität Bochum and Bergische Universität Wuppertal in Bochum, Germany in October 2010, and by Huazhong University of Science and Technology in Wuhan, China in October 2012.

In September 2014, a seminar entitled *Design of wind turbine support structures* was presented to local consulting engineers to disseminate the research results. The seminar was chaired by the author, assisted by colleagues Dr Gert van Rooyen and Etienne van der Klashorst at Stellenbosch University.

References

Alberti L 2006. Flow around cylindrical towers: The stabilising role of vertical ribs. Master's Thesis, Stellenbosch University, South Africa.

Day WP 2012. A contribution to the advancement of geotechnical engineering in South Africa. DEng dissertation, Stellenbosch University, South Africa.

DNV/Risø 2002. Guidelines for Design of Wind Turbines. 2nd ed. Accessed 29th March 2014. Copenhagen: Det Norske Veritas (DNV) and Risø National Laboratory.

ESDU 1998. Engineering Science Data Unit. Response of structures to vortex shedding – structures of circular or polygonal cross section, HIS Standards Store.

Fluri TP 2008. Turbine layout for and optimization of solar chimney power conversion units. PhD dissertation, Stellenbosch University, South Africa.

Fluri TP, Pretorius JP, Van Dyk C, Von Backström TW, Kröger DG, Van Zijl GPAG 2009. Cost Analysis of Solar Chimney Power Plants, Solar Energy 83(2) 246–256.

Fraser ES Computational modelling of concrete footing rotational rigidity. Master's Thesis, Stellenbosch University, South Africa.

Fraser ES, Van Zijl GPAG 2009. Computational Investigations of Concrete Footing Rotational Rigidity, World Academy of Science, Engineering and Technology 50 (2009) 519-528.

Harte R, Van Zijl GPAG 2007. Structural stability of concrete wind turbines and solar chimney towers exposed to dynamic wind action. Journal on Wind Engineering and Industrial Aerodynamics (JWEIA), 95 (9-11) October 2007: 1079-1096.

Kikuchi Hirotoshi, Yukio Tamura, Gideon Van Zijl, Kazuki Hibi, Nadaraja Pillai, Lisa Alberti 2007a. Wind pressures on cylindrical models with serrated roughness and flow fields, 12th International Conference on Wind Engineering (12ICWE), 1-7 July 2007, Cairns, Australia.

Kikuchi Hirotoshi, Yukio Tamura, Gideon Van Zijl, Kazuki Hibi, Sungil Hong, Lisa Alberti 2007b. Wind pressures acting on a circular cylinder with rotors, 12th International Conference on Wind Engineering (12ICWE), 1-7 July 2007, Cairns, Australia.

IEC 2005. IEC 61400-1:2005. Wind turbines. Part 1: Design requirements. International Electrotechnical Commission, Geneva.

NG 2014. http://news.nationalgeographic.com/news/energy/2014/04/140416-solar-updraft-towers-convert-hot-air-to-energy/, accessed July 2016.

Pretorius JP 2007. Optimization and control of a large-scale solar chimney power plant. PhD dissertation, Stellenbosch University, South Africa.

Retief JV 2015. Contributions to the implementation of the principles of reliability to the standardized basis of structural design. DEng dissertation, Stellenbosch University, South Africa.

Rousseau J-P 2005. Dynamic evaluation of the solar chimney. Master's Thesis, Stellenbosch University, South Africa.

Rousseau J, Van Zijl GPAG 2006. Dynamic evaluation of the solar chimney. Concrete / Beton, Nr 114, December 2006, pp. 12-18.

Schlaich J 1995. The Solar Chimney-Electricity from the Sun. Edition Axel Menges, Stuttgart, Germany.

Schlaich J, Bergermann R, Schiel W, Weinrebe G 2004. Sustainable electricity generation with solar updraft towers. Structural Engineering International 3, 225–229.

Talley S, Mungal G 2002. Flow around cactus-shaped cylinders. Center for Turbulence Research, Annual Research Briefs 2002, pp. 363-376.

Van Dyk C 2004. The realisation of the solar chimney inlet guide vanes. Master's Thesis, Stellenbosch University, South Africa.

Van Dyk C 2008. A methodology for radical innovation – illustrated by application to a radical civil engineering structures. PhD dissertation, Stellenbosch University, South Africa.

Van Dyk C, Van Zijl GPAG 2004. Realisation of the inlet guide vanes – an integral part of the solar chimney. Proceedings SEMC 2004, Cape Town, South Africa, 315-320.

Van Zijl GPAG, Alberti L 2007. Paper Ref: SEMC 2007/696: Flow around Cylindrical Towers: the stabilizing role of vertical ribs. Proc. Third International Conference on Structural Engineering, Mechanics and Computation (SEMC 2007), Cape Town, South Africa, Sept 2007, pp. 884-889.

Van Zyl WS 2014. Concrete wind turbine towers in Southern Africa. Master's Thesis, Stellenbosch University, South Africa.

Van Zyl WS, Van Zijl GPAG 2015. Dynamic behaviour of normally reinforced concrete wind turbine support structures. J SAICE 54(4) 35-44.

Von Backström ThW, Harte R, Höffer R, Krätzig WB, Kröger DG, Niemann H-J, Van Zijl GPAG 2008. State and Recent Advances in Research and Design of Solar Chimney Power Plant Technology, VGB PowerTech Journal, July-edition 2008.

Way A 2014. A study on the design and material cost of wind turbine towers in South Africa. Master's Thesis, Stellenbosch University, South Africa.

Way A, Van Zijl GPAG 2015. Material cost comparison between steel, concrete and hybrid wind turbine support structures in South Africa. J SAICE 54(4) 45-54.

Chapter 6 Summary and conclusions

Contributions to structural engineering have been categorised in *advanced cement-based construction materials*, *crack formation and durability*, *renovation and retrofitting* and *sustainable energy harvesting structures*. Highlights of the findings in each category have been outlined in Chapters 2 to 5, citing the roughly 200 dissertations, theses and technical papers containing the original and complete contributions. The conclusions are collected in the next sections.

6.1 Advanced cement-based construction materials

In advanced cement-based construction materials (ACM), the following contributions stand out:

- Design methods and appropriate mixing procedures of ACM with local ingredient materials, for classes of Strain-hardening Cement-based Composites (SHCC), Ultra-high Strength Concrete (UHPC), Steel Fibre Reinforced Concrete (SFRC), Lightweight Aerated Concrete (LWAC) and Lightweight Foam Concrete (LWFC).
- The time dependence of SHCC, in particular the time-dependent widening of cracks under sustained tensile load, and confirmation of the existence of a creep limit and creep fracture of cracked SHCC.
- A constitutive model for mechanical and time-dependent behaviour of SHCC, based in multi-surface computational plasticity has been presented and demonstrated in several verification and validation analyses.
- Industrial manufacturing processes of SFRC and SHCC by extrusion, and in-situ application by spraying (shotcrete) and the characterisation of the influence on mechanical properties by densification and fibre orientation. This expertise has led to the invitation as visiting professor to assist with 3D Printing of Concrete (3DPC) at NTU, Singapore, and holds potential for the immediate future work on 3DPC at Stellenbosch University.
- Tensile test guidelines for SHCC to characterise multiple crack formation and pre-crack specimens for durability investigations. This contribution was selected as one of ten outstanding papers of 2015 by the International Journal Materials and Structures.
- Shear test method for SHCC including optimised specimen size and geometry, to produce and characterise the multiple diagonal cracking and illuminating the mechanism of shear strength enhancement by principal stress rotation. The test and results have been instrumental in devising an SHCC overlay retrofitting strategy for enhanced shear resistance to seismic action described in Section 6.3.
- First to propose acoustic emission as none-destructive test method to distinguish matrix cracking from fibre pull-out in SHCC, with significant potential for further research and development, and in-situ structural condition monitoring.

6.2 Durability

In the era of significantly deteriorated infrastructure internationally, and in light of roughly 50% of construction budgets directed to maintenance and repair, durability of construction materials and structural systems has been a focus of research and development. The following contributions are highlighted:

- Crack formation and deterioration in SHCC under in-service, loaded conditions were investigated in international leadership and collaboration in technical committees. A book on the state-of-the-art of durability of SHCC has been co-edited and sold more than 5000 chapters in 5 years (Van Zijl and Wittmann 2011). In follow-up, a book on the Framework for durability design with SHCC is in print (Van Zijl and Slowik 2016). These activities and contributions have led to several keynote presentations nationally and internationally.
- Crack pattern characterisation in SHCC, chloride ingress and chemical binding, and electrochemical corrosion monitoring and verification. The postulation and first evidence have been presented of the importance of crack spacing as opposed to crack width in chloride-induced corrosion of steel reinforcement in cracked SHCC. The reduced cathode to anode area ratio has been proposed as the driving mechanism of significantly reduced corrosion rates and reinforcing bar deterioration, despite significant amounts of free chloride reaching the steel surface through finely spaced cracks. This holds significant potential for condition monitoring and the design of appropriate intervention strategies for structures subject to chloride-induced corrosion, which is the number one deterioration mechanism in infrastructure world-wide.
- Results of the combined action of mechanical cracking and ASR deterioration in plain concrete and reinforced concrete are emerging from the research group. Mechanical cracks acting as stress-free expansion regions upon continued or re-activated ASR expansion, are to be considered in the design of repair and/or retrofitting intervention for several structures local to Stellenbosch, Western Cape, and internationally.

6.3 Renovation and retrofitting strategies

Advanced cement-based construction materials are in several instances advantageous in repair and retrofitting strategies, as they might be in new construction carefully designed with consideration for overall system cost savings and/or full life cycle cost. Expertise in traditional construction materials and ACM, including constitutive models in computational implementations, have enabled the development of the following retrofitting strategies for unreinforced load-bearing masonry (ULM) structures:

- Carbon fibre reinforced polymer (CFRP) strip reinforcement of ULM walls to control cracking due to restrained shrinkage. The strategy was validated and proposed for renovation of a historic building in Amsterdam, and awarded as best paper at an international conference in 2001.
- In-plane shear resistance enhancement by thin shotcrete, bonded SHCC overlay on ULM walls. The strategy was developed for local residential infrastructure susceptible to damage and in fact collapse in a seismic event of standardised design magnitude for the Western Cape region. International interest has been raised, culminating in invitations to the Netherlands, where gas extraction over decades has led to emergence of seismic events in recent years, and Denmark, where ULM façade instability and collapse caused by construction and repair activities at neighbouring structures are foreseen to be addressed by this thin bonded shotcrete SHCC overlay retrofitting strategy.

Overlay strategies with CFRP for reinforced concrete beams subjected to cyclic loads like in a highway bridge, and with SHCC for a cracked concrete substrate, have also been studied. For the cyclic debonding of CFRP from concrete, a dominant failure mechanism, a test specimen and procedure has been proposed. For SHCC overlays, particular contributions on interfacial preparations and their influence on interfacial properties and crack diffusion through the overlay have been proposed and included in a book chapter on the behaviour of bonded SHCC overlay systems in the *Framework for durability design with SHCC* (Van Zijl and Slowik 2016).

6.4 Renewable energy harvesting structures

In search of renewable and sustainable energy sources to facilitate economic growth in South Africa and address global warming through fossil fuel emissions, the following structural engineering aspects of energy harvesting have been contributed:

- South African project leadership in an international research project on the Solar Chimney Power Plant, which, together with the extended group of international collaborators known as the Solar Chimney Competence Network, brought the SCPP concept to the brink of implementation and pre-feasibility studies.
- The first local design strategies for the structural design of tall steel, reinforced concrete and hybrid wind turbine tower structures for the emerging local energy industry. The strategies were disseminated in a local journal and a symposium on the design of wind turbine support structures.

6.5 Longevity of contributions

Ensuing international conference series with a leadership role by the author in two of the fields of contribution are testament to the research relevance, importance and impact. The SHCC international conference series with roots in Hawaii (2005) and Stellenbosch (2009) and subsequent events in Rio de Janeiro (SHCC2-2011), Dordrecht (SHCC3-2014) and Dresden (SHCC4-2017), has grown to a stable kernel of experienced and emerging researchers in academia and industry on this ACM. The international conference series on solar Updraft Tower Power Technology started as sessions in existing wind engineering conferences and culminated in dedicated events in Bochum (2010) and Wuhan (2012).

The contributions have laid the link between construction material properties, structural behaviour and durability. Through the fundamental experimental research, structural mechanics and computational mechanics, it has been made possible to utilise the advanced properties of ACM to advance structural performance and durability. Human capital well-versed in the fundamental principles of this multi-level structural engineering approach has been developed in the process of research supervision by the author.

Appendix A Student supervision

Completed Post-Doctoral

1. Dr. W.P. Boshoff, 2007. The design, characterisation and implementation of advanced cement-based composites in the South African Civil Engineering Industry, SU.

Completed Doctoral

1. Dr.ir. A.T. Vermeltfoort, 2005. PhD dissertation Brick-mortar interaction in masonry under compression (promotor Prof D Martens, co-promoter Prof GPAG Van Zijl), Eindhoven University of Technology.
2. Dr. W.P. Boshoff, March 2007. PhD dissertation Time-dependent behaviour of ECC (promotor Prof GPAG Van Zijl), Stellenbosch University.
3. Dr. C van Dyk, Dec 2008. PhD dissertation A methodology for radical innovation – illustrated by application to a radical civil engineering structure (promoter Prof GPAG Van Zijl, co-promoters Prof JV Retief, Dr G de Wet), Stellenbosch University.
4. Dr Peter William Day, March 2013. DEng dissertation A contribution to the advancement of Geotechnical Engineering in South Africa (promoter Prof JV Retief, co-promoter Prof GPAG Van Zijl), Stellenbosch University.
5. Dr. Jin Zang, March 2015. PhD dissertation Structural application of UHPFRC in bridge deck systems (promoter GPAG Van Zijl), Stellenbosch University.
6. Dr Johan V. Retief, Dec 2015. DEng dissertation Contributions to the implementation of the principles of reliability to the standardized basis of structural design (promoter Prof GPAG Van Zijl, co-promoter Dr C Viljoen), Stellenbosch University.
7. Dr. Suvash Chandra Paul, Dec 2015. PhD dissertation Crack formation and durability of cement-based construction material (promoter GPAG Van Zijl), Stellenbosch University.

Current Doctoral

8. Mr. Salhin Alaud, Dec 2016. PhD dissertation Durability of concrete under combined action - mechanical load and alkali silica reaction (ASR) (promoter Prof GPAG Van Zijl), Stellenbosch University.
9. Mr. Stephan Zeranka, 2017. PhD dissertation Design-oriented shear constitutive model for steel fibre-reinforced concrete (SFRC) (promoter Prof GPAG Van Zijl), Stellenbosch University.
10. Mrs Susan Engelbrecht, 2016. PhD dissertation Flexural design guidelines for strain–hardening fibre reinforced cement-based composites (promoter Prof GPAG van Zill), Stellenbosch University.
11. Mrs Julia Schönwälder, 2017. PhD dissertation Experimental and computational Investigations into the Mechanical behaviour of Architectural Cardboard (promoter Prof JG Rots (TU Delft), co-promoter Prof GPAG van Zijl), Delft University of Technology.
12. Mr Peter Mbewe, 2017. PhD dissertation Structural system performance evaluation towards sustainable housing (promoter Prof GPAG Van Zijl), Stellenbosch University.
13. Mr Algurnon S. van Rooyen, 2017. PhD dissertation Mechanics and durability of surface treated foamed concrete (promoter Prof GPAG Van Zijl), Stellenbosch University.
14. Mohamad Pourbehi, 2018. PhD dissertation Computational modelling of ASR (promoter Dr JA van Breda Strasheim, co-promoter Prof GPAG Van Zijl), Stellenbosch University.

Completed Masters

1. Mr Gerardo PJ Cirillo, Prediction of Damage to Cement-Based Structures Subject to Tunnelling-induced Settlements, December 2003, Stellenbosch University, cum laude.
2. Mr Cobus van Dyk, The realisation of the solar chimney inlet guide vanes, April 2004, Stellenbosch University.
3. Mr Don de Koker, Manufacturing Processes for Engineered Cement-Based Composite Material Products, December 2004, Stellenbosch University.
4. Mr Gao Song, Matrix Manipulation to Study ECC Behaviour, April 2005, Stellenbosch University.
5. Mr Jurie J. Loots, Computational assessment of seismic resistance of RC framed buildings with masonry infill, December 2005, Stellenbosch University, cum laude.
6. Mr Jean-Pierre Rousseau, Dynamic modelling of the solar chimney, December 2005, SU.
7. Mr Schalk W Marais, Punching shear of flat slabs, April 2005, Stellenbosch University.
8. Ms Lisa T Alberti, Flow around cylindrical towers: the stabilizing role of vertical ribs, December 2006, Stellenbosch University, cum laude.
9. Mr Qinjiang Shang, Shear behaviour of SHCC, December 2006, Stellenbosch University.
10. Mr Heinrich Stander, Experimental and computational characterisation of SHCC-Concrete interfacial bond, March 2007, Stellenbosch University, cum laude.
11. Mr Christo R Visser, Mechanical and structural characterization of extrusion moulded SHCC, December 2007, Stellenbosch University, cum laude.
12. Mrs Susan Victor, Towards Design guidelines for reinforced strain–hardening cement-based composites, March 2008, Stellenbosch University.
13. Ms Elsje Fraser, Computational modeling of footing rotational rigidity, December 2008, Stellenbosch University.
14. Ms WI Dunaiski (co-promotor) Investigation into the effective lengths of web compression elements in parallel chord trusses, December 2008, Stellenbosch University, cum laude.
15. Mr Gerrit Visser, FRP external reinforcement of bridges in SA, December 2009, Stellenbosch University.
16. Mr Katiso Molapo, The behaviour of strain-hardening cement composites under biaxial compression, December 2010, Stellenbosch University.
17. Mr Edson Mucambe, Creep and Shrinkage prediction models for concrete water retaining structures in South Africa, December 2010, Stellenbosch University.
18. Mr Peter Mbewe. Development of analytical flexural models for steel fibre reinforced concrete beams with and without steel bars, December 2011, Stellenbosch University, cum laude.
19. Mr Suvash Chandra Paul. Mechanical behaviour and durability performance of concrete containing recycled concrete aggregate, December 2011, Stellenbosch University.
20. Mr Willie Swanepoel. The behaviour of fibre reinforced concrete (SHCC) under biaxial compression and tension, December 2011, Stellenbosch University.
21. Mr Charl de Jager. A critical appraisal of existing models for nonlinear finite element analysis of reinforced concrete response, March 2012, Stellenbosch University, cum laude.
22. Mr Adriaan Badenhorst. Debonding of external carbon fibre reinforced polymer plates from reinforced concrete structures by cyclic loading effects, March 2012, Stellenbosch University.
23. Mr Algurnon van Rooyen. Energy efficient construction materials: Structural lightweight aerated concrete, March 2013, Stellenbosch University.
24. Mr Willem van Zyl. Concrete wind turbine towers in Southern Africa, December 2014, Stellenbosch University, cum laude.
25. Mr Andrew Way. A study on the design and material costs of tall wind turbine towers in South Africa, December 2014, Stellenbosch University, cum laude.

26. Mr JP de Villiers. Bond behaviour of lightweight foamed concrete for use in structural application, December 2015, Stellenbosch University, cum laude.
27. Mr JD Gerber. Alternative wall-to-slab connection systems in reinforced concrete structures, December 2016, Stellenbosch University, cum laude.
28. Mr L de Beer. Developing and testing a sprayable overlay of SHCC for retrofitting of unreinforced load bearing masonry walls, December 2016, Stellenbosch University, cum laude.

Current Masters

29. Mr Tino Muzofa (2016 - 2017). Wind turbine foundation optimisation, Stellenbosch University.
30. Mr Trevor Dunn (2016 - 2017). Lightweight concrete building systems for sustainable residential infrastructure, Stellenbosch University.
31. Mr Schalk Bezuidenhout (2016 - 2017). Non-destructive measurement of corrosion in RC, Stellenbosch University.